A STATISTICAL LIGHTNING MODEL

by

Marlie van Zyl

Submitted in fulfilment of the requirements for the degree of Master of Science in the School of Physics, University of KwaZulu–Natal.

As the candidate's Supervisor I have/have not approved this thesis for submission

Signed: ..... Name: ..... Date: .....

PREFACE

The experimental work described in this dissertation was carried out at the Hermanus Magnetic Observatory, Hermanus, and in the School of Physics, University of KwaZulu–Natal, Durban, from March 2010 to December 2011 under the supervision of Dr Andrew B. Collier.

These studies represent original work by the author and have not otherwise been submitted in any form for any degree or diploma to any tertiary institution. Where use has been made of the work of others it is duly acknowledged in the text.

DECLARATION 1 - PLAGIARISM

I, ..., declare that

1. The research reported in this thesis, except where otherwise indicated, is my original research.
2. This thesis has not been submitted for any degree or examination at any other university.
3. This thesis does not contain other persons' data, pictures, graphs or other information, unless specifically acknowledged as being sourced from other persons.
4. This thesis does not contain other persons' writing, unless specifically acknowledged as being sourced from other researchers. Where other written sources have been quoted, then:
   (a) Their words have been re-written but the general information attributed to them has been referenced
   (b) Where their exact words have been used, then their writing has been placed in italics and inside quotation marks, and referenced.
5. This thesis does not contain text, graphics or tables copied and pasted from the Internet, unless specifically acknowledged, and the source being detailed in the thesis and in the References sections.

Signed: .....

DECLARATION 2 - PUBLICATIONS

DETAILS OF CONTRIBUTION TO PUBLICATIONS that form part and/or include research presented in this thesis (include publications in preparation, submitted, in press and published and give details of the contributions of each author to the experimental work and writing of each publication)

Signed: .....

Acknowledgements

I would like to thank my supervisor, Dr Andrew Collier, for his patience and guidance as well as excellent learning and travel opportunities. The South African Weather Service (SAWS) for data from their lightning detection network. Kristen Corbosier for lightning data from the National Lightning Detection Network (NLDN). Janos Lichtenberger for lightning data from LINET. Peter Steinbach for Trimpi data from Rothera. The National Research Foundation (NRF) for funding my project. The South African National Space Agency (SANSA) Space Science for accommodating me during my studies and contributing to my funding.

Abstract

The detailed spatial and temporal influence of lightning on precipitation losses from the Earth's radiation belts is not yet well known. The precipitation is mainly due to the pitch angle scattering of electrons by lightning induced whistler mode waves. The World Wide Lightning Location Network (WWLLN) gives continuous real-time global lightning coverage with excellent time resolution. The detection efficiency of WWLLN is unfortunately relatively low. This led to the normalisation of WWLLN with reference to Lightning Imaging Sensor (LIS)/Optical Transient Detector (OTD) data. LIS/OTD has very good detection effiency and spatial resolution. However, whereas WWLLN records strokes, LIS/OTD record flashes. Therefore the flash multiplicity had to be taken into account. The normalised WWLLN flash densities were compared to those of the South African Weather Service (SAWS) data, National Lightning Detection Network (NLDN) and the European LINET network. Then the average power per lightning flash was calculated to determine the energy flux incident on the ionosphere. Finally the WWLLN data was transformed to geomagnetic (MAG) coordinates using the Altitude Adapted Corrected Geomagnetic (AACGM) code. By applying absorption curves, the energy flux into the magnetosphere was estimated. These values were then compared to Trimpi produced Whistler-Induced Electron Precipitation (WEP) rates.

Contents

List of Figures

List of Tables

Acronyms

AACGM Altitude Adjusted Corrected GeoMagnetic

ALDIS Austrian Lightning Detection and Information System

CG Cloud-to-Ground

CC Cloud-to-Cloud

CGM Corrected Geomagnetic

CME Coronal Mass Ejection

EIWG Earth-Ionosphere Waveguide

ELF Extremely Low Frequency

DF direction finder

DE detection efficiency

FWM Full Wave Method

GPS Global Positioning System

HRAC High Resolution Annual Climatology

HRMC High Resolution Monthly Climatology

HRFC High Resolution Full Climatology

IC Intra-Cloud

IGRF International Geomagnetic Reference Field

IRI International Reference Ionosphere

LA location accuracy

LEP Lightning-Induced Electron Precipitation

LDN Lightning Detection Network

LIS Lightning Imaging Sensor

LLS Lightning Location Systems

LPI Lightning Protection Index

MDF Magnetic Direction Finder

NLDN National Lightning Detection Network

OTD Optical Transient Detector

PSD Power Spectral Density

SAWS South African Weather Service

TOA Time of Arrival

TOGA Time of Group Arrival

TRMM Tropical Rainfall Measuring Mission

VLF Very Low Frequency

WEP Whistler-Induced Electron Precipitation

WWLLN World Wide Lightning Location Network

Chapter 1

Introduction

Lightning is a large scale electric discharge occurring in the Earth's atmosphere. A lightning stroke consists of long current branches that can extend to several kilometers. It typically lasts a few milliseconds. Since lightning emits radiation over a broad frequency range it is an effective source of electromagnetic waves. It has been commonly accepted that the statistics of many observable lightning parameters are best described by a lognormal distribution (Ogawa, 1995). Ground flash density (flashes/km^2) is one of the few exceptions. It has been found to vary on a seasonal, annual and latitudinal basis.

A Cloud-to-Ground (CG) lightning stroke starts with a large charge separation occurring between a cloud and the ground. The charge in the cloud is thought to occur due to the friction between graupel and ice crystals. The negative charge in the lower part of the cloud travels down towards the Earth, called the stepped leader. As the stepped leader gets very close to the ground, positive charges from the Earth surge up. When the two streams connect, a channel is created which discharges huge amounts of energy. This is called the return stroke. The huge energy release causes the air around it to expand quickly and this is the cause of thunder.

A lightning flash only lasts about a second, but it can consist of multiple strokes. Flashes that have subsequent strokes with a polarity opposite to the first stroke are called bipolar flashes. Schulz et al. (2005) inferred that the majority of positive bipolar flashes are the result of a so called true positive first CG stroke followed by one or more negative CG strokes. Negative CG are believed to account for about 90% of all CG discharges (Rakov and Uman, 2003).

Lightning emits most of its radiation in the Very Low Frequency (VLF) (3–30 kHz) range. The VLF energy from lightning can travel long distances in the Earth-Ionosphere Waveguide (EIWG) with low attenuation. A portion of this energy can penetrate through the ionosphere and into the magnetosphere. Once in the magnetosphere the energy from a lightning discharge is guided by the magnetic field lines. As the radio waves travel along this path, they undergo dispersion. This means that different frequencies travel at different velocities. With the high frequencies usually traveling faster than the lower frequencies. This leads to a signal of gliding tones at the end of the path. This

phenomena is called a whistler. Recent studies have shown that waves in the whistler mode play an important role in energetic radiation belt losses (Johnson et al., 1999; Rodger and Clilverd, 2002).

1.1 Outline

First a basic background of Space Physics, the regions of interest, lightning and whistlers are discussed in Chapter 2. Then a description of lightning detection and lightning detection networks is given in Chapter 3.

Chapter 4 gives discussion of the data analysis methods and results in the study. The global lightning stroke density in geographic coordinates is determined from World Wide Lightning Location Network (WWLLN) data. Since the detection efficiency (DE) of WWLLN is low, the subsequent data is then normalised with reference to the global lightning flash densities of Lightning Imaging Sensor (LIS)/Optical Transient Detector (OTD). Since WWLLN measures strokes not flashes, multiplicity (the number of strokes per flash) has to be incorporated in order to change the values to flashes. The normalised WWLLN flash densities are then compared to data from regional networks in order to do a validation. The flash densities are then converted to geomagnetic coordinates. From here the VLF power density incident on the bottom ionosphere is calculated. The classical absorption coefficients of Helliwell (1965) are used to calculate the power entering the magnetosphere.

Chapter 5 gives a discussion of the methods that were used and results that were obtained. A conclusion is reached and recommendations for possible further studies are given in Chapter 6.

Chapter 2

Background

2.1 Space Physics

Space Physics is a study of the Sun-Earth environment depicted in Figure 2.1. It is related to the study of the often violent changes in the space environment surrounding the Earth, called Space Weather.

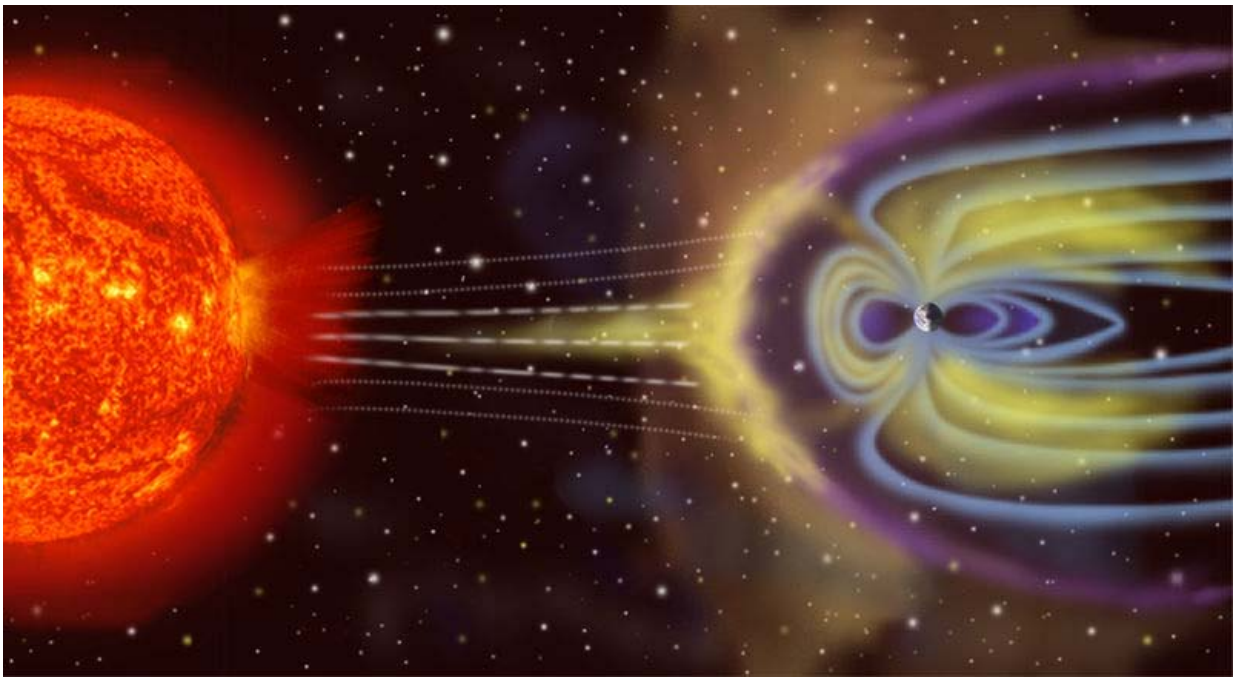

Figure 2.1: The Sun-Earth connection by Steele Hill/NASA. For release 04/29/2002. Image from `http://http://sec.gsfc.nasa.gov/sec_resources.htm`.

The Sun radiates energy which is the product of violent nuclear reactions inside its core. Energy gets transported to the surface via radiation and convection (White, 1970)

from where it is ejected. One of the ways in which energy gets ejected is as a hot plasma, called a Coronal Mass Ejection (CME). CMEs can be hazardous as they sometimes travel in the direction of the Earth. CMEs are carried via a solar wind and move at speeds of 1000 km/s or more. Solar winds are often the carriers of strong magnetic fields and highly energetic particle fluxes (Scherer et al., 2005). Some of the energy can reach Earth and have damaging effects to objects like satellites, rockets, aeroplanes and power cables.

2.2 Studied regions

2.2.1 Magnetosphere

The Earth is surrounded by a magnetic field, the magnetosphere (Figure 2.2), that is often regarded as a dipole. The magnetic field lines are described by a parameter called the L-value. As an example: $L = 2$ describes a set of the Earth's magnetic field lines which cross the Earth's magnetic equator two Earth radii 6371 km $\times 2$ from the centre of the Earth. Without inter planetary plasma the Earth's magnetic field would be perfectly symmetrical, but due to the presence of the solar wind it is not.

Once the streams of energetic particles from a CME and magnetic fields carried by the solar wind reaches the magnetosphere it distorts its magnetic dipole shape by compressing it on the dayside and stretching out the nightside to create a tail of many hundreds of Earth radii long (Scherer et al., 2005). The International Geographic Reference Field (IGRF) model is often used to represent the magnetic field of the Earth more accurately by including higher quadrapole and multipole terms.

The inner part of the magnetosphere is called the plasmasphere, which is bounded by the plasmapause. (Budden, 1988). The bulk of the plasma contained within the plasmasphere is composed primarily of "cold" (low energy) electrons and protons with typical energies of < 1 eV, and is relatively dense with concentrations of 10^2 to 10^4 electrons/cm ^{3} at the inner edge of the plasmapause (Bortnik, 2004).

Inside the cold plasma of the plasmasphere is a torus of "hot" (high energy) electrons and protons called the Van Allen radiation belts. These hot particles typically have energies of > 100 keV and experience long-term trapping in the geomagnetic field. This type of trapping requires stable magnetic fields which are not present at the magnetopause due to the magnetic field fluctuations induced by the variable solar-wind and but are present between 200 km and $L \approx 7$.

A region of depleted electron flux, called the slot region, divides the radiation belts into an inner and outer section where the inner section stretches out to $L \approx 2$ and the outer section constitutes the rest. One possible contributor of particles in the inner radiation belts are solar protons that penetrate the inner magnetosphere during strong magnetic storms and become trapped during the recovery of the magnetosphere configuration (Lazutin et al., 2009). The geomagnetic field in between the ionosphere and solar plasma consits of particles from both of the regions. The electric and magnetic fields

in the radiation belt region accelerate and trap the particles the electrons and protons over a long period before eventually returning them to their source regions (Walt, 2005).

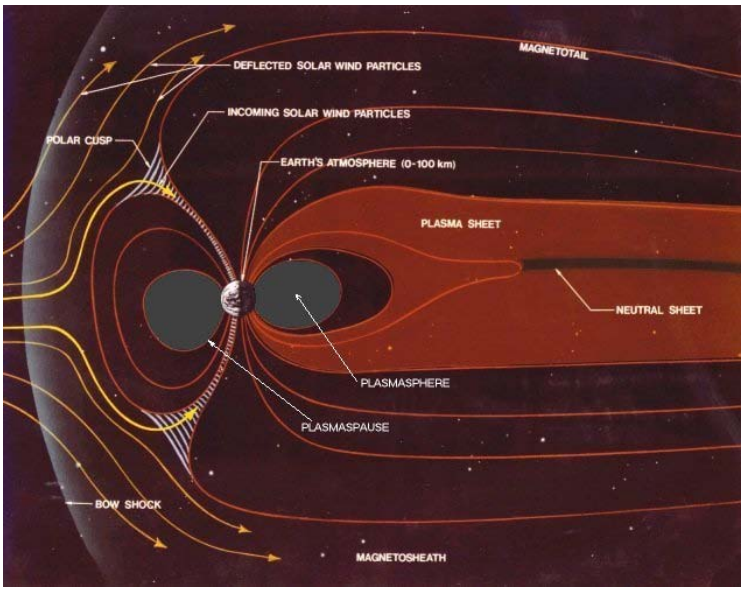

Figure 2.2: A portion of the Earth's magnetosphere. The yellow arrows indicate the different paths that solar wind particles can follow to enter into the inner magnetosphere. Author: Dave Dooling. Curator: Linda Porter. NASA Official: Gregory S. Wilson. Article title: Rocket will study Space Weather effects. Image from `http://science.nasa.gov/science-news/science-at-nasa/1999/ast07jan99_1`.

The trapped energetic radiation belt electrons undergo three main periodic motions: cyclotron motion, where the particle gyrates around the magnetic field lines; a bouncing motion, where the particle bounces between the Northern and Southern hemispheres along the field lines and a drifting motion where the particle drifts around the Earth. These occur on time scales of $\approx 10^{-3}s$, $\approx 1s$ and $\approx 10^{3}s$ respectively. Waves originating from the Earth often lead to wave-particle interactions which cause these energetic electrons to be lost from the radiation belts.

A gradient drift arises due to the particles experiencing the effect of a stronger magnetic field closer to Earth and a weaker magnetic field further from the Earth. This causes the gyroradii of the particles to increase and decrease with each orbit around a field line which causes the particles to drift. Curvature drift arises from the centrifugal force felt by particles as the magnetic field lines cause them to move along a curved path (Chen, 1984).

The gradient drift

$$\mathbf{V}_{\bigtriangledown B} = \pm\frac{1}{2}v_{\perp}r_{L}\frac{\mathbf{B}\times\bigtriangledown_{\perp}\mathbf{B}}{B^{2}} \tag{2.1}$$

and the curvature drift

$$\mathbf{V}_R = \frac{mv_\parallel^2}{qB} \times \frac{\mathbf{R}_c \times \mathbf{B}}{R_c^2} \tag{2.2}$$

can be added together to give the total drift in a a curved vacuum field, the gradient-curvature drift:

$$\mathbf{V}_{\nabla B} + \mathbf{V}_R = \frac{m}{q}\frac{\mathbf{R}_c \times \mathbf{B}}{R_c^2 B^2}(v_\parallel^2 + \frac{1}{2}v_\perp^2) \tag{2.3}$$

where m is the mass of a particle, q is the electric charge of a particle, B is the magnetic field, R_c is the constant radius of curvature and r_L is the Larmor radius.

What makes the gradient and curvature drifts so important is that their magnetic effects along with the mirroring of particles are the primary controlling factors related to long-term trapping of particles in the magnetic field Walt (2005) and especially the inner magnetic field where the VLF waves radiated by lightning first enter the magnetosphere.

2.2.2 Ionosphere

The ionosphere is a region of the Earth's atmosphere of which the greater region is made up of ionised particles due to radiation. It stretches from an altitude of 60 km–1000 km and can be divided into three main regions. An E (90 km–130 km) and F (>130 km) region are always present whilst the bottom D-region (60 km–90 km) (Kivelson and Russell, 1995) only exists during the day due to an increase in solar radiation and therefore ionisation.

An electron density profile as a function of altitude, Figure 2.3, is often helpful in illustrating the difference between the three main regions. These differences exist not only due to the different wavelengths of the radiation incident at different altitudes, but also due to the composition of the different layers. The D-region is created by the most energetic types of radiation like solar x-ray photons and galactic cosmic ray particles. The E-region ions are mostly O_2^+ and NO^+ whilst the F-region is mostly composed of O^+ ions, Figure .

The ionosphere is usually studied using ionospheric models that depend on location, altitude, day number, sunspot cycle phase and geomagnetic activity. One of the most popular models is the International Reference Ionosphere (IRI) which predicts the height distribution of the electron concentration N(z) and features such as ion concentration as well as electron, ion and neutral temperatures.

2.2.3 Earth-Ionosphere Waveguide

The Earth can be seen as a solid conducting sphere surrounded by a thin dielectric atmosphere (Nickolaenko and Hayakawa, 2002). The conductivity of the air decreases by six orders of magnitude upon moving downward out off the ionosphere. A rapid decrease

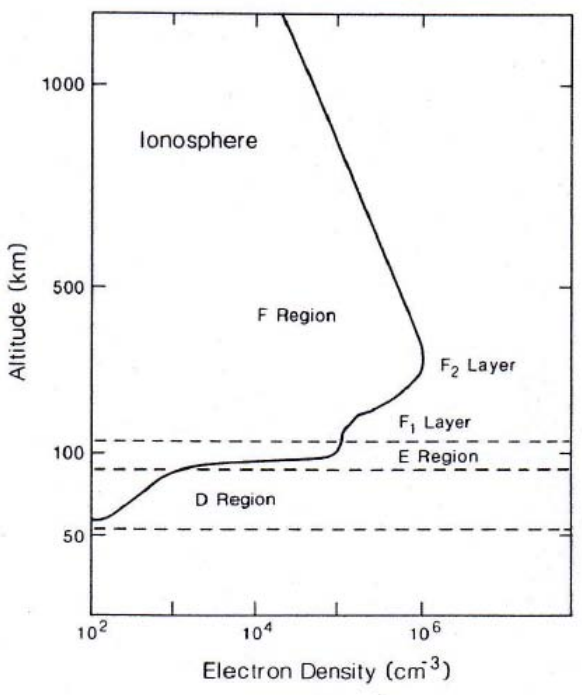

Figure 2.3: Electron density profile of the ionosphere

of conductivity with altitude allows one to treat the lower parts of the atmosphere as a thin dielectric layer located between two relatively good conductors of which the upper layer is the plasma of the ionosphere and the lower is the Earth. These two layers form a spherical cavity, called the Earth-Ionosphere Waveguide (EIWG). During the daytime the EIWG is much narrower, due to the absorbing D-region in the ionosphere. The VLF energy radiated by lightning propagates through multiple reflections in the EIWG over long distances with low attenuation (2–3 dB/100 km) with a propagation distance that varies from $1500 - 8000$ km.

2.3 Lightning

2.3.1 Charging mechanisms

A lightning discharge usually begins with a charge build-up in a cloud. The primary source of lightning is the cumulonimbus cloud type, commonly known as the thundercloud (Rakov and Uman, 2003). Electric charges produced inside the cloud are thought to be primarily due to collisions between graupel, supercooled droplets of water that collect and freeze on a falling snowflake, and small ice crystals in the presence of water droplets that facilitate significant charge transfer (Rakov and Uman, 2003).

While falling to the bottom of the cloud the heavy graupel particles acquire a charge

from their collisions with the ice crystals. If the graupel is near the top of the cloud and below a critical temperature, called the reversal temperature (T_R), it will acquire a negative charge. Lower in the cloud, at a temperature above T_R, the graupel acquire a positive charge. The huge charge difference between the top and bottom of the cloud causes very high potential differences that leads to the development of electric fields between these two regions (Lynch, 1980). As a charged cloud moves over the ground it can cause electric fields to build-up between the cloud and the ground. This is due to the negative charges in the bottom of the cloud that repel the negative charges in the ground causing it to aquire a positive charge in the region closest to the cloud.

2.3.2 Discharge process

Stroke

The most basic element of a lightning discharge is a stroke. It can be divided into two main processes: a leader and a return stroke. For a lightning discharge to occur an initial breakdown, that bridges the negative and positive regions, has to take place (Rakov and Uman, 2003). The first leader, called the stepped leader, creates a conducting path between the cloud and the ground. By doing this, it effectively distributes negative charge from the cloud all the way along the downward path.

As the leader approaches the ground, the electric field at the ground surface increases until it exceeds a critical value for the initiation of one or more upward-connecting leaders. When contact is made between the downward and upward moving leaders, an energetic return stroke will rush along the same conducting path from the ground towards the cloud and neutralise the charge that the negative leader has deposited (Rakov and Uman, 2003). An example of the process of a stroke is illustrated in Figure 2.3.

Subsequent Stroke

Sometimes a lightning discharge ends at one stroke, but more often the residual first stroke channel is traversed by a leader that appears to move continuously, the dart leader (Rakov and Uman, 2003). Before the dart leader the J (junction) and K processes occur. The J process leads a charge redistribution in the cloud whilst the K process can be seen as a dart leader of some kind. These processes play an important role in a CG discharge by transporting additional negative charges into and along the existing channel, stopping before it reaches the ground.

When a dart leader approaches the ground a process very similar to that of the first stroke occurs. However it takes place over a shorter distance and therefore takes less time. Once the dart leader is connected to the ground, the subsequent return stroke is launched upward and once again neutralises the leader charge. This process can continue until there is no longer a large enough negative charge region at the bottom of the cloud.

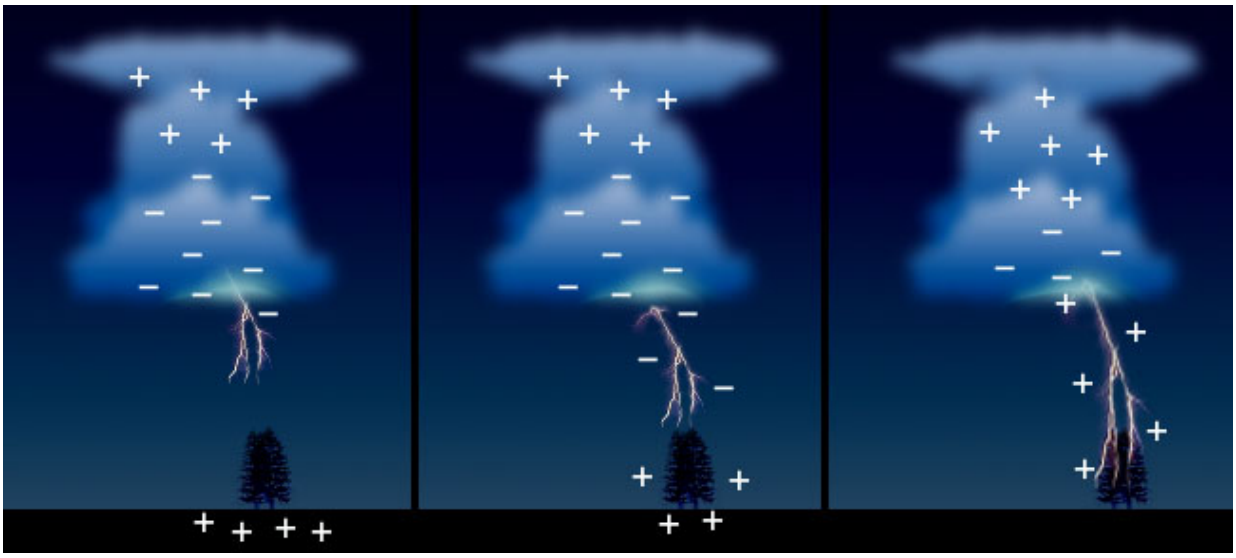

Figure 2.4: A Cloud-to-Ground lightning discharge starts with a charge difference between the cloud and the ground. Image from Windows to the Universe `http://windows2universe.org`, National Earth Science Teachers Association.

Various types of lighting discharges are illustrated in Figure 2.5. Clearly identifiable are negative CG, Intra-Cloud (IC) and Cloud-to-Cloud (CC) lightning discharges originating from and in cumulonimbus clouds.

Positive Discharges

But a lightning flash does not only occur due to a negative charge region in a cloud. A positive flash, that transports charge from the Earth and the positive region at the top of the cloud can also occur. However less than 1 out of 10 global lightning CG is thought to be positive (Rakov and Uman, 2003). Positive flashes mainly have only one stroke, but they have the highest measured lightning currents (near 300 kA), the largest charge transfer to the ground and have been found to be more dominant during the winter season (Orville and Huffines, 2001).

Upward Discharges

Lightning discharge have also been known to start from the ground upward. Sometimes the electric field enhancement of a grounded vertical object becomes so large that the upward-moving leader from the object's tip can be initiated, by in-cloud charges, or, more likely, by in-cloud discharge processes, as opposed to being initiated by the charge on the descending stepped leader. The object then becomes capable of initiating upward lighting (Rakov and Uman, 2003). Objects with a height less than 100 m are usually only struck by downward lightning, whilst those with a height greater than 500 m have been known

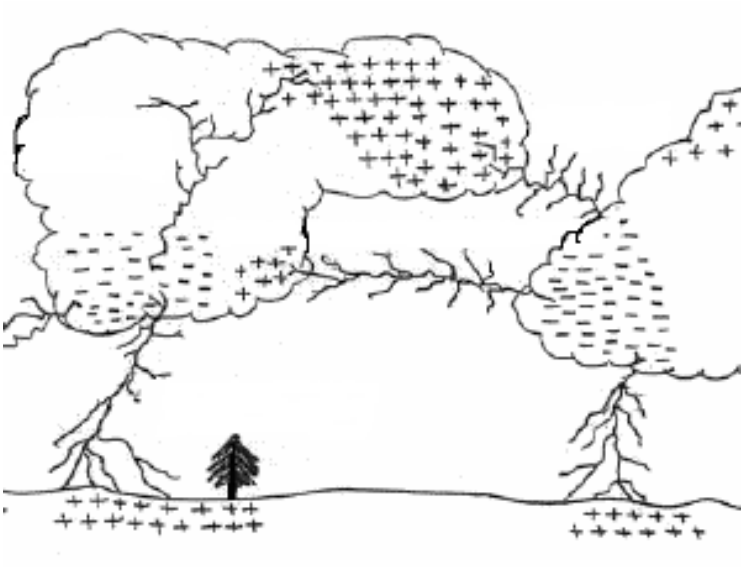

Figure 2.5: An illustration of the different kinds of connection between the clouds and the ground. Image from an article titled "Where Lightning Strikes ", NASA Science - science news. `http://science.nasa.gov/science-news/science-at-nasa/2001/ast05dec_1`

to initiate upward lightning.

Cloud Discharges

Cloud discharges include intracloud (within one thundercloud), intercloud (between thunderclouds) and air discharges (between a thundercloud and the air). It is thought that the majority of cloud discharges are of the IC type. These can be viewed as being composed of an early and a late stage. Overall, the early stage processes are probably similar to the initial breakdown and stepped-leader processes in negative CG lightning (Rakov and Uman, 2003). In general the upper and lower boundaries of a negative charge region, where the electric fields are highest, are the most likely places for a cloud flash to begin.

2.3.3 Intra-Cloud to Cloud-to-Ground ratio

The ratio of IC to CG flashes is called the z-ratio: $z = \frac{N_c}{N_g}$, where N_c is the cloud flash density, N_g is the ground flash density. Some studies have used a constant z-ratio. However, it has mostly been found to vary.

Prentice (1977) found a mean z-ratio value of 5.7 for latitudes of 2°–19°, 3.6 for latitudes of 27°–39°, 2.6 for latitudes of 43°–50° and 1.8 for latitudes of 52°–69°. They used the following to fit 29 observations:

$$z = 4.16 + 2.16(\cos 3\lambda) \tag{2.4}$$

where λ is the latitude. Most experimental data for z fell within a factor of 2–3.

Mackerras et al. (1998) did a global study and also found that z varies with latitude. They obtained a value of 3.96 for latitudes of 0°–20°, 3.18 for latitudes of 20°–40° and 1.92 for latitudes of 40°–60°. Boccippio et al. (2001) found an average value of 2.94 for the continental United States.

In one of the latest z variation studies, De Souza et al. (2009) looked at geographic distribution, latitude, percentage of positive CG flashes and total flash density as well as the hourly variation. They found a small diurnal variation and a relation to the lightning flash density, with z increasing with increasing flash density.

From these results it is clear that values of z can have variations due to storm type, location and other factors, but an average value has been found to be around 3 (Rakov and Uman, 2003). An average value of around 3–3.5 was assumed by Rodger et al. (2004a, 2005) following (Mackerras et al., 1998). Due to all the different values in literature, and for the purpose of this study, an average global value of $z = 3$ was also assumed.

2.3.4 Multiplicity

There is a saying that lightning never strikes in the same place twice. In reality this is very seldom true. The number of lightning strokes per flash is known as the lightning stroke multiplicity and multiplicity is often > 1. A CG lightning stroke is the process of a single CG connection (leader) and reconnection ground-to-cloud (return stroke). If there is charge left in the cloud, another stroke will occur. This means that multiple strokes can occur in the same location.

Multiplicity has been found to vary with the stroke grouping criteria of the various lightning detection networks both during the detection and analysis process. As an example Christian et al. (2003) considered multiple events for LIS/OTD data to be a part of the same flash if there was not more than a 333 ms time gap between successive events and not a separation distance of more than 15 km between geolocated events.

According to Ogawa (1995) and Pinto et al. (1996), who examined CG lightning in Brazil, multiplicity obeys a long-tailed distribution. From a 1996 data set Watkins et al. (2001) found 52.5% of the flashes to have one stroke, 20.7% to have two strokes and 11.2% have three strokes. This agrees well with the 59.5%, 21.8% and 10.1% of Pinto et al. (1996) and supports the long-tailed distribution of multiplicity. Watkins et al. (2001)

used this multiplicity property to compare the Halley stroke rate data to the National Lightning Detection Network (NLDN) flash rate data, by assuming that multiplicity does not have a strong variation with position due to the long-tailed distribution property.

Schultz and Diendorfer (2006) also noted a long-tailed multiplicity distribution and found an average multiplicity of 2 for negative flashes in Austria. This differs from an average multiplicity of 4.6–6.4 obtained by Rakov and Huffines (2003) from NLDN data in 2003. Schultz and Diendorfer (2006) attribute the difference to different data acquisition techniques, the use of different amounts of data, an increased DE of singles strokes and the misclassification of strokes as CG.

More recently Pinto Jr. (2008) found that the percentage of multiple negative CG flashes in Brazil from the Moro do Cachimbo Station (52%) was much higher than those from two detecting towers in Switzerland from the San Salvatore Station (31% and 35%). These differences could be either due to the different latitudes or different meteorological conditions. Pinto Jr. (2008) also found a multiplicity of 3.8 in the Southeast region of Brazil. Gill (2008), using the South African Weather Service (SAWS) lightning detection network, found the highest multiplicity values in South Africa were over KwaZulu-Natal and the Eastern Cape with more than 3 strokes per flash. Over the entire interior plateau they found a multiplicity of 2–3.

Except for a variation in detecting system and latitude a variation with climate, terrain (Orville and Huffines, 2001) and seasonal variation has also been found. Orville et al. (1987) studied a lightning detection system along the northeastern United States from a year of data. They found that whilst positive flashes tend to keep their one-stroke property throughout the year, the negative flashes had an increase in one-stroke flashes from 40% to 80% from summer to winter. The polarity link was also confirmed by Pinto Jr. (2008) who found that positive flashes are usually single stroke. The multiplicity of negative flashes has been found to have regional variation, thought to be due to variations in the horizontal dimensions of the thunderstorms at different locations.

Taking all the different multiplicity values and variations into account, an average global lightning stroke multiplicity value of 3.5 strokes/flash was assumed for the purpose of this study (Thomson, 1980; Thomson et al., 1984; Cummins et al., 1998).

2.3.5 Estimates of the Energy radiated by Lightning

Lightning radiates energy over all frequencies, but has a peak in the VLF range. Lightning is the most effective terrestrial source of VLF radiation with the biggest portion coming from the return stroke, due to its heavy current flow. The main lightning discharge, the return stroke, has an energy spectrum that peaks around 9 kHz to 10 kHz (Prasad and Singh, 1982).

Hill (1957) found that the peak of the radiation spectrum from a CG stroke was around 11.2 kHz and estimated the total energy radiated in the leader and return stroke in the VLF range to be at 220 kJ.

Hill (1979) aimed to find a typical average value for the energy dissipated in a lightning return stroke. This was done by creating a survey of lightning energy estimates and then taking lightning characteristics like current, charge, multiplicity and the height of strokes into account. From electric, optical and acoustic measurements Hill (1979) calculated an average value of 5×10^4 kJ over all frequencies.

Borucki and Chameides (1984) found a value for the global average energy dissipation rate derived from the energy per flash. First Borucki and Chameides (1984) considered the energy of one stroke, the number of strokes per flash and the distribution of energy among the first and subsequent strokes and then incorporated the global average flash rate. By calculating the energy/ flash from optical and electric field change measurements Borucki and Chameides (1984) found an average of 4×10^5 kJ/flash.

More recently Cooray (1997) found that a typical lightning ground flash with 4 strokes dissipates about 9.5×10^5 kJ. Of this energy 4.5×10^5 kJ dissipates into the leader stages and 5×10^5 kJ in the return stroke stages.

From these studies one could consider an average energy per flash of around 10^5 kJ. This is in sharp contrast with the 220 kJ. It should be noted that Hill (1957) only looked at the VLF range and used a theoretical estimate of the average energy per stroke. Since the 10^5 kJ per flash values were determined from energy estimates across all the frequencies the energy radiated in the VLF range will be smaller.

2.3.6 Lightning Spectrum

The VLF energy radiated by a lightning discharge over a range of frequencies spreads throughout the EIWG, suffering subionospheric attenuation and absorption consistent with that of multimode waveguide models (Poulsen et al., 1993). In some cases, the ionosphere has been modeled as a set of thin, homogeneous layers that combine to form a stratified medium (Helliwell, 1965; Lauben et al., 1999; Lehtinen and Inan, 2009). Due to reflection in the EIWG, a fraction of the VLF lightning energy penetrates the horizontally stratified ionosphere and enters the magnetosphere.

In order to calculate the VLF energy from lighting Lauben et al. (2001) derived a function for the Power Spectral Density (PSD) of a lightning stroke, based on the widely used Bruce and Golde (1941) model for a lightning return stroke and the expression for an electric field at a distance R from the base of a vertical CG discharge (Uman, 1984). The location of the lightning discharge within the EIWG at a source geomagnetic latitude, λ_s was assumed to be given by $R_l = 0$. Where R_l is the height at which the discharge enters the ionosphere.

The far-field power spectral density of waves that enter the ionosphere at $R_l = 100km$ is given by

$$P(\omega) = \frac{1}{Z_0}(\frac{h_e I_0}{2\pi\epsilon_0 c^2})^2(\frac{\sin\theta}{R_l})^2\frac{\omega^2(a-b)^2}{(\omega^2+a^2)(\omega^2+b^2)}. \quad (2.5)$$

where ω is the angular frequency, Z_0 is impedance of free space ($\approx 377\Omega$) and ϵ_0 (8.854×10^{-12} N/A^2) is the permeability of free space, θ is the angle observer with respect ot the local zenith and h_e is the height of the initial $+Q$ charge above ground. The parameters a $= 5 \times 10^3$ Hz and b $= 1 \times 10^5$ Hz are chosen to give a typical spectrum that is broadly peaked between 2 kHz and 6 kHz. A stroke height $h_e = 5km$ and reference current $\mid I_0 \mid = 10.53kA$ are adopted to give reasonably strong wave intensity values (Lauben et al., 2001). According to the PSD function (2.5) a CG discharge radiates energy in all directions within the area between the EIWG. Therefore the $\frac{1}{R_l{}^2}$ factor was added to (2.5) to account for additional subionospheric attenuation due to absorption and wave mode interference.

Bortnik et al. (2003a,b) did a study of the wave power density at a free-space distance, R, from a lightning source. It is derived from the expression given by Uman (1984) for the lightning radiated electric field, together with a model for the discharge current profile by (Cummer and Inan, 1997). The equation was almost identical to (2.5)

The wave power density along the bottomside ionosphere was calculated for the region surrounding the lightning discharge. The PSD function predicts a radiation pattern with a null value directly above the lightning source ($sin(\theta = 0) = 0$), but due to the inhomogeneities in the EIWG the radiation pattern will get smeared out. By assuming the source to be slightly displaced from the vertical, one can ignore the null radiation pattern (Bortnik, 2004).

2.3.7 Distribution

The most recent estimates of the average annual global lightning flash rate have been found to be around 44 ± 5 flashes/s (Christian et al., 2003) as shown in Figure 2.5. With a annual global flash rate of 55 flashes/s in the Northern Hemisphere summer to a minimum of 35 flashes/s in the Northern Hemisphere winter which indicates a seasonal variation. The total lightning flash rates in the northern hemisphere have been found to be much higher than those in the Southern Hemisphere (Mackerras et al., 1998). This is thought to be due to a larger land area in the Northern Hemisphere. The mean annual land to ocean flash ratio found by Christian et al. (2003) was 10:1. With the average global annual flash rate for the oceanic regions around 5 flashes/s compared to a continental $31 - 49$ flashes/s.

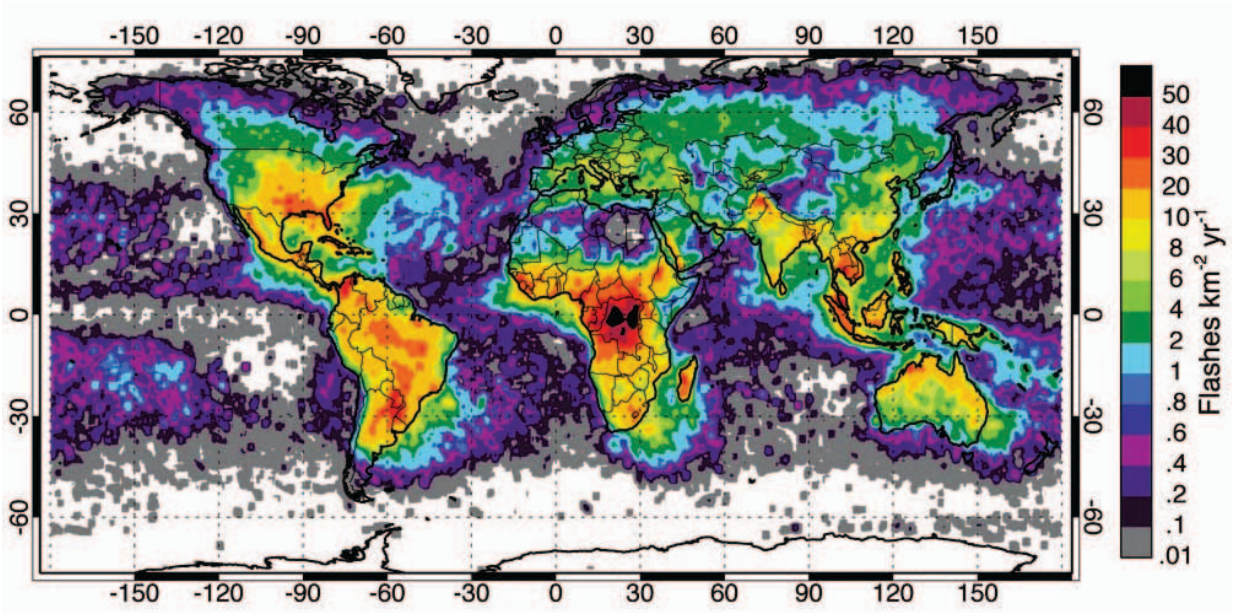

Figure 2.6: Christian et al. (2003), created a map of the Annual Distribution of Lightning Activity using OTD data.

A variation in latitude has also been found by comparing the tropics to the sub-tropics (Christian et al., 2003).

2.4 Whistlers

2.4.1 General Mechanism

When whistlers were observed on Earth for the first time, it was as whistling sounds of an unknown origin heard over long-distance telephone lines (Barkhausen, 1919). We now know that whistlers are an electromagnetic phenomena that originate in the magnetosphere. When a pulse is radiated by a lightning discharge it can travel great distances in the EIWG since it undergoes minimal attenuation. Due to the fact that the ionosphere is partially permeable to VLF waves, a pulse may move upward, penetrate the ionosphere and enter the magnetosphere.

Once in the magnetospheric plasma the waves propagate along the Earth's magnetic field lines in the whistler mode. If a wave is trapped in a field-aligned plasma density irregularity or duct, the direction of the wave normal will be more strongly confined to the magnetic field. Such a wave will travel back to the ionosphere and enter the EIWG in the conjugate region. A non-ducted wave will probably be reflected back into the magnetosphere. While travelling along the magnetic field lines the waves become dispersed, so as to arrive as whistling tones decreasing in frequency, thus the name "whistler". A typical frequency spectrum of a whistler is shown in Figure 2.6.

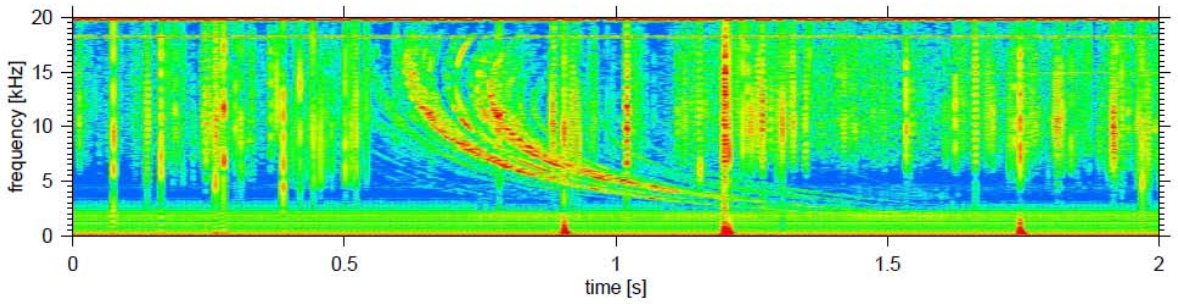

Figure 2.7: The frequency spectrum of a whistler recorded in Dunedin at 04:19:37 UTC on 14 December 2006, (Collier et al., 2010).

The quasi-longitudinal approximation to the whistler mode dispersion relation is

$$\mu^2 = \frac{\Pi^2}{\omega(\Omega\cos\theta - \omega)} \tag{2.6}$$

where μ is the refractive index, Ω and Π are, respectively, the plasma- and gyrofrequency and θ is the angle of propagation with respect to the static magnetic field. The derivation of (2.3) only takes the electron component of the plasma into account since ions do not contribute significantly due to their low gyrofrequency (Collier et al., 2009, 2010).

The condition $\Omega\cos\theta - \omega = 0$ defines a resonance cone outside of which propagation is evanescent. Since the refractive index of the neutral atmosphere ($\mu \sim 1$) is much less than that of the ionosphere ($\mu > 1$), waves entering from below are refracted into a transmission cone defined by wave normal directions which lie close to the vertical. The half-width of the transmission cone is determined by μ in the ionosphere, and is generally in the range 2°–3°. A whistler only becomes trapped in a duct or field-aligned plasma density irregularity when the refracted wave normal lies inside the trapping cone, which is symmetric around the magnetic field direction (Helliwell, 1965). At low latitudes there is almost no overlap between the transmission and trapping cones. This means that whistlers are mostly observed at middle to high geomagnetic latitudes.

Whistlers are known to have a nocturnal occurrence assumed to be due to an increase in transparency in the ionosphere (Helliwell, 1965). Fiser et al. (2010) found that, for the same range of source lightning currents, the average whistler amplitudes are three times higher at night than in the daytime.

2.4.2 Ionospheric Absorption

Estimates of VLF wave power entering the ionosphere have typically been calculated by combining a model of power entering from the EIWG with an estimate of ionospheric absorption. However due to the coupling of waveguide modes below the ionosphere into upward travelling power at higher altitudes is a difficult process that will need Full Wave Method (FWM) electromagnetic solutions. Unfortunately the FWM is computationally intensive and FWM estimates of transmitter power in the ionosphere are highly dependent on frequency, transmitter location, and details of the ionospheric plasma, for which no globally applicable models thus far exist (Starks et al., 2008).

This prompted Starks et al. (2008) to adopt a two-model approach, where they used a wave guide power model and an ionospheric absorption model of VLF transmissions. To model the ionospheric absorption, they applied the wave absorption curves that Helliwell (1965) generated for 2 kHz and 20 kHz for typical nighttime and daytime conditions. Helliwell (1965) created an averaged D-region model since the absorption contribution from the lower ionosphere is usually dominant. For the lower ionosphere, three electron-density models were used, representing normal daytime, normal nighttime, and polar blackout conditions (Helliwell, 1965).

In the upper ionosphere Starks et al. (2008) used only one electron density model, but this may be scaled to correspond to any value of foF2 by multiplying the density at each height by the factor $(\frac{foF2}{9})^2$. In order to apply them on a global basis, they were interpolated in frequency and extended to cover all local times done. The latter was done by creating a transition function between the day and night curves in order to copy the rapid production and recombination procesess in the ionosphere due to an increase in ionisation during the day.

By modeling wave propagation from VLF transmitters Starks et al. (2008) could estimate the wave normal angles and the field of whistler mode waves in the plasmasphere. The model combines a simulation of the fields in the EIWG, ionospheric absorption estimates and geomagnetic field and plasma density models, with full 3D raytracing. Their output was found to be consistent with that of previous models.

However a comparison of all the models to data from five satellites revealed that away from the magnetic equator, all of the models systematically overestimate the median field strength in the plasmasphere due to terrestrial VLF transmitters by 20 dB at night and at least 10 dB during the day (Starks et al., 2008). In addition wavefield estimates at $L < 1.5$ in the equatorial region appeared to be about 15 dB too low. Starks et al. (2008) thought discrepancies to be due to important physics in or below the ionosphere that was not being modeled. After adjusting the low-altitude field estimates downward by constant factors the model outputs were closer to those of satellite observations.

2.4.3 Wave Particle Interactions and Precipitation

Whistler waves are often studied as they are thought to be one of the most significant inner radiation belt loss mechanisms to wave-particle interactions (Kennel and Petschek, 1966; Abel and Thorne, 1998a,b). One of these interactions is called WEP. WEP arises from whistlers interacting with cyclotron resonant radiation belt electrons near the equatorial region (Tsurutani and Lakhina, 1997). Pitch angle scattering of energetic radiation belt electrons (Kennel and Petschek, 1966) by whistler mode waves drives some resonant electrons into the bounce loss cone, resulting in their precipitation into the atmosphere (Rycroft, 1973). The range of L-shells over which WEP is taken to occur ($1.9 \leq L \leq 3.5$) spans the radiation belts.

WEP leads to localized ionospheric modifications produced by secondary inonisation just below the D-region of the ionosphere. These are then observed as Trimpi perturbations in subionospheric VLF transmissions (Helliwell et al., 1973). A Trimpi perturbation begins with a fast (~ 1 s) change in the received amplitude and/or phase, followed by a slower relaxation (< 100 s) back to the original undisturbed signal. Trimpi perturbations are therefore caused by WEP from the Van Allen radiation belts that increase the electron concentration in the D-region and therefore the properties of the EIWG (Helliwell et al., 1973; Rycroft, 1973).

Trimpi perturbations observed at Faraday on the Antarctic Peninsula are known to be strongly associated with the high-current CG lightning occurring around 34° N, 76° W (Clilverd et al., 2002, 2004) close to the footprint of $L = 2$ flux tubes. From these observations, combined with the seasonality of lightning activity , Rodger et al. (2004b) argued that the representative rate of mean WEP activity affecting the ionosphere observed from Faraday at all times throughout the year would be $0.79\ ^{-1}$min.

Using the Faraday Trimpi rate Rodger and Clilverd (2002) considered the global distribution in WEP producing Trimpi, assuming that the WEP rate is directly linked to lightning activity around the base of the field line where the WEP occurs. In this manner lightning occurrence rates at Faraday L-shells were used to produce an expected longitudinally varying WEP producing Trimpi rate. Using the relationship between Faraday Trimpi and lightning in the expected source region (Rodger and Clilverd, 2002) a global WEP rate could be estimated by applying the relationship to the global flash rate densities. However WEP is very scarce at low L-shells Voss et al. (1998), despite the records of high lightning activity, due to increasingly unfavorable gyroresonance conditions (Friedel and Hughes, 1992). The L-variation in WEP rates were therefore estimated from satellite measurements (Voss et al., 1998). After taking this effect into account an estimation of the global distribution of WEP rates was done(Rodger et al., 2003; Rodger and McCormick, 2004; Rodger et al., 2004b).

From the expected global variation in the mean rate of Trimpis one can estimate the global variation in energy transferred from the Van Allen radiation belts into the atmosphere. Clilverd et al. (2004) did a comparison between the relative scattered

amplitudes of Trimpi with the return stroke peak current of the associated lightning discharges and found a direct relationship, with stronger lightning producing larger Trimpi due to higher energy fluxes. Clilverd et al. (2004) showed that the magnitude of the WEP mean energy precipitation flux is linked to the return stroke peak current of the lighting, I (in kA), by

$$F_{WEP}(I) = 2 \times 10^{-6}(|I|/147)^{2.3} \text{kg/ s}^3$$

On the basis of CG lightning current distributions, Rodger et al. (2005) determined the mean energy precipitation flux of typical WEP bursts. For WEP that produced observable Trimpi perturbations, mean precipitation energy fluxes were $2 - 3 \times 10^{-6}$ kg/s^3, for lightning with larger currents. Taking into account the full range of lightning currents, a typical WEP burst at $L \sim 2.3$ was thought to have a have a mean precipitation energy flux of 1×10^{-6} kg/s^3.

Chapter 3

Lightning Detection

The earliest lightning detection units were lightning flash counters (Rakov and Uman, 2003). These are instruments that register whether the filtered electric (or magnetic) field from lightning exceeds a fixed threshold. The output of the lightning flash counter is the number of lightning events and/or time sequence of lightning events at a given location. The first flash counter was called the "grozootmetchik" (Russian for thunderstorm detector), invented by Popov in 1895.

The annual number of thunderstorm days is the only parameter related to lightning incidence for which worldwide data is available extending over many decades (Rakov and Uman, 2003). In certain locations there is data available for more than a century. A thunderstorm day is defined as a local calender day during which thunder is heard at least once at a given location. The practical range of audibility of thunder is about 15 km where the maximum range of audibility is typically around 25 km (Rakov and Uman, 2003).

Lightning flash density studies started gaining momentum about a century ago with Brooks (1925), combining his climatological thunderstorm frequency studies with the flash rates observed by Mariott (1908). He went on to estimate a global flash rate of 100 flashes/s . Until recently his estimate has been accepted and widely used in various studies. Since the invention and application of satellites we now have what we assume to be a more accurate value of 44 ± 5 flashes/s occurring around the globe (Christian et al., 2003). Locating lightning with a good accuracy requires the use of multiple-instrument networks. Hence the development of lightning detection networks.

3.1 Types of Detectors

Lightning can be detected via satellite or ground receivers. Satellite detectors usually rely on optical techniques. Whereas there are two main methods of detecting lightning activity via the ground, via Magnetic Direction Finder (MDF) or Time of Arrival (TOA).

A MDF uses the electromagnetic signature of a lightning return stroke, which presents itself as a sudden increase in the voltage, to detect a CG lightning flash. The system uses two vertical orthogonal loop antennas and a horizontal flat plate antenna. The lightning stroke induces a current in the loops which allows the measured voltage to be used to determine the direction of arrival of the incident wave. The flate plate is used to resolve a 180° ambiguity that will arise in the calculations. Multiple direction finders are used to triangulate the data to determine the position of a lightning stroke which each send the data of a registered stroke to a position analyser Rakov and Uman (2003).

The TOA system is usually combined with the MDF and uses the TOA of the leading edge of a lightning pulse at each station. More specifically, the first few microseconds of a lightning pulse in the $0.3 - 3$ MHz frequency range are used. Only the first pulse is used to avoid the sky wave (a wave reflected off the ionosphere), which arrives slightly later. Since the lightning pulse is dominated by the CG return stroke it finds the location of the ground point of the lightning stroke to within a few meters. The high density of ground stations that are required for accurate detection makes the system unsuitable for coverage of large areas.

An adaption of the TOA method is the Time of Group Arrival (TOGA). By using the VLF band ($3 - 30$ kHz) which contains the highest PSD of lightning radiation, lightning can be easily detected and measured at several thousand kilometers. Propagation over such ranges in the EIWG disperses the initial sharp pulse of the lighting stroke into a wave train that lasts a millisecond or more. The dispersed waveform or sferic is processed at each station and the TOGA is determined from the progression of phase versus frequency, using the whole wave train (Dowden et al., 2002). For methods of radio location using only timing, at least four sites are needed for unambiguous location (Dowden et al., 2002).

3.2 Lightning Detection Systems

3.2.1 World Wide Lightning Location Network

WWLLN makes use of spherics in the VLF waveband to detect lightning strokes using the TOGA method(Rodger et al., 2006). Since VLF waves undergo stable propagation with low attenuation in the EIWG, this allows the WWLLN nodes to be spaced at distances of thousands of kilometers. The nodes each consist of an whip antenna, a Global Positioning System (GPS) receiver and an Internet connected processing computer.

WWLLN is mostly used to study high peak current lightning. It gives continuous observations in real time and has excellent time resolution, although the DE is only around 10% (Abarca et al., 2010). The number of nodes has increased from 25 in 2005 to more than 40 in 2010. Figure 3.1 is an example of WWLLN data in real time. The increasing number of nodes along with increasingly sophisticated signal processing

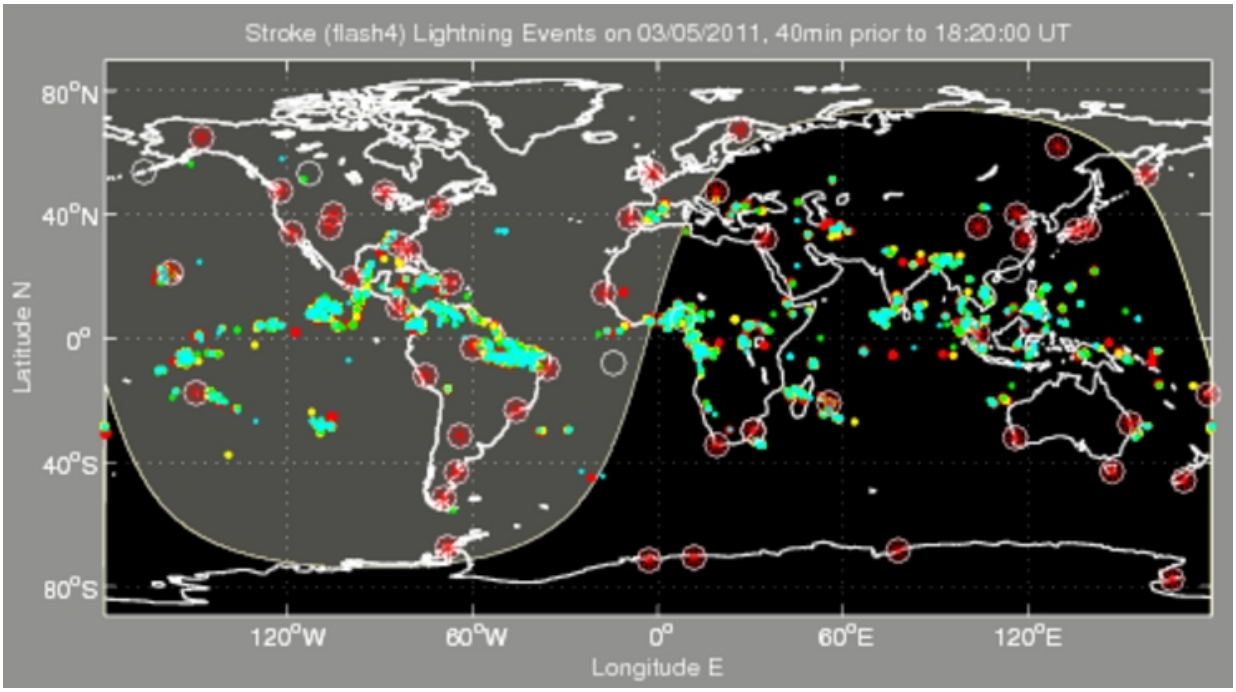

Figure 3.1: An example of WWLLN data which are available in real time (`http://webflash.ess.washington.edu/`). The red stars indicate the nodes.

algorithms has led to an increased DE over the years (Rodger et al., 2004a, 2005, 2006).

Figure 3.2 illustrates the location of lightning strokes as detected by the SANAE, Hermanus and Durban WWLLN stations as well as their combined detected strokes for the month of September. The locations of the various stations are indicated by a red triangle. The total lightning activity for that month is shown in Figure 3.3. This illustrates the power of using VLF techniques since a lower node density is needed than for other lightning detection networks that rely on different techniques. WWLLN clearly detects the general pattern in lightning distribution with peaks in the Americas, Africa and Martitime Continent Figure 3.3. However the stroke densities are very low. The overall DE of cloud-to-ground flashes increased from 3.88 % in 2006–2007 to 10.30 % in 2008-2009 (Abarca et al., 2010). The WWLLN CG DE has been found to be strongly dependent on peak current (Rodger et al., 2004a). The location accuracy (LA) is found to have a northward and westward bias as well as strong limitations in capturing the diurnal cycle (Abarca et al., 2010).

WWLLN has been found to have different capabilities in different parts of the world due to its variations in global network density. A reason for the discrepancies between WWLLN and regional datasets in previous evaluations has to do with the diversity of networks used as ground truth to evaluate the WWLLN. Regional networks have a high DE, but only for a limited area. It is important to note that the overall DE from the

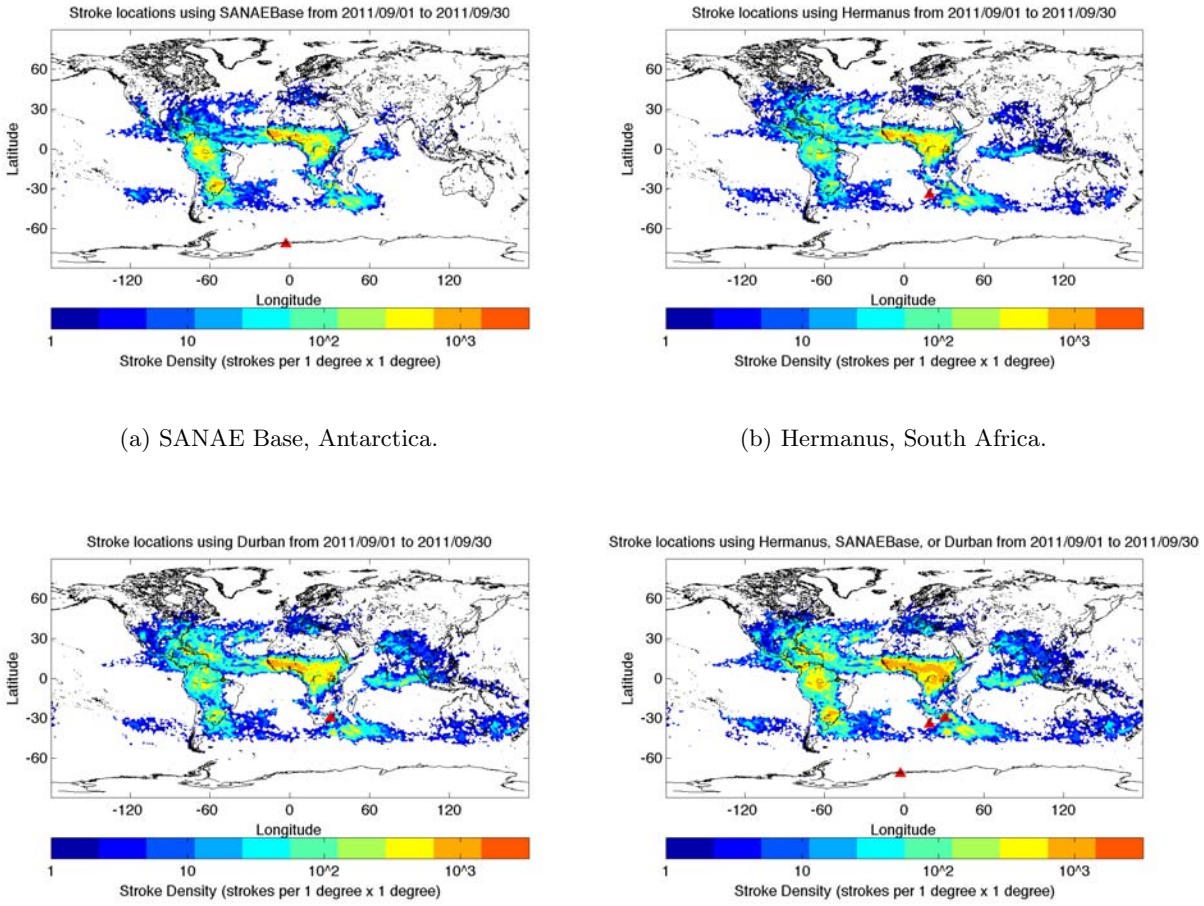

(a) SANAE Base, Antarctica.

(b) Hermanus, South Africa.

(c) Durban, South Africa.

(d) SANAE, Hermanus and Durban.

Figure 3.2: WWLLN stroke locations for September 2011. (a),(b),(c) represent strokes identified with contribution from each of the individual stations, whilst (d) illustrates their combined effect. (Figures by Holzworth, R. H., personal communication, 2011.)

networks that measure only CG flashes, rough estimates of the corresponding number of IC flashes are made. To do this, Rodger and McCormick (2004) and Rodger et al. (2005) assumed that there are 3.5 times more IC flashes than CG flashes following (Mackerras et al., 1998).

3.2.2 Lightning Imaging Sensor/Optical Transient Detector

The Optical Transient Detector (OTD) and Lightning Imaging Sensor (LIS) are satellite borne lightning detectors using narrow band infrared filters and image processing techniques to identify the time and location of lightning discharges. The optical technique

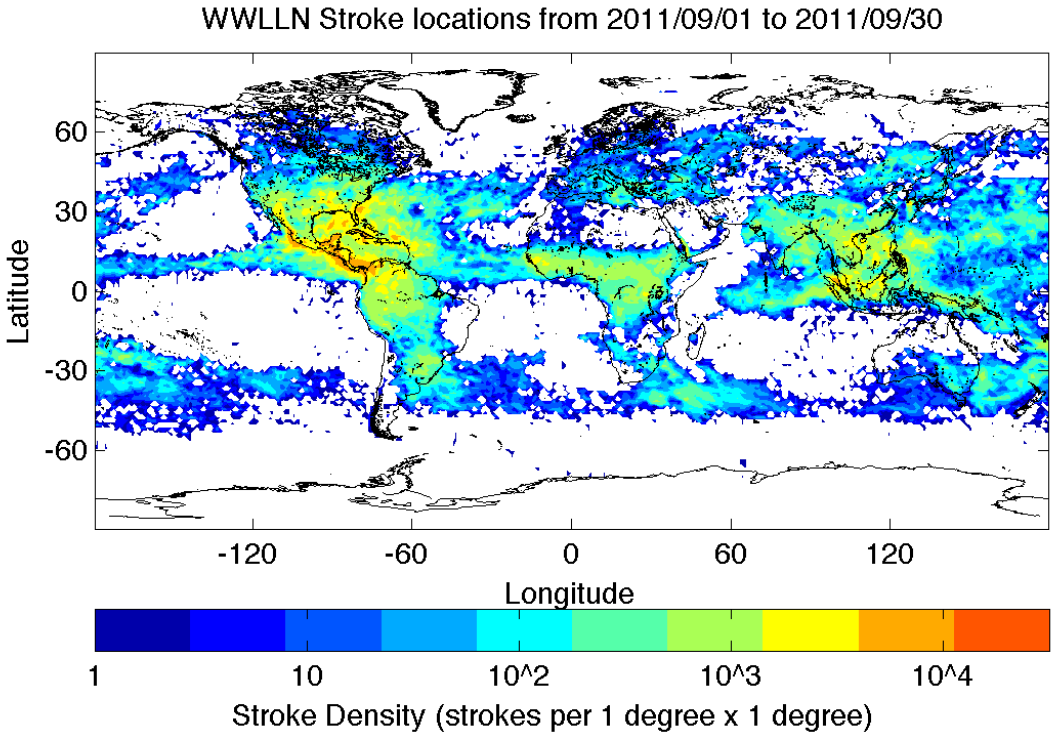

Figure 3.3: Total WWLLN stroke locations for September 2011. (Figure by Holzworth, R. E., personal communication, 2011.)

and location of the detectors allow for the detection of CG, IC and CC discharges. Of the many available formats of LIS and OTD data, two were used in this study. The 0.5° High Resolution Annual Climatology (HRAC) and High Resolution Monthly Climatology (HRMC) gridded LIS/OTD data. The OTD data runs over a 5 year period (May 1995 to April 2000) and LIS over 8 years (January 1998 to December 2005). The two data sets have been merged and intercalibrated to obtain consistency. The gridded products are generally preferable for a time series analysis since they incorporate the appropriate spatial and temporal variations.

The HRAC data have daily temporal resolution but each measurement represents a 110 day centered moving average, reducing the effect of diurnal aliasing. The smoothed rates are formed by independently averaging the aggregated flash counts and view times over the 110 day period and then dividing to obtain the rate. The variance of the data is further improved by averaging over a number of years to form an annualised climatology. The data are also spatially smoothed with a 2.5° moving average. The HRMC data also

have a daily temporal resolution, however the values are averaged over a month for every month of the year. Both these formats give flash rate densities in flashes/km^2/yr .

3.2.3 South African Weather Service

The South African Weather Service (SAWS) has a set of 19 sensors that have been running since November 2005. The sensors have been located as to ensure a DE of 90% and a LA of 500 m over South Africa. It has a high density of sensors in the Highveld and KwaZulu-Natal region since this is where most of the lightning activity happens during the Austral summer months.

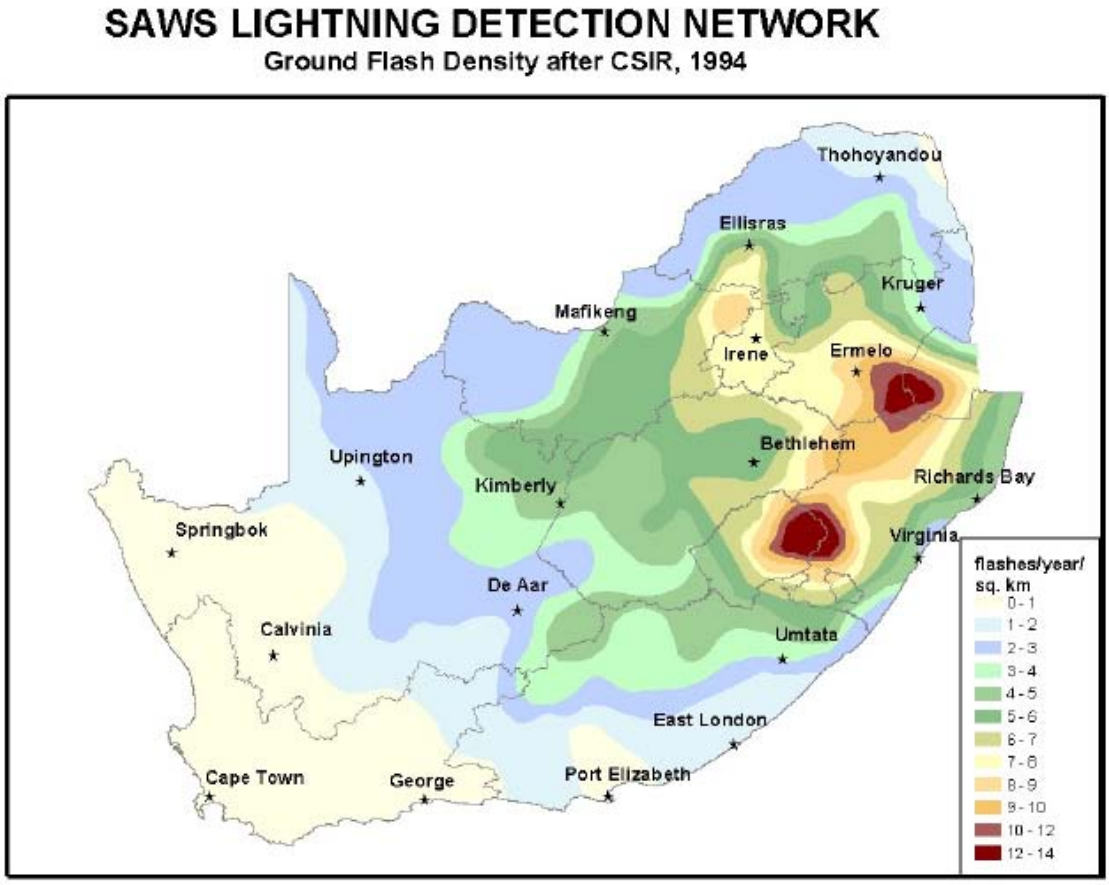

Figure 3.4: The locations of the SAWS sensors overlain over the flash-density maps (after CSIR, 1994).

The system determines the time and location of a lightning stroke in real-time by using MDF and TOA. Both these methods use the electromagnetic nature of lightning. The detecting antennas have a bandwidth that ranges from 1 kHz to 1 MHz. The SAWS

detection system makes use of ground-wave propagation which does not allow for very long propagation distances. This is the reason that the network has to have quite a few stations covering South Africa. It also means that the coverage of the system, whilst very good over the country, declines rapidly beyond the borders of the country. Figure 3.4 illustrates the locations of the SAWS lightning detectors overlain on the lightning flash rate density as detected by the system.

3.2.4 National Lightning Detection Network

The National Lightning Detection Network (NLDN) is a commercial system that has been giving complete lightning detection coverage of the continental United States since 1989 (Orville and Huffines, 2001). The system uses direction finders which are located over the United States with distances between two sensors ranging from less than 75 km to more than 525 km. This causes the DE of the network to vary. Since the NLDN uses the MDF and TOA method it requires $>$ 100 ground stations to cover the contiguous United States. The DE has been found to be at 80%–90% since 1995 (Cummins et al., 1998). Besides the time and position of a lightning stroke, the system also records the flash peak current and polarity. Strokes are grouped into flashes using a spatial and temporal clustering algorithm (Cummins et al., 1998). The primary objective of the system is to detect CG flashes, however some IC flashes are also included due to data retrieval and processing limitations. Figure 3.5 gives a representation of the NLDN detectors (Orville and Huffines, 2001).

3.2.5 LINET

The LINET lightning detection system was developed at the University of Munich and started operating in May 2006. The network consists of 100 sensors over 20 European countries as shown in Figure 3.6. LINET detects both CG and IC lightning discharges. The system also combines TOA and MDF techniques. The system reaches a location accuracy of down to 150 m. Data comparisons have revealed that LINET reports more lightning events than other lightning detection networks with comparable sensor geometry. This is probably because the LINET system analysis all incoming signals above the noise level, irrespective of their pulse shapes (Betz et al., 2008).

The system uses baselines of 200–250 km which gives very good coverage in the central parts of the network. In many border areas, with the inclusion of the Mediterranean Sea, the baselines are larger leading to a reduced DE, thus weak CG and IC signals are not located (Betz et al., 2008). LINET detects and locates both CG and IC strokes using the same procedure, but with a preference to IC strokes.

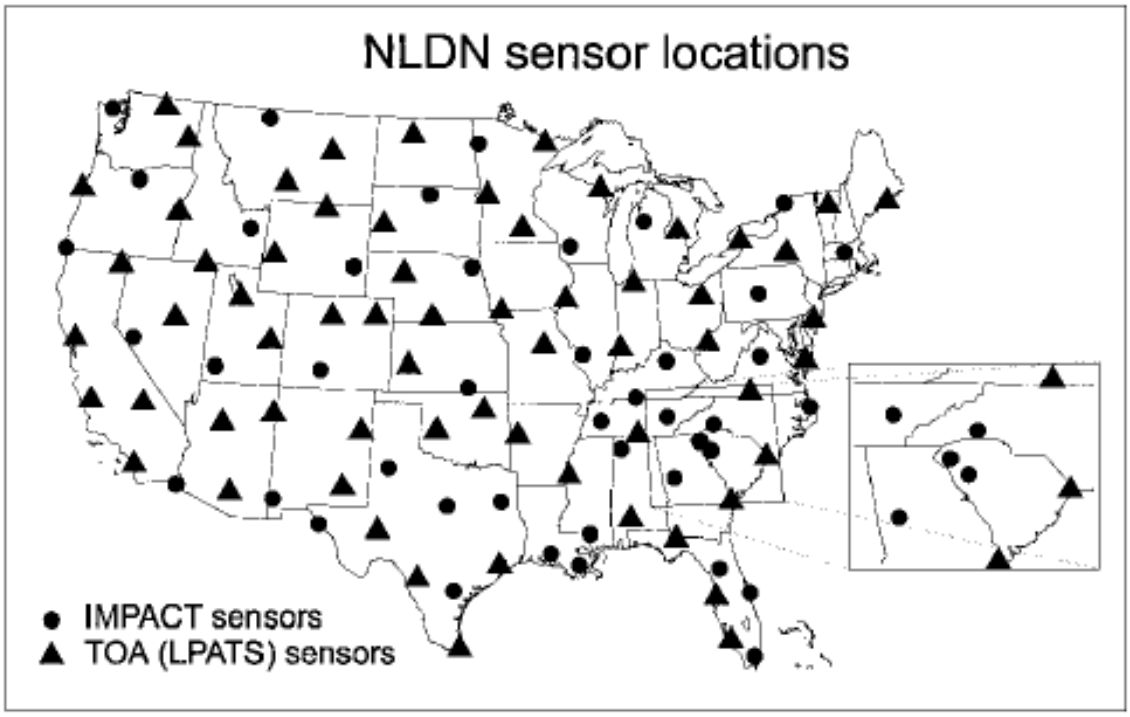

Figure 3.5: Lightning sensor locations for the NLDN. (Orville and Huffines, 2001). The locations of the IMPACT [DF and TOA method] sensors are plotted with a filled circle and the locations of the Lightning Positioning and Tracking System (LPATS) TOA sensors are plotted with a filled triangle.

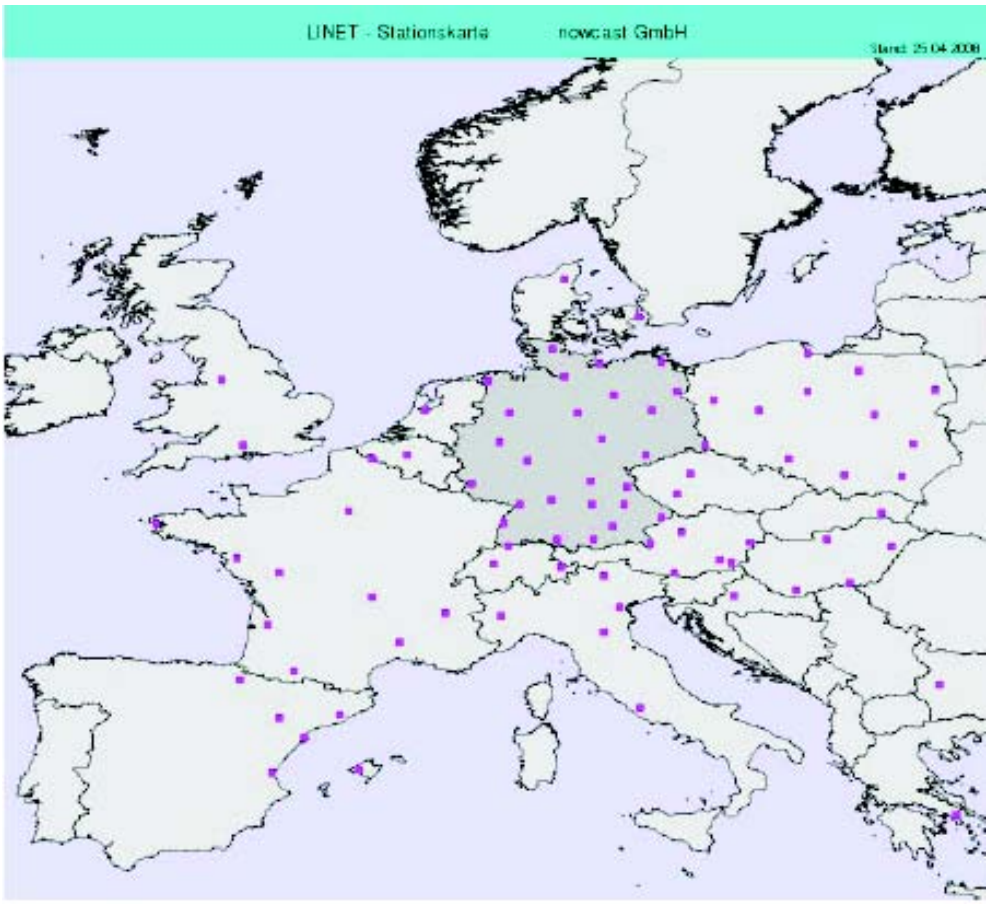

Figure 3.6: LINET sensor locations. (Betz et al., 2008)

Chapter 4

Results

4.1 Statistical Lightning Model

Lightning that leads to whistler waves is thought to be the primary cause of energetic electron losses in the Earth's radiation belts. Their temporal and spatial effect is not yet very well known. A statistical lightning model can be used to give an estimate of the VLF energy from lightning that leaks through the ionosphere and penetrates the magnetosphere. This energy distribution can then be compared to known values of energy losses from the radiation belts due to WEP, to see what fraction is caused by lightning.

The WWLLN data set has a excellent time resolution, but the DE of the data set is not ideal. This prompted the use of a second data set to normalise the WWLLN data. Studies by Christian et al. (2003) and Rodger and McCormick (2004) inspired the use of OTD lightning data for the current study. Christian et al. (2003) created a map of the annual geographic distribution of lightning activity using OTD data. Rodger et al. (2005) created a map of the annual geomagnetic distribution of lightning activity, by transforming the OTD data to geomagnetic coordinates.

LIS/OTD data was ultimately used as it has been averaged over a long time period of ten years, thus reducing the variance. The LIS/OTD data set also has a very good DE. The HRMC LIS/OTD data set was used since it gives monthly averages of the lightning flash rate densities in flashes/km^2/ day. Figure 4.1 shows the monthly averages that were used in the normalisation of seasonal WWLLN flash rate densities. It also gives a good illustration of the seasonal and latitudinal variation of lightning activity, with the maximum flash rate densities occuring in the Northern Hemisphere during their summer months.

WWLLN data for individual lightning strokes were projected onto a $0.5^\circ \times 0.5^\circ$ grid to get the data into the same format as the LIS/OTD data. High resolution maps of the seasonal flash rate densities, averaged over 5 years (2005-2009), derived from WWLLN data are shown in Figure 4.2. Although WWLLN gives a general indication of the global lightning activity, its observed densities were quite low as compared to Figure 4.1. With the lightning flash rate density maximum being around 3 flashes/km^2/yr. Multiplicity

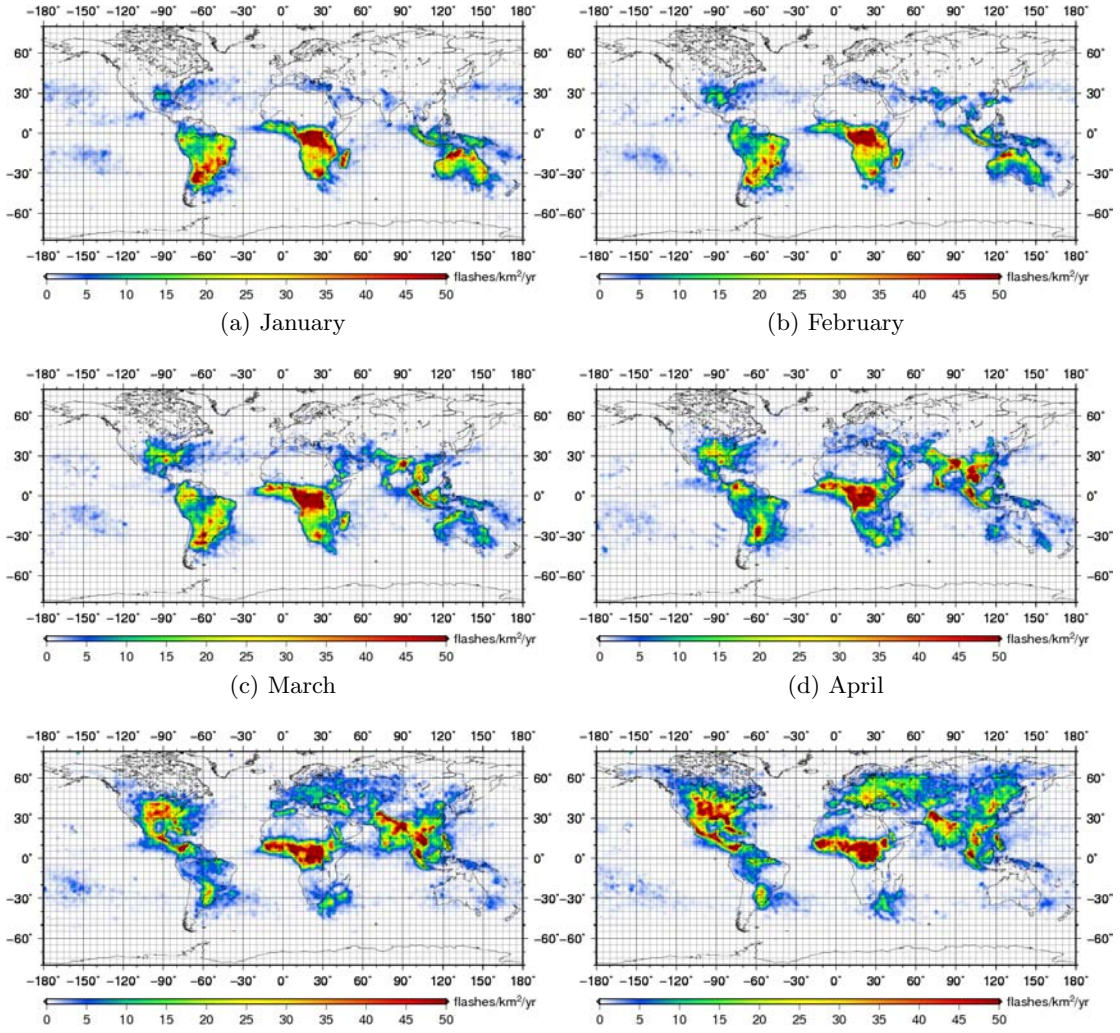

(a) January (b) February

(c) March (d) April

(e) May (f) June

Figure 4.1: Monthly LIS/OTD HRMC transformed to flashes /km^2/yr averaged over 1995-2005.

had to be incorporated since WWLLN measures strokes and not flashes by dividing with a factor of 3.5 strokes/flash. The WWLLN data were then corrected for undetected lightning flashes by scaling WWLLN to the the mean and standard deviation of LIS/OTD.

Thereafter normalisation factors, that vary on a longitude and latitude scale, were created to alter the DE of WWLLN. Figure 4.3 represents the factors which are the ratio of a LIS/OTD average to a WWLLN average for every $15° \times 15°$ grid block. A different set of factors were created for and applied to every season. From Figure 4.3 the normalisation factors were found to vary with the WWLLN node distribution. Where a higher normalisation factor often agreed with a lower number of WWLLN nodes in the same block. However this was not always found to be the case as there are no nodes over

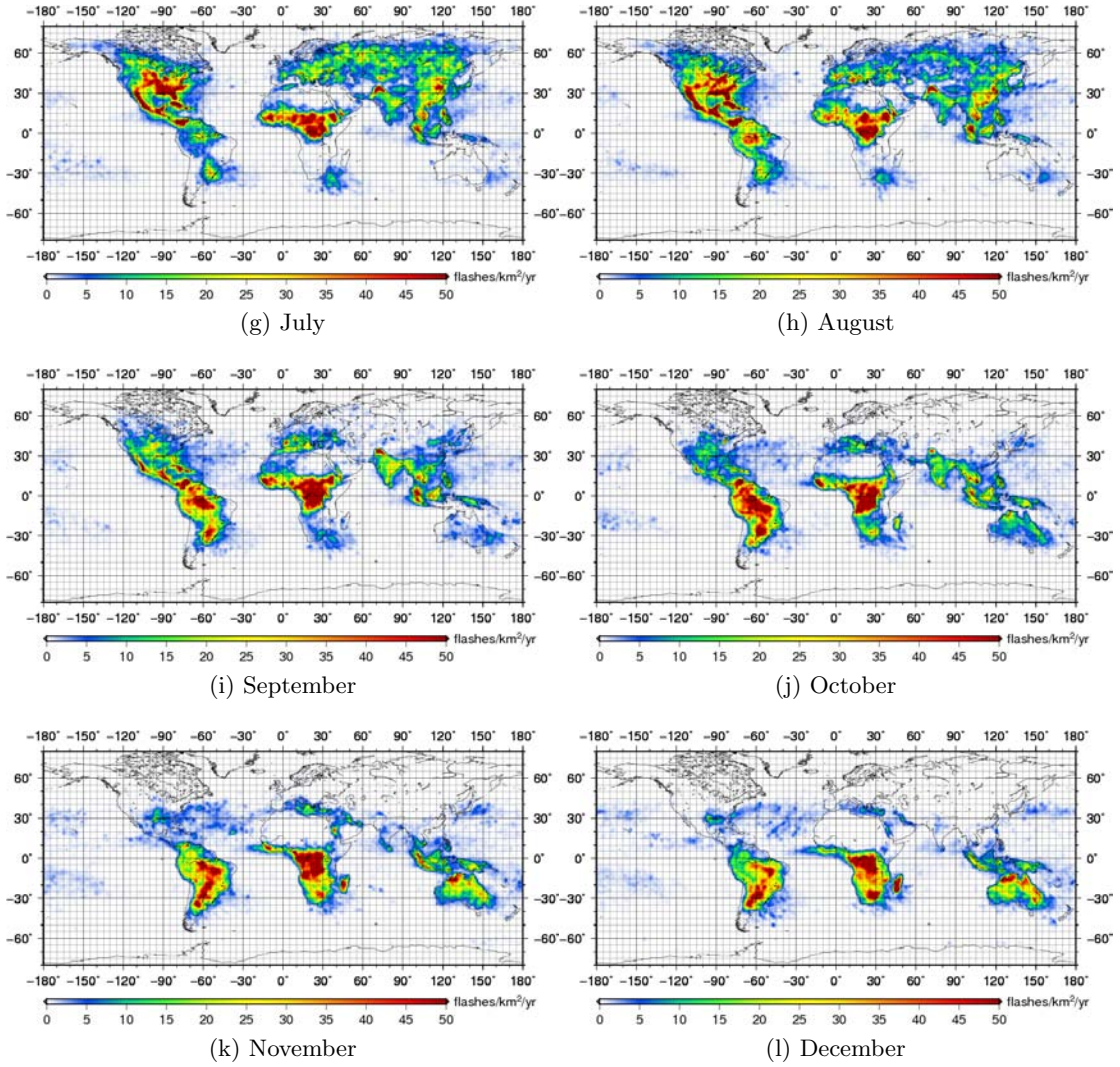

(g) July (h) August

(i) September (j) October

(k) November (l) December

Figure 4.1: (Continued) Monthly LIS/OTD HRMC flashes /km^2/yr averaged over 1995-2005.

the ocean, but the normalisation factors were low. This might be because the flash rate densities over the oceans are very low as illustrated in both Figures 4.1 and 4.2. Therefore the normalisation factors will be close to 1 as both WWLLN and the LISOTD flash rate densities are almost the same over the oceans. There was also an increase in the normalisation factor around a WWLLN node. This is probably due to the WWLLN lightning detection not being that good close to a node. Due to the low propagation-produced dispersion of a stroke a waveform might not have the expected dispersion waveform at the node (Rodger et al., 2006). This could then lead to the stroke being rejected.

Figure 4.4 represents the seasonal variation of the normalised WWLLN flash rate densities. L-values of 1.9, 2.7, 3.5 are added to the maps. These L-values are included

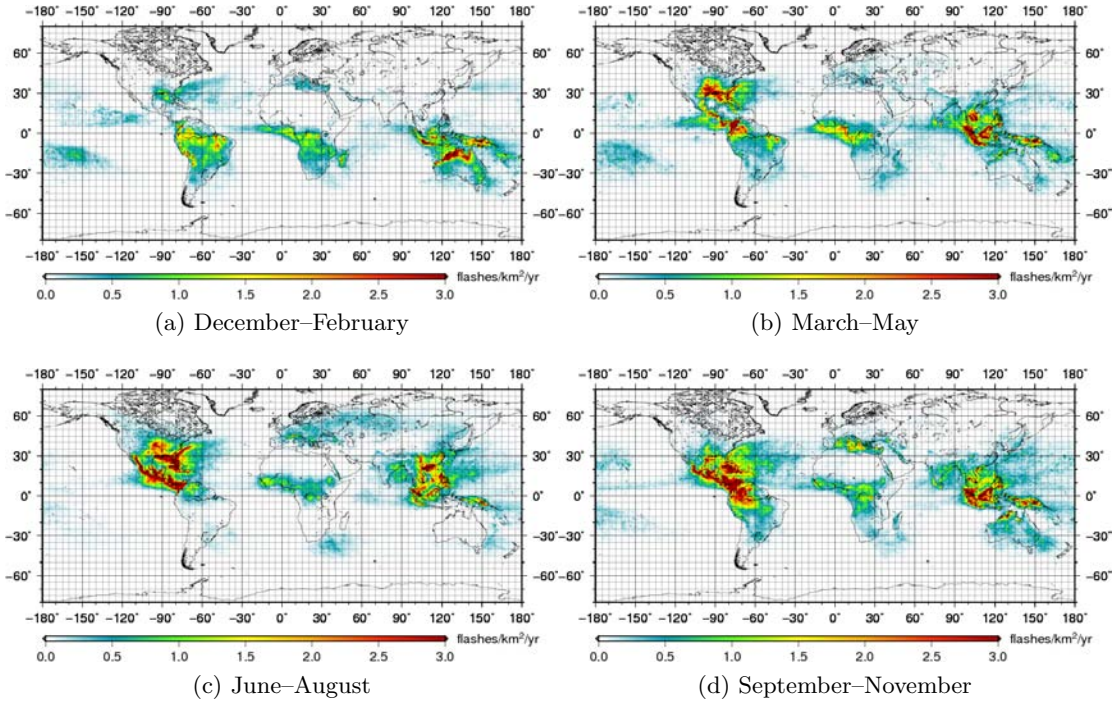

(a) December–February (b) March–May

(c) June–August (d) September–November

Figure 4.2: WWLLN before: flash rate densities in flashes/km^2/ yr, averaged over 2005–2009.

since they are in the range of L-shells over which WEP is most likely to occur. Since the distribution of lightning flash rate densities vary over the seasons, the energy radiated from lightning being transported into the radiation belts will also vary. From Figure 4.4 it is clear that North America is the greatest contributer to lightning activity around the $L \approx 2$ region, with the Southern Hemisphere making a very small contribution. However, before any energy distributions from the normalised WWLLN could be done and compared to the WEP rates, a validation of the normalised WWLLN flash rate densities had to be done first.

4.2 Comparison with regional data sets

A statistical χ^2 test is done between WWLLN and the regional data sets in order to do a validation of the normalised WWLLN data. The WWLLN flash rate densities are transformed to a $1^\circ \times 1^\circ$ grid to view the lightning flash densities on a scale that is slightly larger, as to get the bigger picture when doing a comparison over larger regions such as the United States and Europe. The flash rate densities are in units of flashes /km^2/day as the comparison of WWLLN to the regional data sets is done on a daily scale. Therefore the HRAC LIS/OTD format was used as it gives daily lightning flash rate densities for every day of the year.

The main purposes of a statistical test is to determine how well the observed data agrees with the expected data. The null hypothesis (H_0) is set up to be refuted in order to

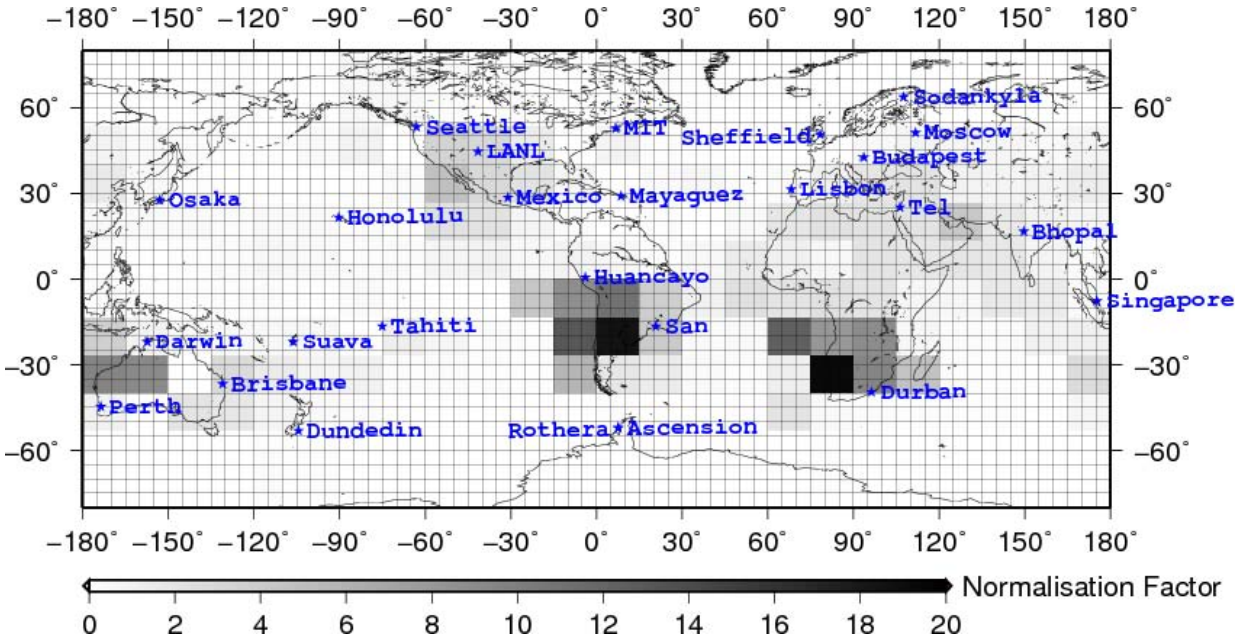

Figure 4.3: An example of normalisation factors for WWLLN in geomagnetic coordinates.

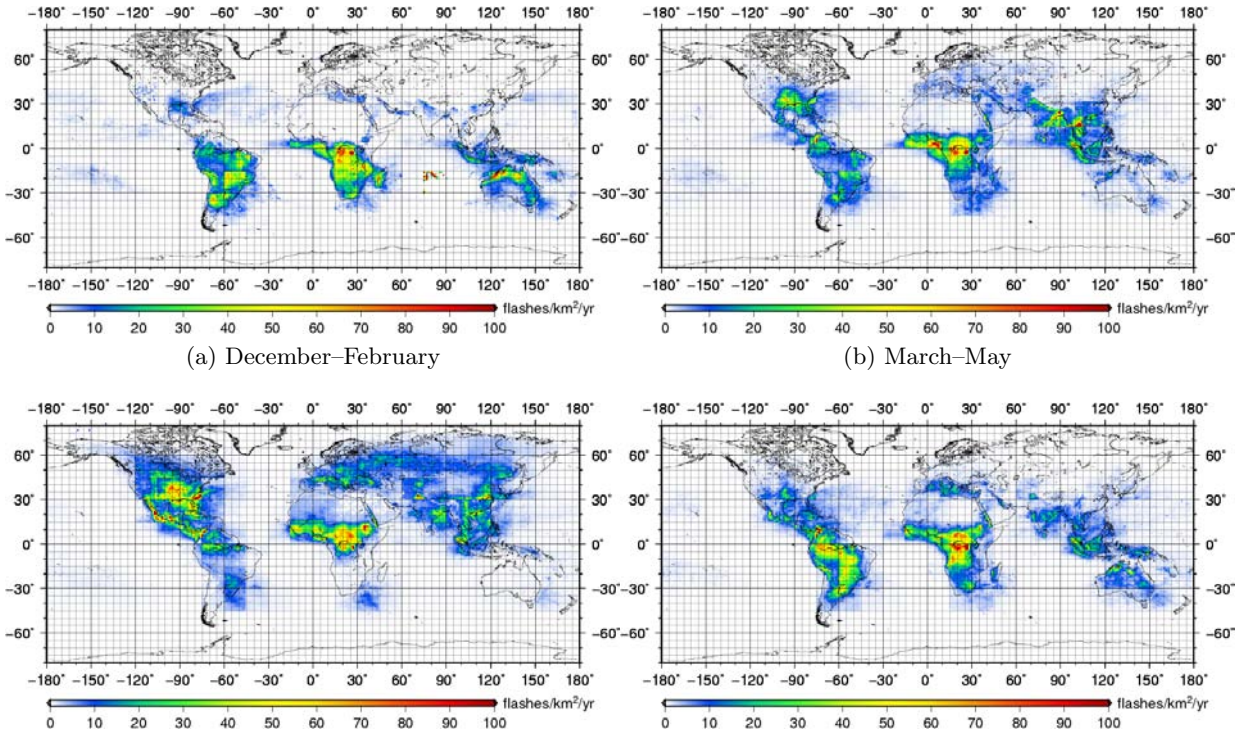

(a) December–February

(b) March–May

(c) June–August

(d) September–November

Figure 4.4: The seasonal variation of the lightning flash rate density at the bottom of the ionosphere in geographic coordinates, averaged over 2005–2009.

support an alternative hypothesis (H_α). In general the null hypothesis implies that there is no difference between the observed and the expected data. The null hypothesis is rejected if the p-value of the χ^2 test is less than a chosen significance level, where the p-value is the probablity that a given result could have been obtained by chance.

4.2.1 Comparison to SAWS data

To validate the normalised WWLLN data for the Southern Hemisphere, it was compared to data from the SAWS lightning detection system. A few days during February 2007 were selected, since this month falls in the season when South Africa has its highest lightning activity. Most of the lightning occurs over KwaZulu-Natal and the Highveld region during the summer months. Since South Africa is not well-confined within a certain latitude and longitude block, the data were reduced to only consider values within the borders of South Africa. This allowed for a better comparision of the normalised WWLLN and SAWS data sets. Since SAWS measures strokes, a multiplicity of 2.5 as found by Gill (2008) was assumed to convert the SAWS data from stroke- to flash rate densities.

Both of the lightning detection systems identified strokes that occured mostly over the east-coast of South Africa for 4 January 2007 in Figure 4.5 (a) and (b). The distribution of strokes then moved westward towards the KwaZulu-Natal and Highveld region as the month continued, Figures 4.6 (a) and (b) to Figure 4.8 (a) and (b). However WWLLN initially seemed to detect a lot less lightning strokes than SAWS does. This might be contributed to the low node density of WWLLN over South Africa which would give very low stroke rate densities over South Africa as shown in Figures 4.5 (c) and (d) to Figure 4.8 (c) and (d). The scale of the WWLLN stroke rate densities are less than a $\frac{1}{4}$ of the LIS/OTD stroke rate densities.

After the normalisation the WWLLN data was found to agree quite well with the SAWS data inside the South African border. Both had flash rate densities that were on the same scale. This is confirmed by the χ-square test results in Table 4.1. The first column gives the date of comparison, the second column gives the χ-square test value and the third column gives the degrees of freedom = n - 1, where n is the number of values used in the comparison. Lastly the fourth column is the p-value. All the p-values are = 1 which would mean that there is a 100% probablity that the two datasets have the same distribution. However outside the South African border over the oceans, WWLLN detects more lightning which SAWS, due to its lack of sensors over the ocean, does not.

4.2.2 Comparison to NLDN data

The variation of the normalised WWLLN data on a seasonal scale was studied by taking one day out of each 2009 season and comparing the flash rate densities to those of the NLDN. This gave a representation of the normalised WWLLN flash rate densities over the United States. The NLDN comparison was done for 26° to 49° N and −124° to 66° E.

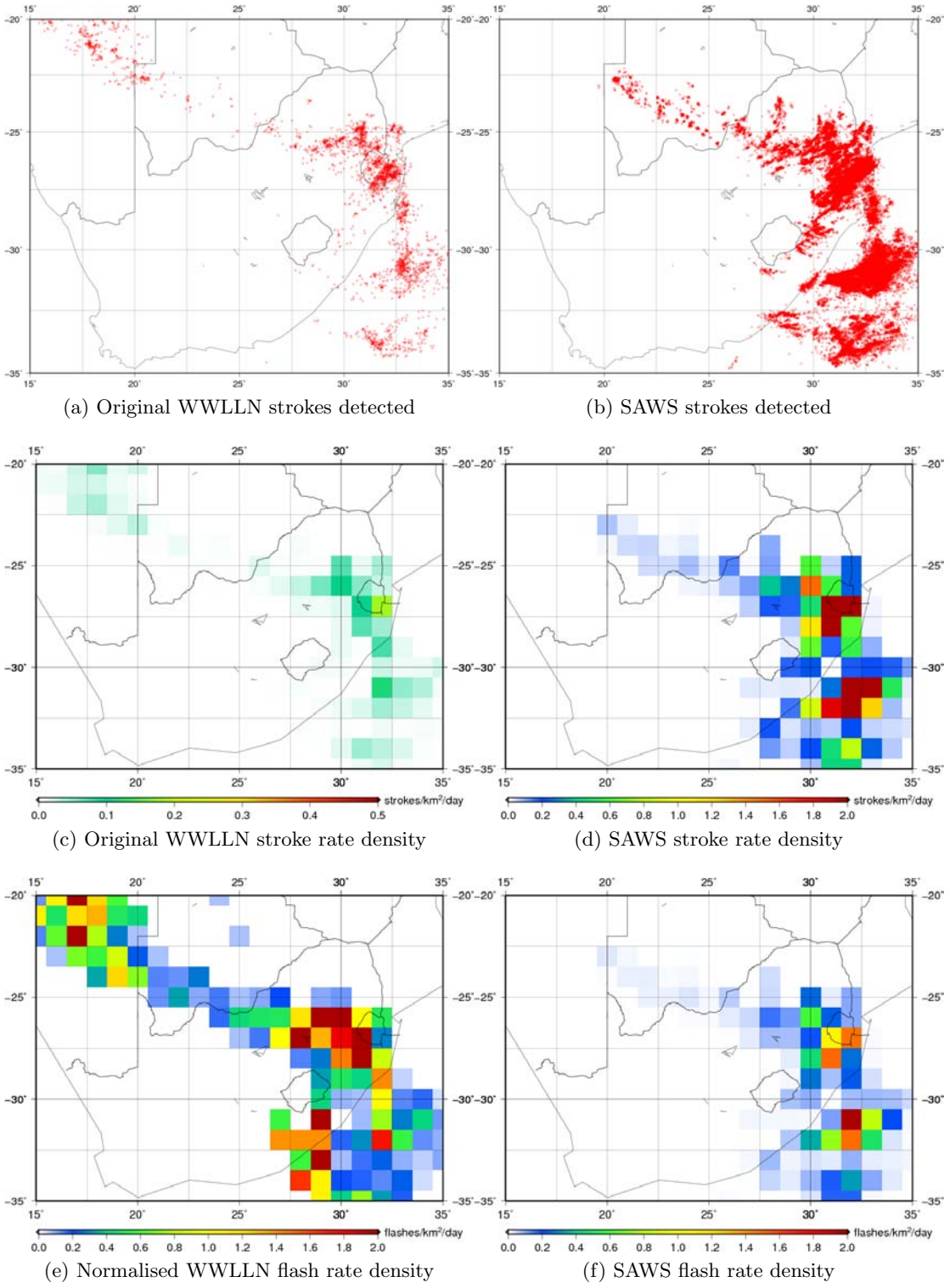

(a) Original WWLLN strokes detected

(b) SAWS strokes detected

(c) Original WWLLN stroke rate density

(d) SAWS stroke rate density

(e) Normalised WWLLN flash rate density

(f) SAWS flash rate density

Figure 4.5: WWLLN and SAWS comparison for 4 February 2007 with (b), (c) in strokes /km^2/day and (d) and (e) in flashes /km^2/day .

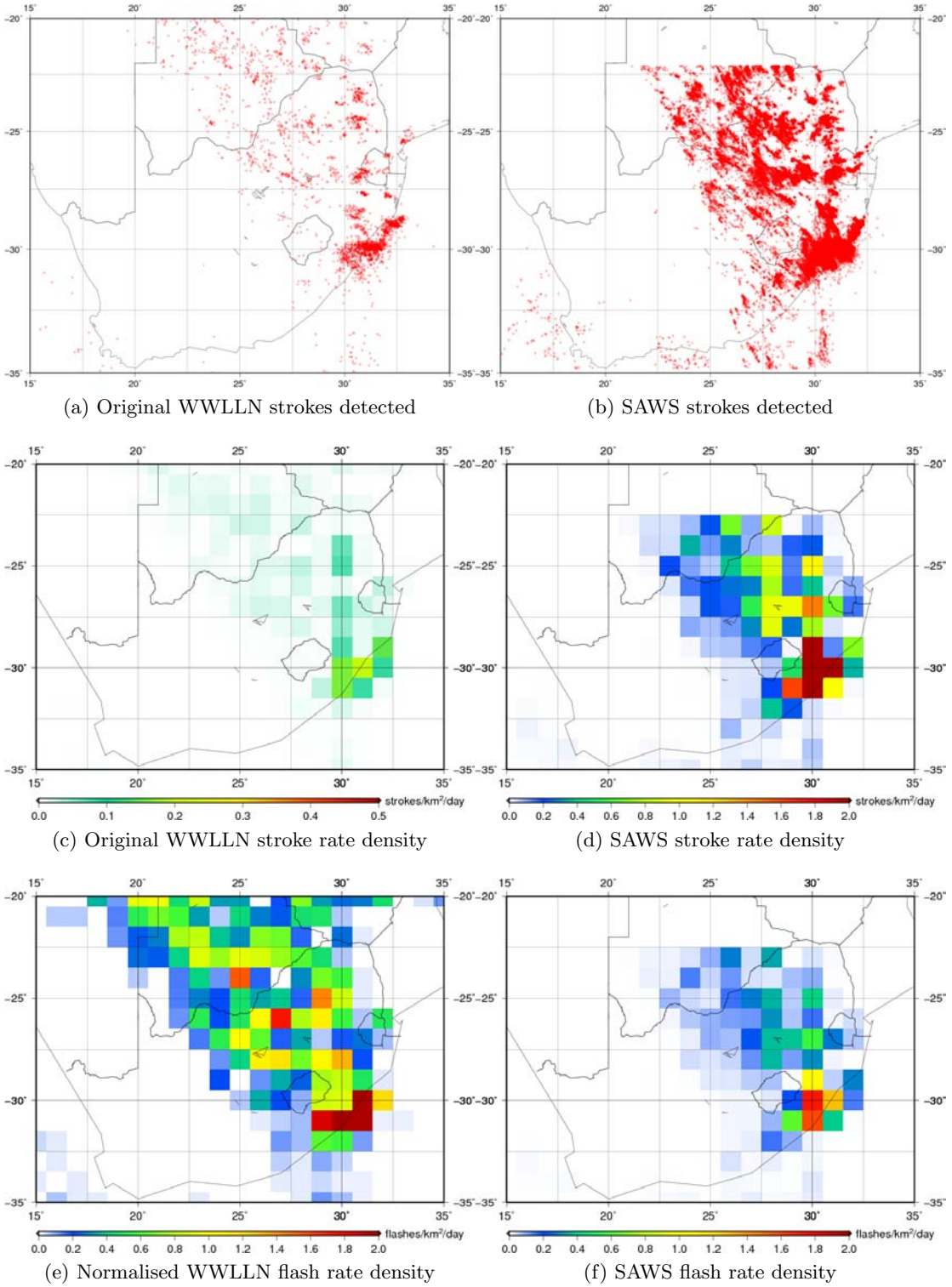

(a) Original WWLLN strokes detected

(b) SAWS strokes detected

(c) Original WWLLN stroke rate density

(d) SAWS stroke rate density

(e) Normalised WWLLN flash rate density

(f) SAWS flash rate density

Figure 4.6: WWLLN and SAWS comparison for 10 February 2007.

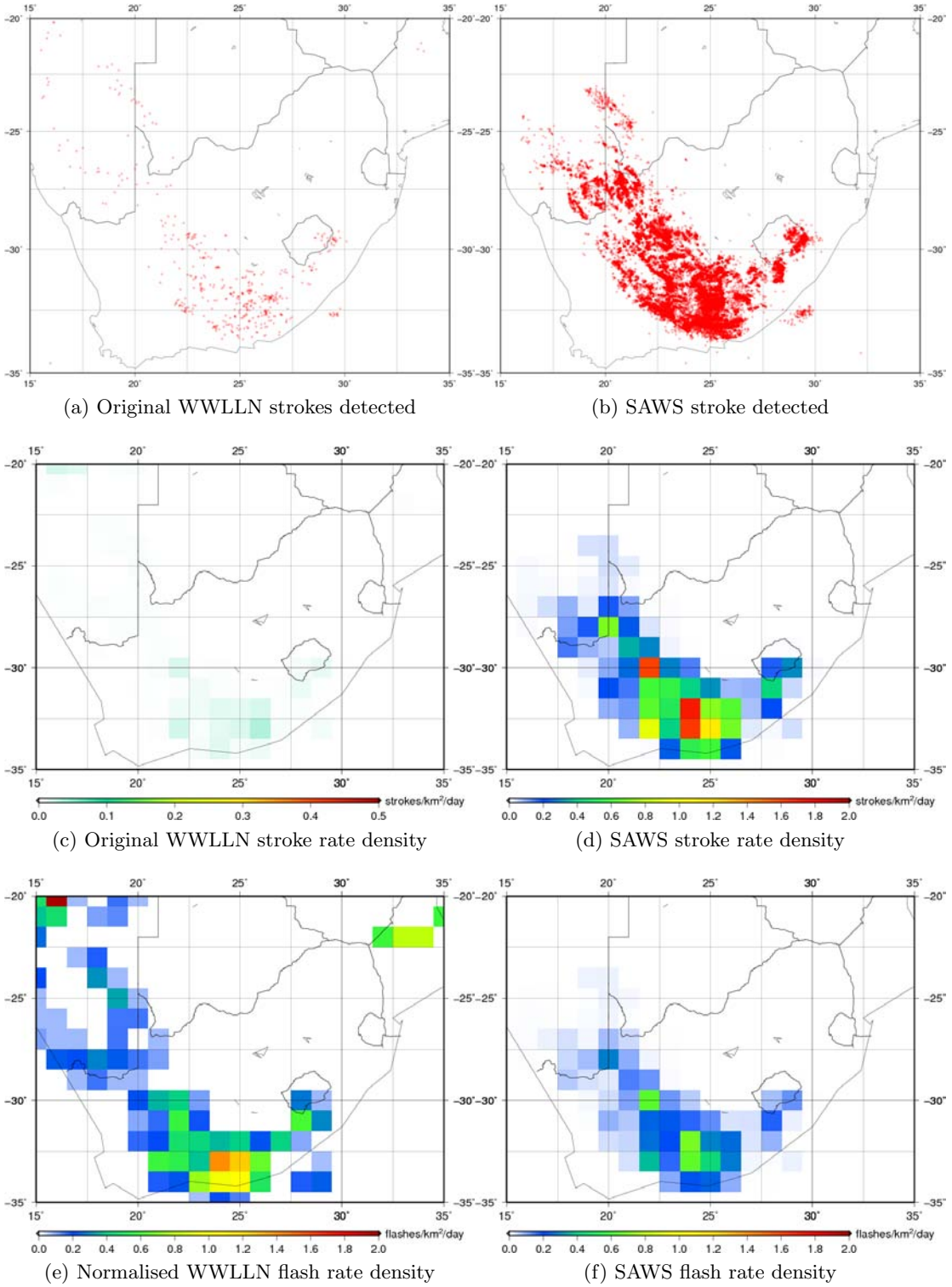

(a) Original WWLLN strokes detected

(b) SAWS stroke detected

(c) Original WWLLN stroke rate density

(d) SAWS stroke rate density

(e) Normalised WWLLN flash rate density

(f) SAWS flash rate density

Figure 4.7: WWLLN and SAWS comparison for 27 February 2007.

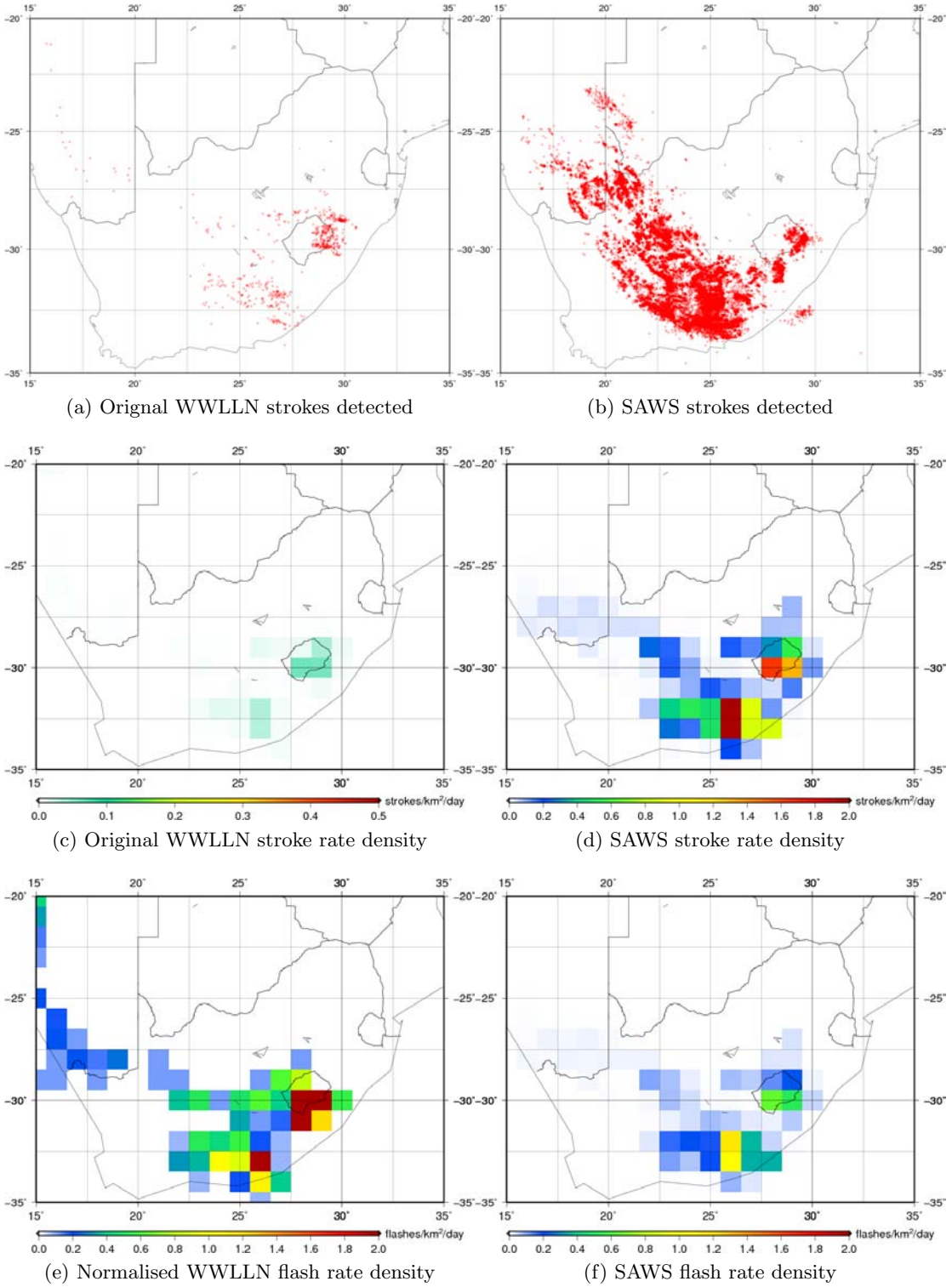

(a) Orignal WWLLN strokes detected

(b) SAWS strokes detected

(c) Original WWLLN stroke rate density

(d) SAWS stroke rate density

(e) Normalised WWLLN flash rate density

(f) SAWS flash rate density

Figure 4.8: WWLLN and SAWS comparison for 28 February 2007.

Table 4.1: SAWS chi-square test.

Dataset	Chi-square	Degrees of Freedom (df)	P-value
20070204	23.9907	69	1
20070210	14.8031	97	1
20070227	3.9593	55	1
20070228	9.7084	41	1

The four days in 2009 were selected by identifying the day with highest stroke distribution in each season from WWLLN. Initially the comparison of the original WWLLN to NLDN number of strokes detected seemed very similar for all four of the days, panels (a) and (b) of Figures 4.9 to 4.12, representing the different seasons. This can be better illustrated in the stroke rate density maps in panels (c) and (d) of Figures 4.9 to 4.12. One reason for this might be the relatively high node density of WWLLN in the United States, as compared to over Africa for example. Another reason might be due to the inner workings of the two lightning detection systems. WWLLN DE is biased toward stronger discharges and the NLDN assigns the peak current of the first stroke to the flash, which is often the strongest (Biagi et al., 2007). Therefore very often the identified coincident flashes are also expected to be coincident strokes (Abarca et al., 2010).

After the normalisation WWLLN flash rate densities were found to agree with those of NLDN as also confirmed by the χ-square test results Table 4.2. The p-values in the test were all equal to 1 which means that there is a 100% probablity that the two distributions are the same. The best comparisons were in the Northern Hemisphere winter (Figure 4.9) and spring (Figure 4.10) and less so in the summer(Figure 4.11) and autumn (Figure 4.12) months when the WWLLN flash rate densities seemed to be bit higher in some regions. A possible reason for this might be due a multiplicity of 3.5 being used to convert the NLDN data from strokes to flashes instead of around 2–2.5 as found by Orville and Huffines (2001). Another reason might be due to the application of the normalisation factors, were certain flash rate densities might have been on the edge of falling into one normalisation factor block, but were assigned to fall another.

Table 4.2: NLDN chi-square test.

Dataset	Chi-square	Degrees of Freedom (df)	P-value
20090227	4.0279	144	1
20090427	33.9648	227	1
20090611	72.8867	44	1
20091029	16.0131	137	1

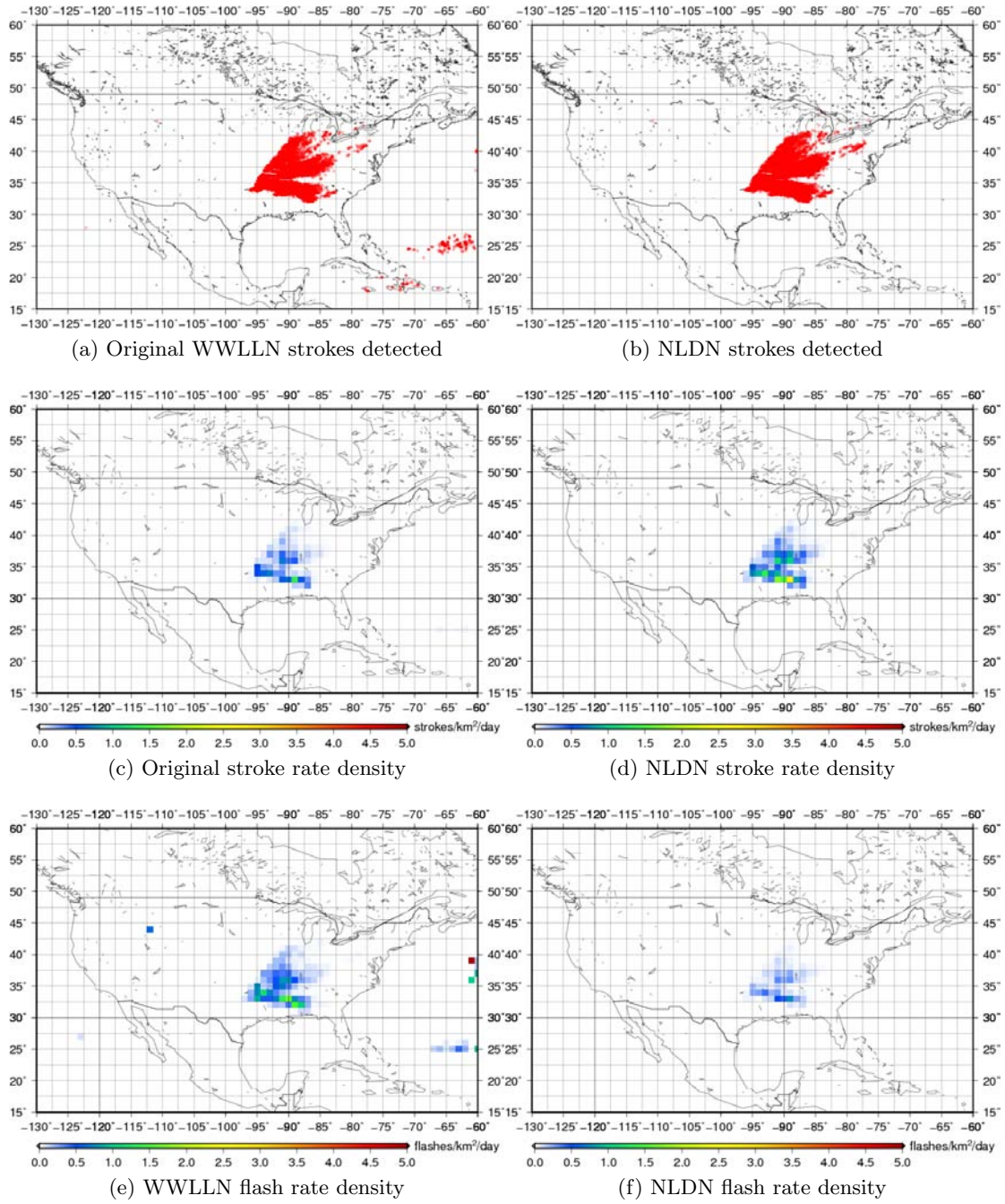

(a) Original WWLLN strokes detected

(b) NLDN strokes detected

(c) Original stroke rate density

(d) NLDN stroke rate density

(e) WWLLN flash rate density

(f) NLDN flash rate density

Figure 4.9: WWLLN and SAWS comparison for 27 February 2009.

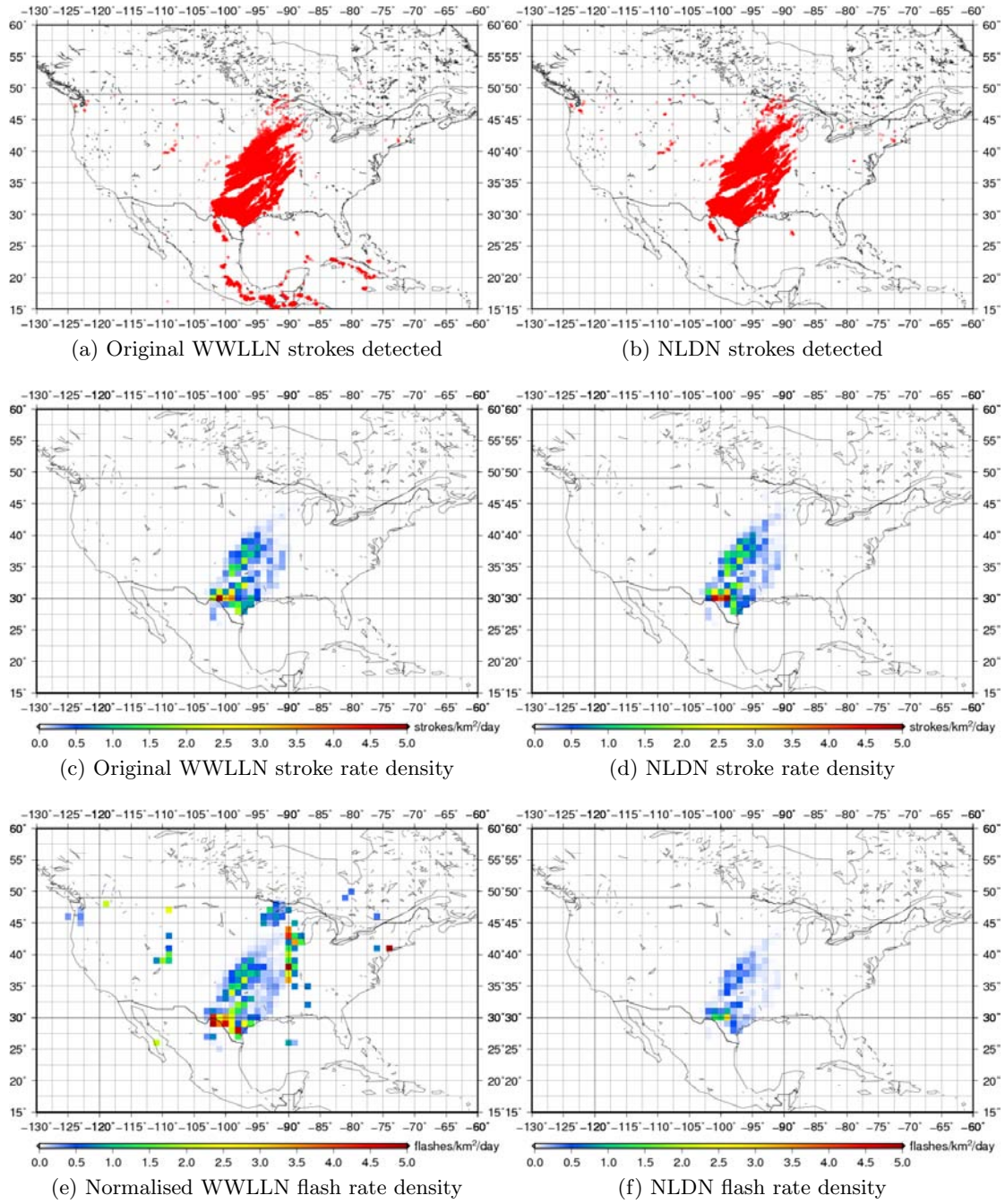

(a) Original WWLLN strokes detected

(b) NLDN strokes detected

(c) Original WWLLN stroke rate density

(d) NLDN stroke rate density

(e) Normalised WWLLN flash rate density

(f) NLDN flash rate density

Figure 4.10: WWLLN and NLDN comparison for 27 April 2009.

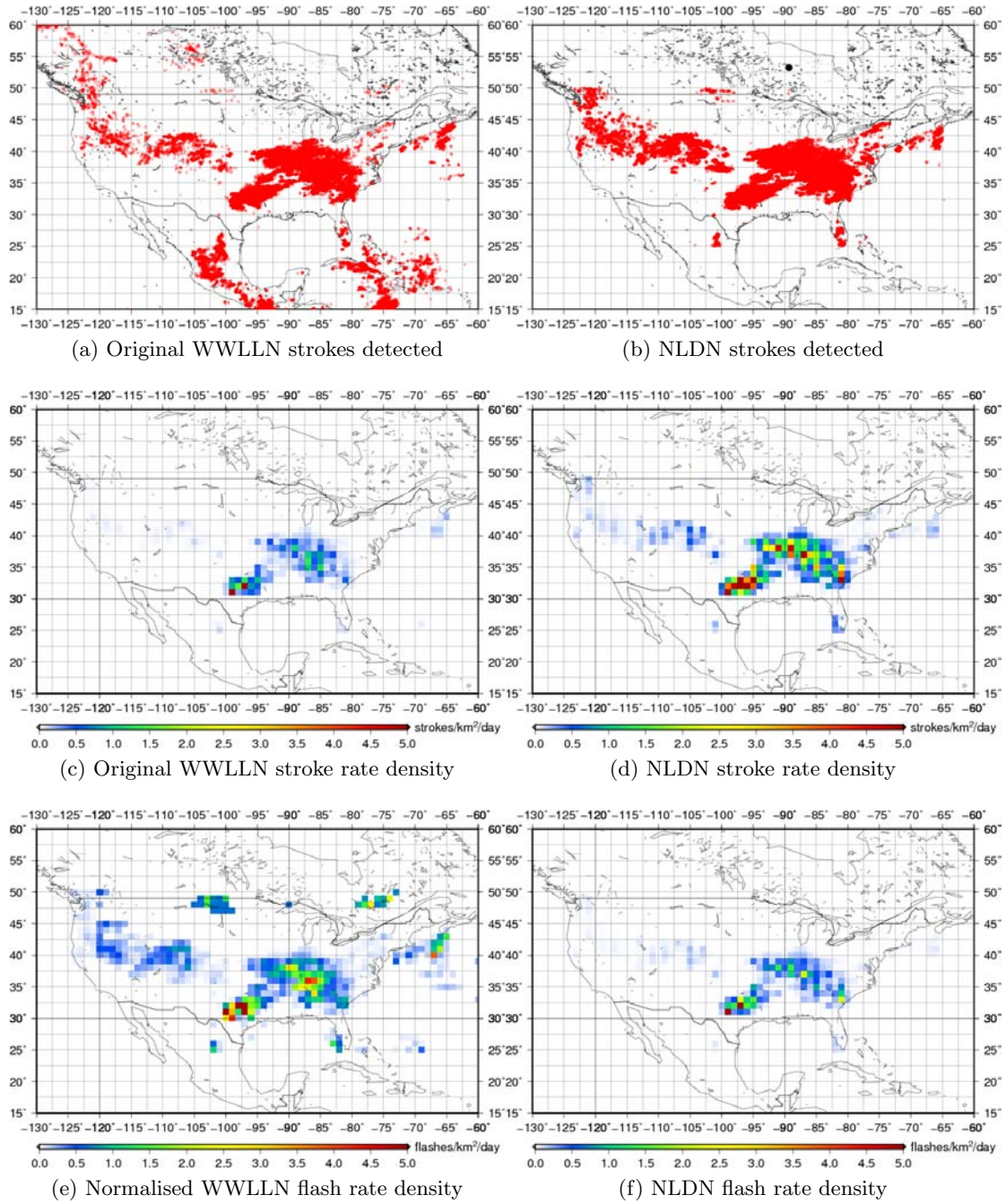

(a) Original WWLLN strokes detected

(b) NLDN strokes detected

(c) Original WWLLN stroke rate density

(d) NLDN stroke rate density

(e) Normalised WWLLN flash rate density

(f) NLDN flash rate density

Figure 4.11: WWLLN and NLDN comparison for 11 June 2009.

4.2.3 Comparison to LINET data

The data used to do the validation of WWLLN to that of a European lightning detection network, LINET runs from 2007–2009. A day is chosen for each year in the Northern Hemisphere summer, when the continent has its highest lightning activity. The LINET comparison was done for 36° to 64° N and −9° to 24° E. Using LINET data the variation of the normalised WWLLN over three years was studied.

Initially WWLLN detected a lot less strokes than LINET does between −5° to 40° longitude. Stroke rate densities show just how low the original WWLLN values are in this region in Figures 4.13 to 4.15. The stroke rate densities of WWLLN are a $\frac{1}{4}$ of those of LINET. After the normalisation the flash rate densities from WWLLN were much more agreeable with those from LINET. For July 2007, shown in Figure 4.13 the LINET flash rate densities were slightly lower than those of the normalised WWLLN. This is probably due to the system still only having run for a year in 2007, which might have meant that there were not as many lightning sensors as there are now.

For July 2008 and July 2009 , represented in Figure 4.14 and 4.15 respectively, LINET had flash rate densities that were found to agree very well with those of WWLLN. Most of the sensors from LINET (60 +) are in Germany and the rest are mostly spread over Western-Europe. Therefore it has a high DE in this region. The normalised WWLLN flash rate densities represent lightnig activity in the eastern part of Europe, which is not covered very well by LINET. It seems that the normalised WWLLN flash densities show an improvement over all three of the years which is probably due to the DE of LINET improving over the last three years with and increase in sensors. Table 4.3 gives p-values of 1 for all three days which would mean that there is a 100% probablity that the normalised WWLLN and LINET flash rate densities have the same distribution.

Table 4.3: LINET chi-square test.

Dataset	**Chi-square**	**Degrees of Freedom (df)**	**P-value**
20070702	32.8044	305	1
20070722	25.4131	198	1
20080702	61.121	336	1
20080714	57.7586	233	1
20090716	49.9279	306	1
20090718	82.2365	220	1

4.3 VLF energy from Lightning incident on the Ionosphere

After Lauben et al. (2001) a wave illumination profile along the lower boundary (assumed to be at a 100 km) of the ionosphere is assumed for a single vertical CG lightning stroke

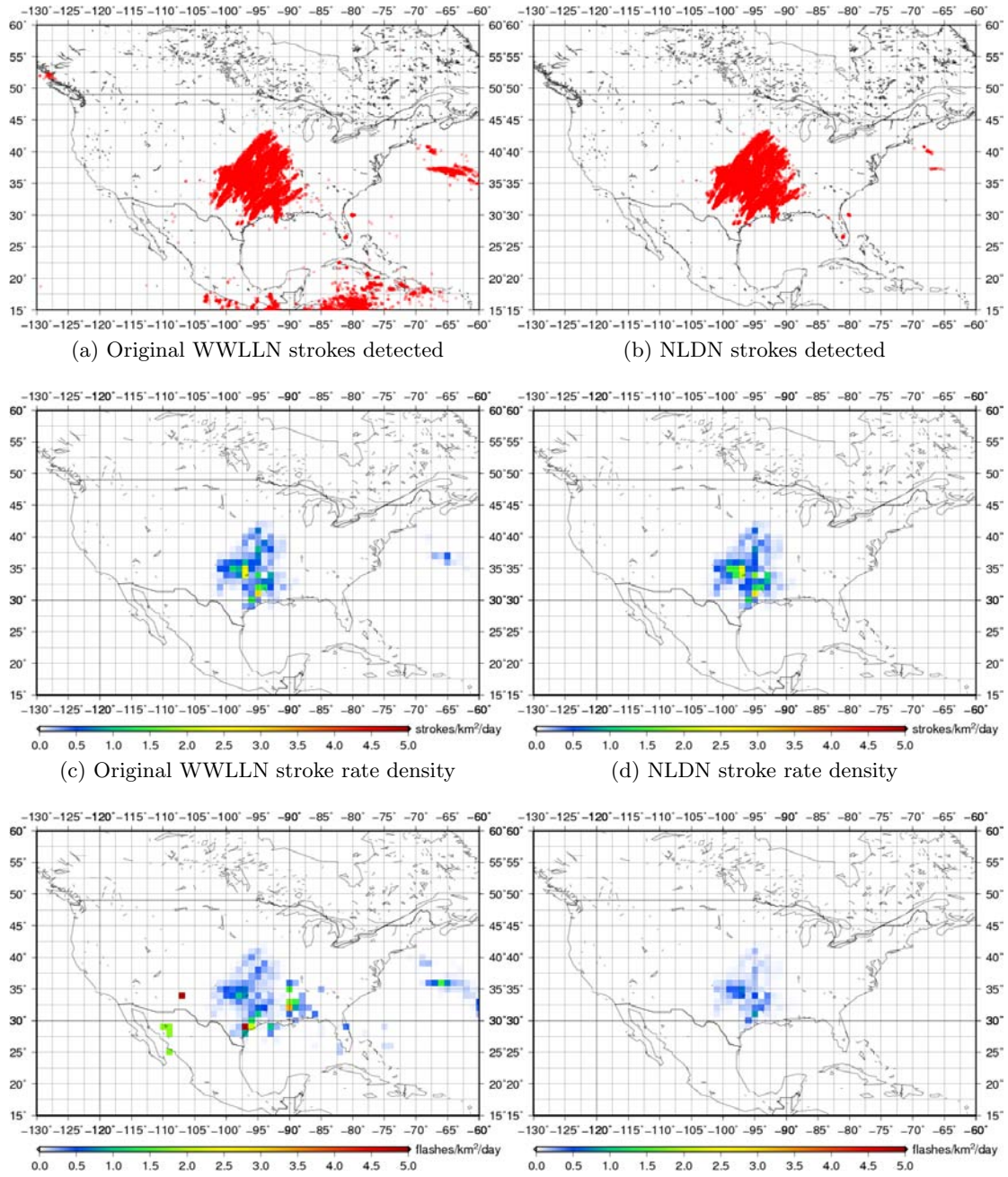

(a) Original WWLLN strokes detected

(b) NLDN strokes detected

(c) Original WWLLN stroke rate density

(d) NLDN stroke rate density

(e) Normalised WWLLN flash rate density

(f) NLDN flash rate density

Figure 4.12: WWLLN and NLDN comparison for 29 October 2009.

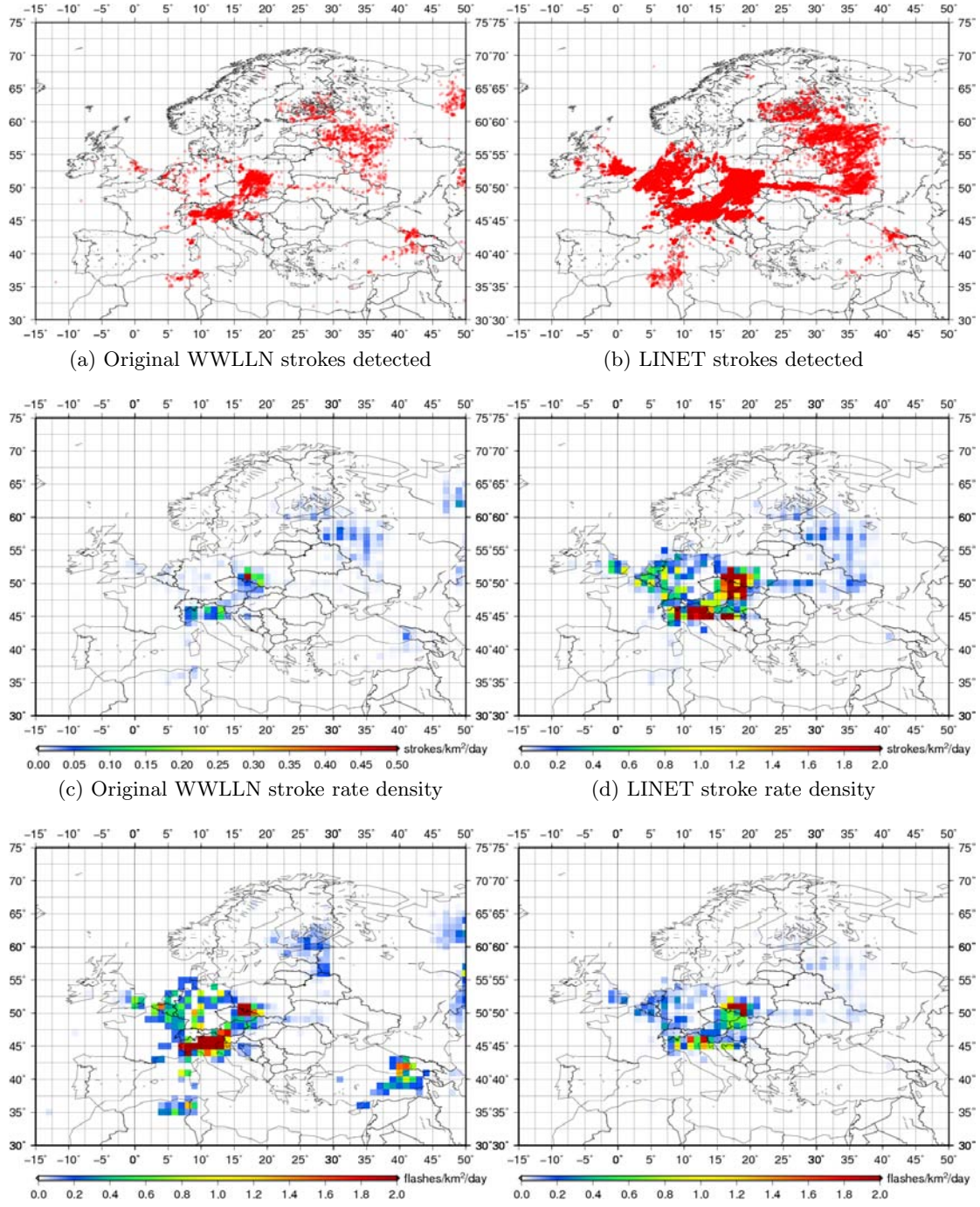

(a) Original WWLLN strokes detected

(b) LINET strokes detected

(c) Original WWLLN stroke rate density

(d) LINET stroke rate density

(e) Normalised WWLLN flash rate density

(f) LINET flash rate density

Figure 4.13: WWLLN and LINET comparison for 2 July 2007.

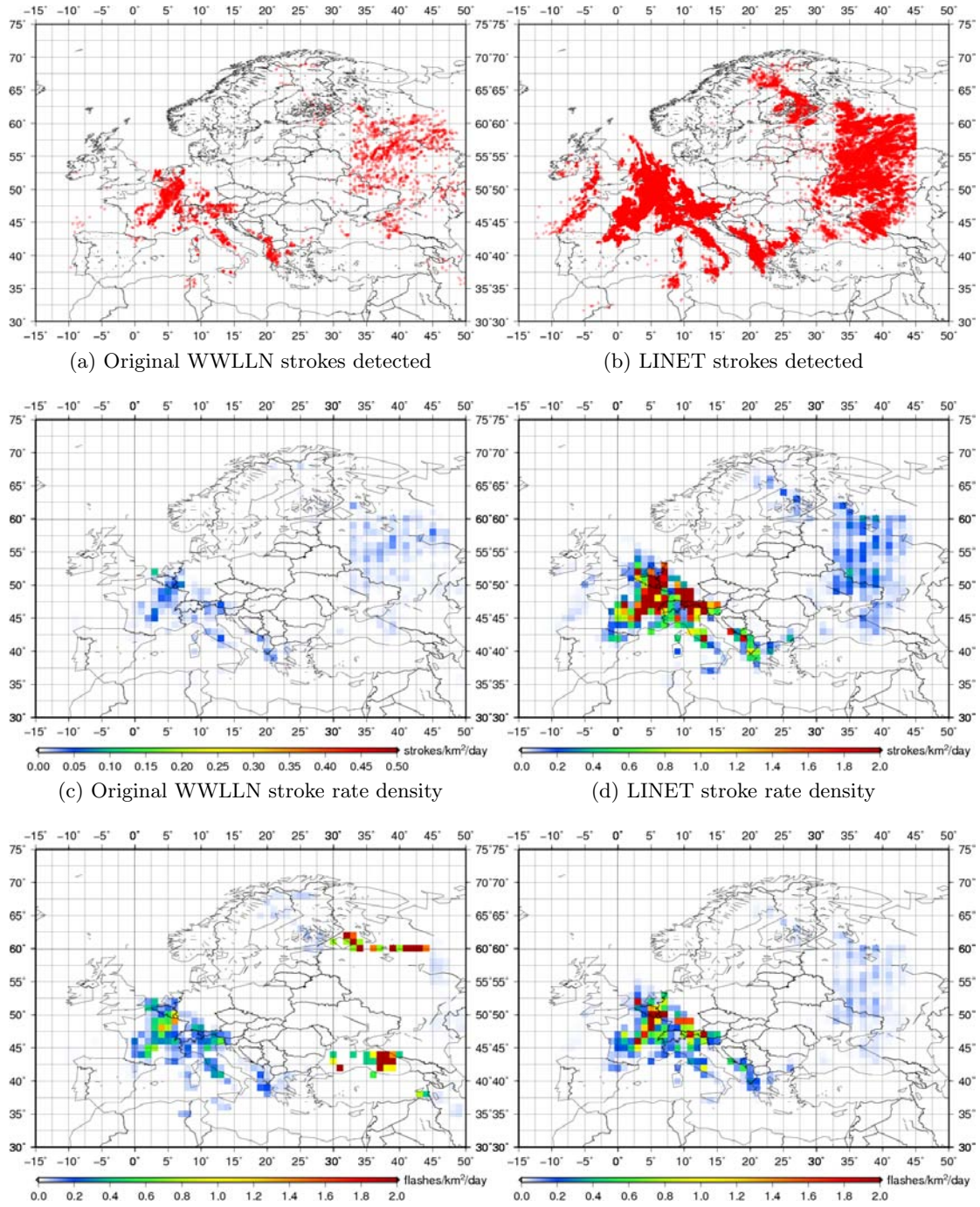

(a) Original WWLLN strokes detected

(b) LINET strokes detected

(c) Original WWLLN stroke rate density

(d) LINET stroke rate density

(e) Normalised WWLLN flash rate density

(f) LINET flash rate density

Figure 4.14: WWLLN and LINET comparison for 2 July 2008.

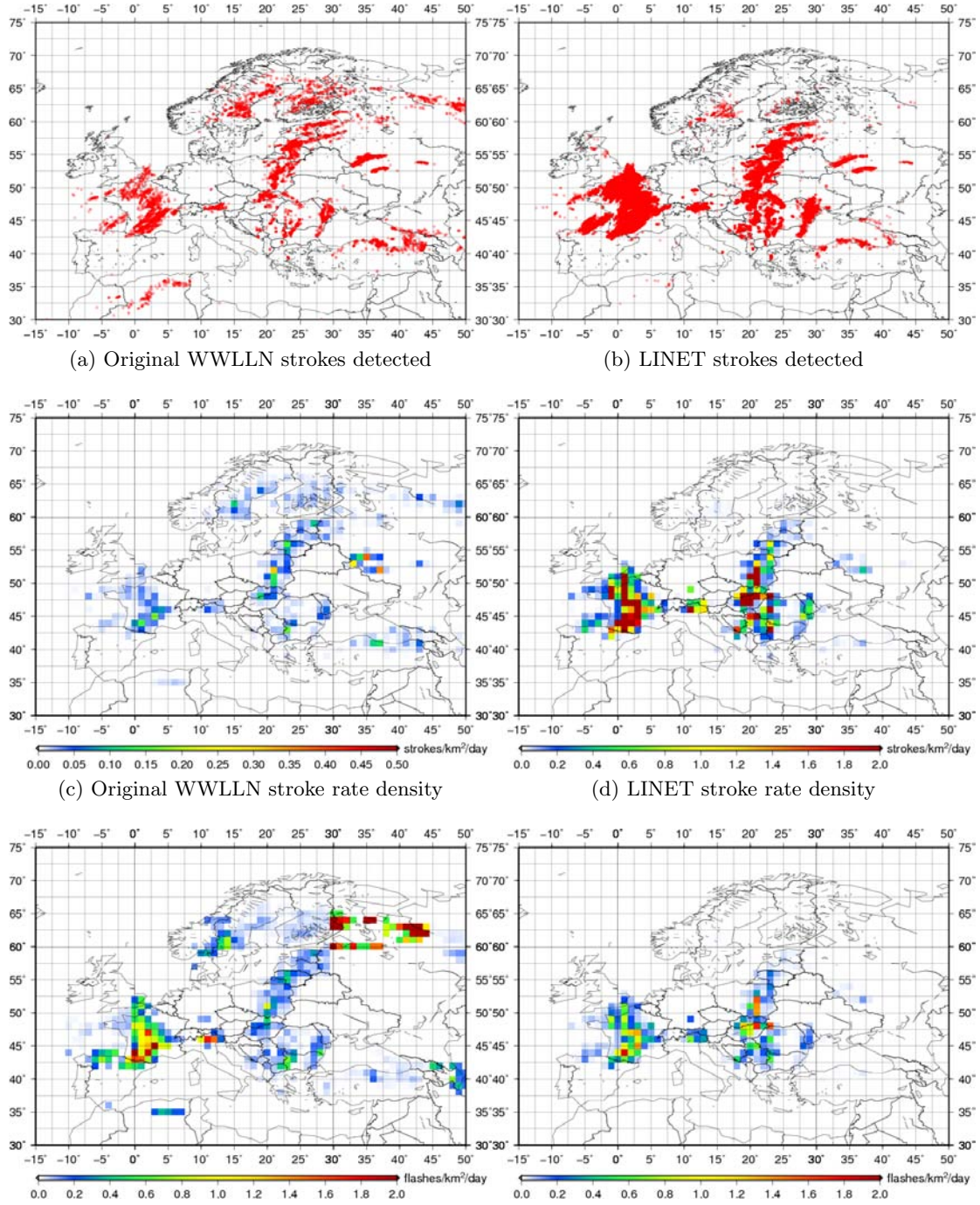

(a) Original WWLLN strokes detected

(b) LINET strokes detected

(c) Original WWLLN stroke rate density

(d) LINET stroke rate density

(e) Normalised WWLLN flash rate density

(f) LINET flash rate density

Figure 4.15: WWLLN and LINET comparison for 16 July 2009.

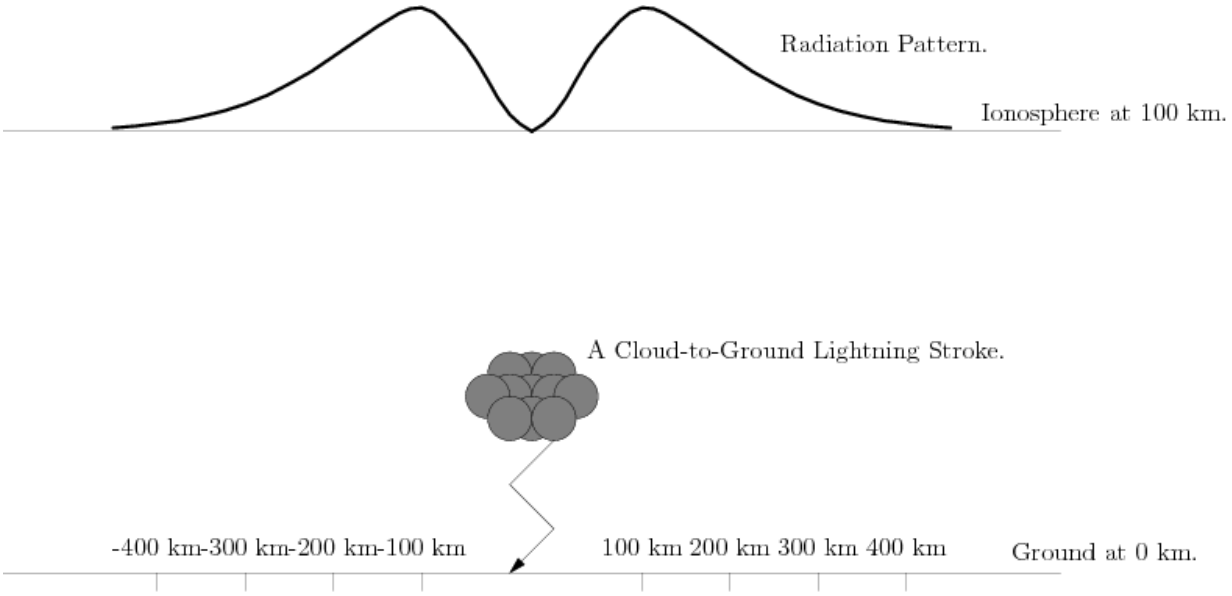

Figure 4.16: The radiation pattern from a single CG lightning stroke typically resembles that of a vertical dipole. Modeled after a figure by (Lauben et al., 2001).

as illustrated in Figure(4.16). The resulting radiation pattern resembles that of a vertical dipole, which the radiation pattern from a CG lightning stroke is often modeled after.

Since this study is for VLF, the spectral information of a lightning stroke has to be incorporated. The PSD function (2.2) is used for this purpose. The PSD function in units of $W/m^2/Hz$ is integrated over the VLF range to give the power flux in units of W/m^2 :

$$P = \int_{2\pi\times 3kHz}^{2\pi\times 30kHz} P(\omega)d\omega = \int_{2\pi\times 3kHz}^{2\pi\times 30kHz} \frac{1}{Z_0}(\frac{h_e I_0}{2\pi\epsilon_0 c^2})^2(\frac{\sin\theta}{R})^2 \frac{\omega^2(a-b)^2}{(\omega^2+a^2)(\omega^2+b^2)}d\omega \qquad (4.1)$$

The PSD function predicts a null radiation pattern directly above the lightning source ($sin(\theta = 0) = 0$), but due to inhomogeneities in the EIWG the radiation pattern gets smeared out. The lack of such a null has also been confirmed in satellite observations. By assuming the source to be slightly displaced from the vertical, one can ignore the null radiation pattern (Bortnik, 2004). Most of the energy from the lightning stroke gets radiated upward at the ends of a torus with a 100 km radius around the stroke location. The rest of the energy will travel through the EIWG with minimum attenuation, where some of it may eventually leak through into the ionosphere.

The total radiated power can be found be integrating the power flux over a spherical area surrounding the lightning stroke, by assuming an area element on the surface of a

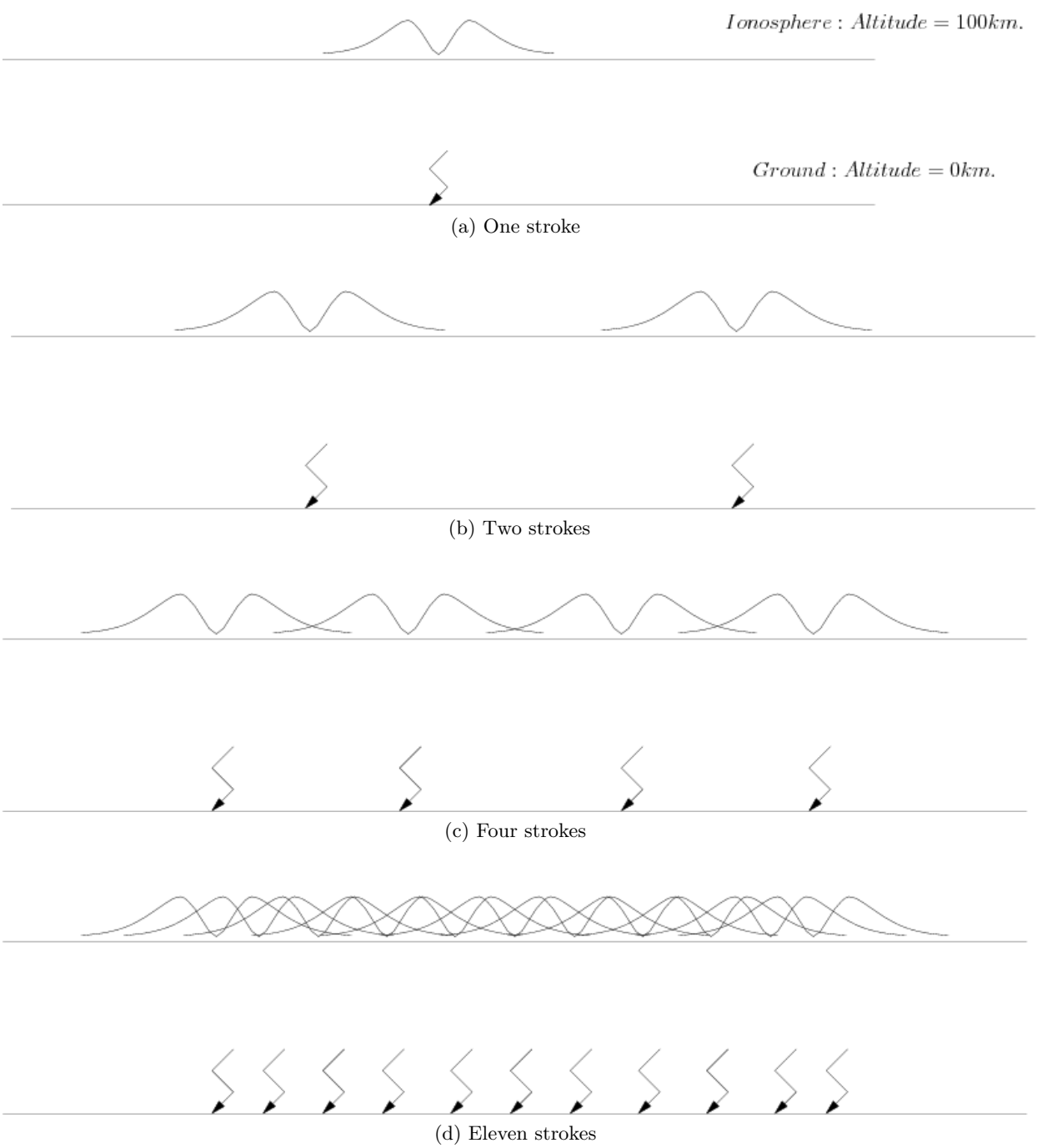

(a) One stroke

(b) Two strokes

(c) Four strokes

(d) Eleven strokes

Figure 4.17: Radiation pattern for an increasing number of lightning strokes. The radiation pattern ends up being uniform and flat, if enough strokes happen in a certain area.

sphere in spherical coordinates $dA = r^2 \sin\theta d\theta d\phi$:

$$P_{total} = \int_{\phi=0}^{2\pi} \int_{\theta=0}^{\pi} Pr^2 \sin\theta d\theta d\phi \tag{4.2}$$

After integrating over the wave frequencies and the spherical area surrounding the lightning stroke the duration of a typical lightning stroke (0.25 s) is incorporated and the following value is obtained for the energy radiated by a single lightning stroke:

$$2.951628 \times 10^5 J/s \times 0.25s = 73790.7J \tag{4.3}$$

This value might seem to be low at first, especially when compared to the energy values from Section 2.3.5 , but it has to be taken into consideration that this value is only for the VLFs. By applying an average multiplicity of 3.5 the total energy radiated per flash would amount to 258267.4 J = 2.582674×10^2 kJ. Although this value might seem a bit small, it should be noted that this value is only for VLF. This value is on the same scale as the 2.2×10^2 kJ found by Hill (1957).

The energy value is applied to the lightning flash densities using the following argument: If you assume that you have 2 lightning strokes happening at almost the same time and place, you would have an illumination profile that has a peak that is twice as high as for one stroke. So as part of a thought experiment: if you have two "half-strokes", happening close to each other, they will give you an energy distribution that combines to almost give the same energy as for one stroke. The same will happen with 4 quarter-strokes and 8 eight-strokes and so forth. In reality there are no half or quarter strokes, but if you have enough strokes which are almost uniformly distributed in the same area, you will have an illumination profile that will flatten out around the peaks, and appear to be uniform as illustrated in Figure 4.17.

Combining the VLF energy rate of a lightning stroke, the duration of lightning flash and the lightning flash densities in units of flashes km^2/yr, the VLF lightning energy flux rates that are incident on the ionosphere can be calculated. This was done for the four seasons using the normalised WWLLN data that was averaged over 2005–2009 as shown in Figure 4.18. As would be expected from the global flash rate densities shown in Figure 4.4 the highest energy flux values were found for June, July and August with some of the higest flash rate densities found over North America then Europe and Asia in Figure 4.18 (c). The values are typically on a scale of $10^5 - 10^6$ J/km^2/yr and has a mean value of 3.45×10^5 J/km^2/yr.

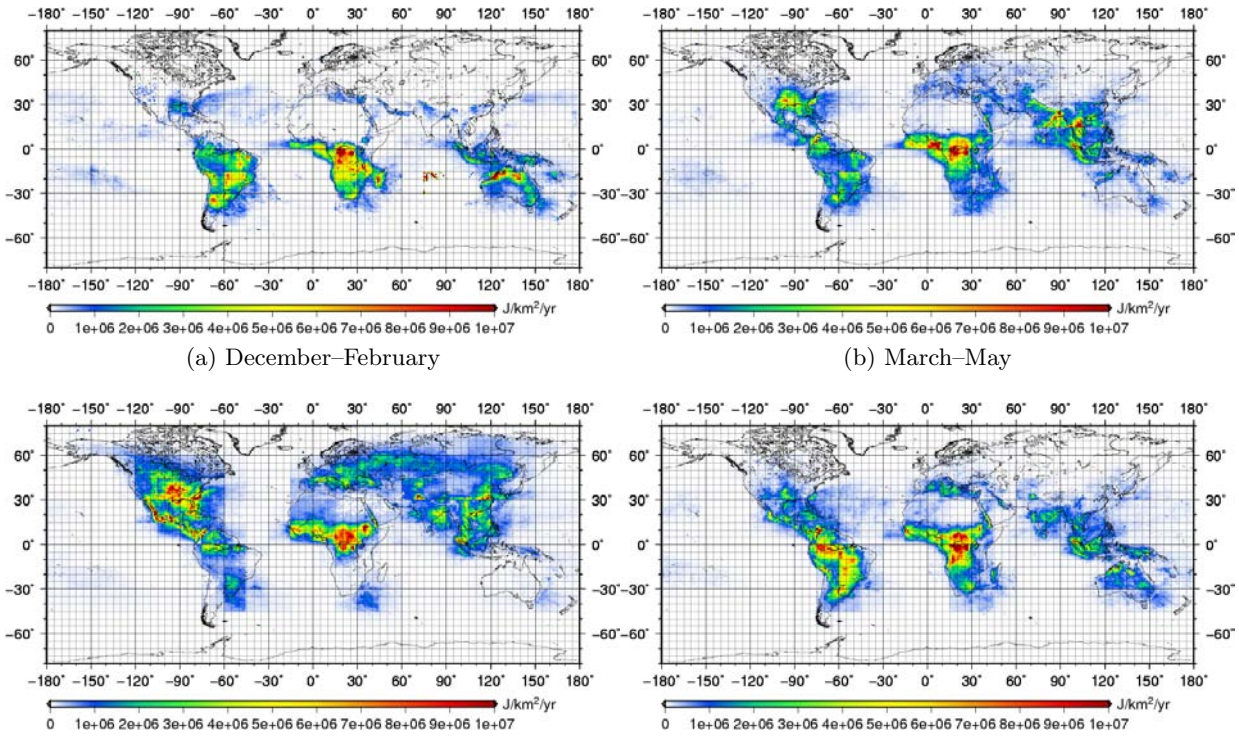

(a) December–February (b) March–May

(c) June–August (d) September–November

Figure 4.18: The seasonal variation of the lightning energy flux in geographic coordinates, averaged over 2005-2009.

4.4 Geographic to Geomagnetic coordinates

However the power flux values from Figure 4.18 have to be converted from geographic to geomagnetic coordinates since the effect of a certain lightning discharge on the radiation belts will be influenced by its geomagnetic latitude (Rodger et al., 2005). With the equatorial lightning having the smallest effect and mid-latitude lightning the highest.

Geographic coordinates can be represented by a three-dimensional cartesian coordinate system with its origin at the centre of the Earth. The x-axis is in the equatorial plane of the Earth, but fixed with the roation of the Earth so it passes through the Greenwich meridian. The z-axis would then be parallel to the rotational axis of the Earth which leaves the y-axis to complete the system with its direction determined according to the right-handed rule (Russell, 1971).

Geomagnetic coordinates can also be represented by a three-dimensional cartesian coordinate system where its z-axis is parallel to the magnetic dipole axis, which is about 11 °north of the Earth's rotational axis. The y-axis would then be perpendicular to the geographic poles and the x-axis completes the orthagonal set according to the right-handed rule (Russell, 1971).

One way of transforming from geographic to magnetic coordinates is by use of the corrected geomagnetic coordinate system (CGM). CGM involves tracing any point, P, in the ionosphere along a geomagnetic field line to the opposite hemisphere, taking into account the full magnetic field (internal dipole and non-dipole sources) model. The point where the field line crosses the dipole equator plane is the new point, Q. P and Q will have the same altitude, but Q will have a magnetic latitude and longitude (Gustafsson et al., 1992).

While the CGM coordinates are very good for working with ionospheric data, points on the same field line have different coordinates(due to different altitudes) and the CGM coordinates therefore do not show the conjugate relationship between two points. It is also difficult to trace magnetic field lines near the geographic poles as well as the equator which leads to regions where the magnetic coordinates cannnot be defined. This led Baker and Wing (1989) to develop the AACGM coordinate system, originally called PACE. It uses the same basic principles as CGM, but it traces the field lines all the way back to the ground. This means that all the points on a field line now have the same latitude and longitude. The coordinate transformation is defined in terms of spherical harmonic coefficients, with a different set for every altitude.

The WWLLN data was transformed from geographic to Altitude Adjusted Corrected GeoMagnetic (AACGM) coordinates, by assuming an altitude of 100 km. The transformed normalised WWLLN energy flux rates are displayed on a seasonal basis and geomagnetic coastline grid in Figure 4.19.

4.5 Absorption into the Magnetosphere

The classic absorption curves of Helliwell (1965) shown in Figure 4.20 were used to transform the energy flux values from the ionosphere to the inner magnetosphere. The curves were created for different ionospheric models. The curves are for a daytime (upper and lower), nighttime (upper and lower) and polar blackout ionosphere. The curve values were used as scaling factors.

Since the lightning energy values were calculated for VLFs, the daytime and nighttime curves from Figure 4.20 were integrated over the VLF range. These new values were then applied to the seasonal flash rate densities to give estimates of the VLF energy flux rates. The day and night energy flux rate distributions for all four of the seasons are shown in Figure 4.21 to Figure 4.22. From these it is clear that the highest energy flux rates were found to affect the ionosphere at night, during the Northern Hemisphere summer (June–August). The VLF lightning energy flux rates in Figure 4.23 (d) typically has values of 3×10^6 to 1×10^7 J/km^2/ yr over North America and Europe. The Northern Hemisphere summer was further investigated by looking at the WEP producing Trimpi rate during these months using data from Rothera, Antarctica.

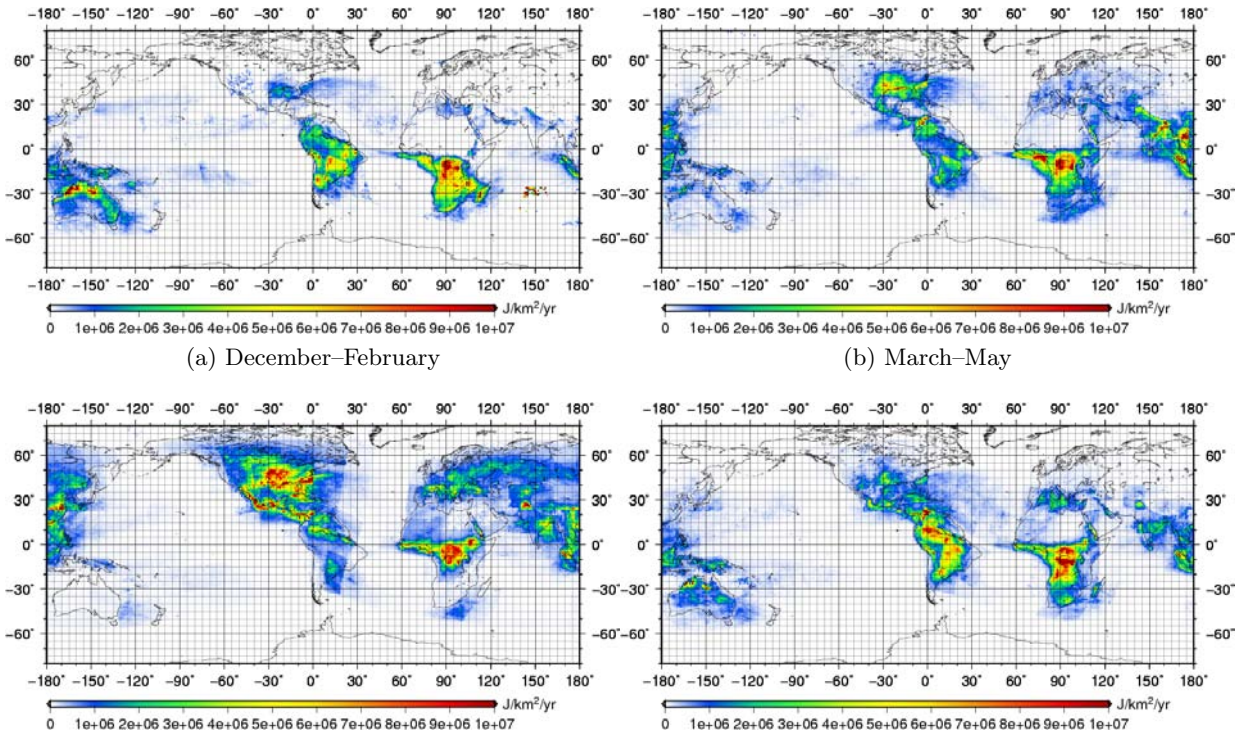

(a) December–February (b) March–May

(c) June–August (d) September–November

Figure 4.19: The seasonal variation of the lightning energy flux at the bottom of the ionosphere in geomagnetic coordinates, averaged over 2005-2009.

Trimpi perturbations that are observed in the Antartic Peninsula are greatly affected by high-current CG lightning around 34°N, 76°W close to the footprint of the $L \sim 2$ flux tubes (Clilverd et al., 2002). Rodger and Clilverd (2002) assumed that the WEP rate in the Antarctic Peninsula would vary in the same way that lightning occuring in the Trimpi perturbation source region over North America, around $L \sim 2$, would across a day. A map of the primary (due to lightning in same hemisphere) and secondary (due to lightning in the conjugate hemisphere) WEP rates was created by scaling the ratio of the Faraday (65.25° S, 64.27° W, $L = 2.45$) WEP rate of 0.79 WEP/ min (Rodger et al., 2005) and flash rate densities over North America found in latitude bands across $L = 2$ to global OTD flash rate densities. The global mean WEP rate of was applied across all L-shells between $L = 1.9$ and $L = 3.5$ by accounting for the variation in L-shell coupling based on detector measurements from a low altitude (200 km, $L = 2.2$) polar-orbititing satellite S81-1/SEEP used by Voss et al. (1998).

Rothera perturbation events from June–July 2009–2010 were then used for the analysis of WEP rates. The detector at Rothera, Antartica that was used to identify the perturbation events was set so that only stronger events were picked. Periods with a signal level lower than -65dB, which included terminator effects and some daytime hours,

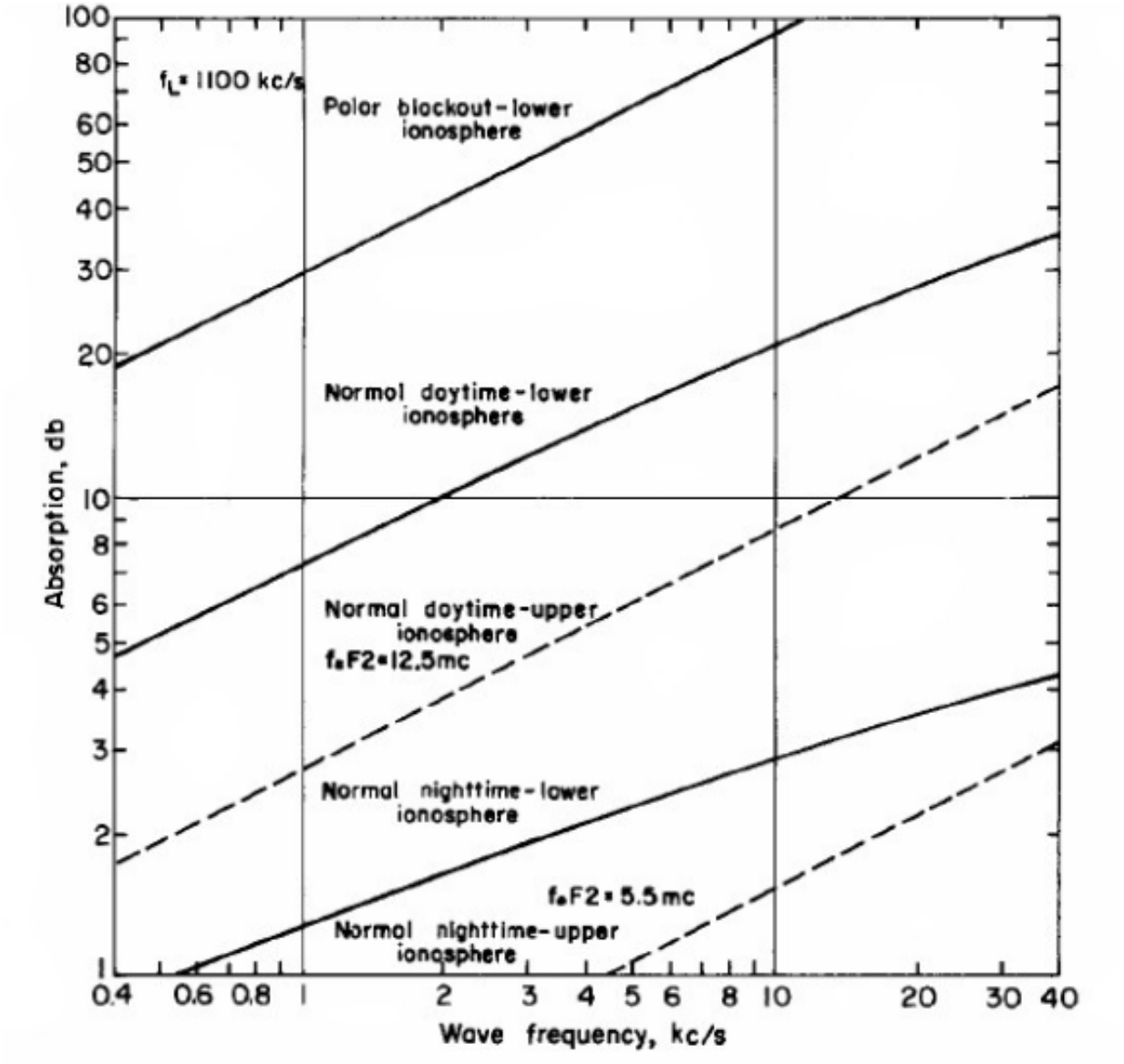

Figure 4.20: The absorption curves of (Helliwell, 1965). The curves are a function of frequency and are displayed for five different ionospheric models.

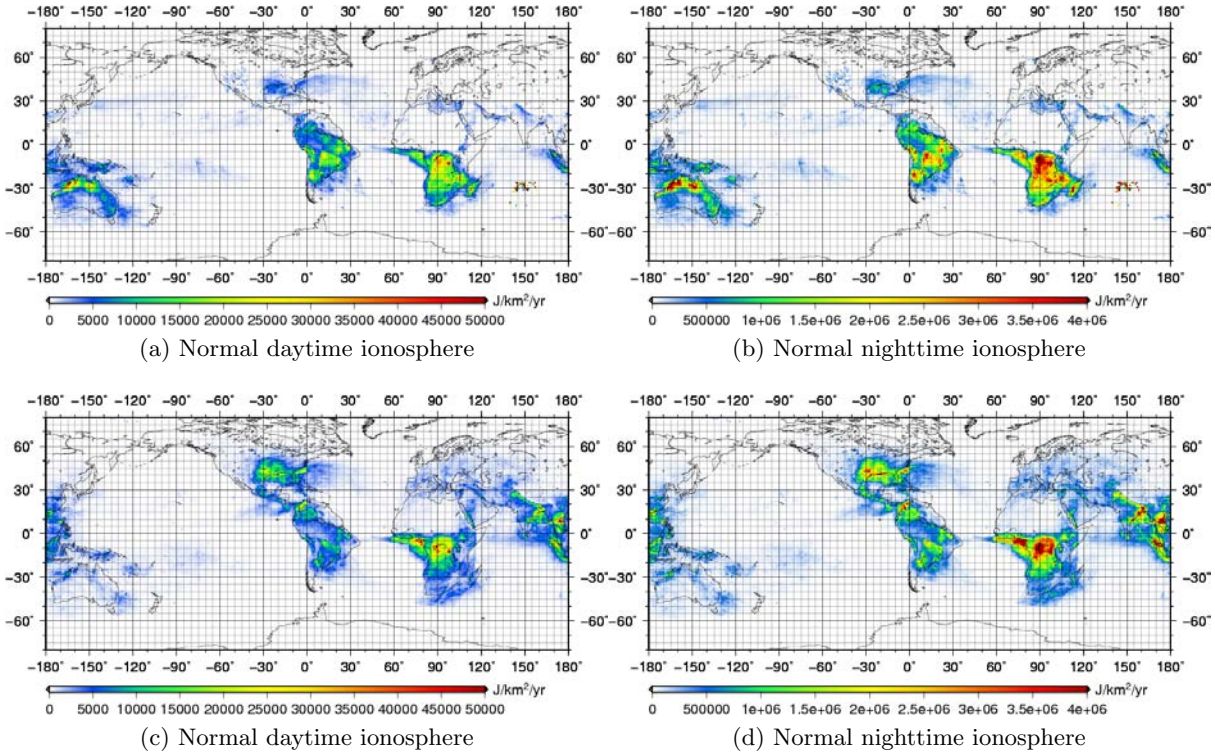

(a) Normal daytime ionosphere

(b) Normal nighttime ionosphere

(c) Normal daytime ionosphere

(d) Normal nighttime ionosphere

Figure 4.21: Power into the magnetosphere in geomagnetic coordinates for December–February (a), (b) and March–May (c), (d) averaged over 2005–2009.

were ignored as well as days where huge phase shifts were present (Steinbach, P., personal communication, 2011).

Figure 4.23 compares the Rothera WEP rates and the lightning flash density rates over North America across $L \sim 2$ that is thought to cause the WEP events at Rothera, Antarctica. The data that was used for both the WEP and lightning density rates are for July 2010. Peak values, here assumed to be those values larger than the mean, were chosen for both the WEP and lightning density rates. According to the peak value critera, 12 peaks were found in the lightning flash rate density data whilst 14 were found in the WEP rate data. From these peaks, 9 were found to be on the same day. This shows that there is a good possibility that lightning at the expected source region may cause WEP at Rothera since the higher lightning flash rate densities also correlated with the higher WEP rates.

A few events were chosen from the data set and were all selected on the following criteria: an amplitude or phase perturbation had to occur and the perturbation had to be a classic Trimpi event. The same method was used to find the WEP rate as described above from the studies by Rodger and Clilverd (2002); Rodger et al. (2004b), except that normalised WWLLN flash rate densities for June–August averaged over 2005–2009 and a Rothera WEP rate were used. An average Trimpi rate of 0.033 WEP/ min was found for

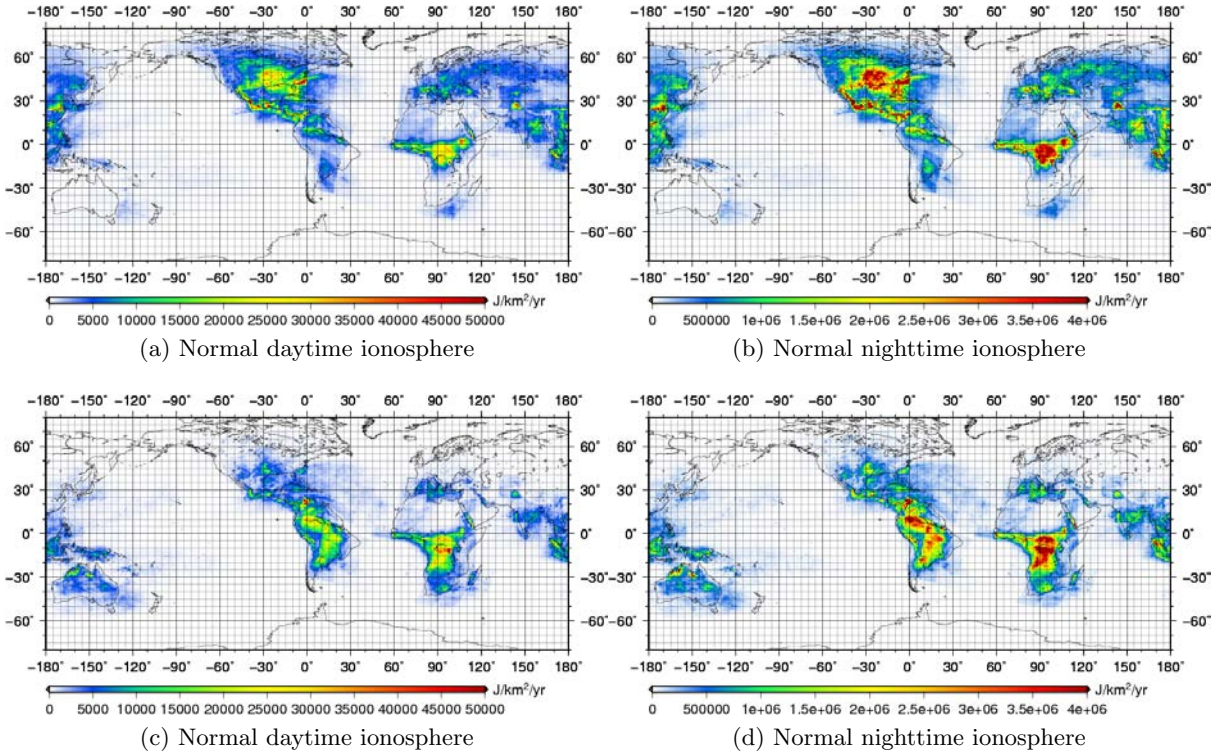

(a) Normal daytime ionosphere (b) Normal nighttime ionosphere

(c) Normal daytime ionosphere (d) Normal nighttime ionosphere

Figure 4.22: Power into the magnetosphere in geomagnetic coordinates for June–August (a), (b) and September–November (c), (d) averaged over 2005–2009.

Rothera as averaged over June–July 2009–2010 and applied on a global scale as shown in Figure 4.24. In order to acount for the latitudinal variation in WEP the satellite measurements of Voss et al. (1998) were first applied to the global WEP rates over $L = 1.9$ to $L = 3.5$ which is the region thought to cause most of the radiation belt losses.

The WEP rates in Figure 4.24 are lower than those found in the Rodger et al. (2005) since a lower WEP rate of 0.033 WEP/ min was estimated for Rothera. There is however still a strong presence from lightning over North America and Europe. This is to be expected as June–August falls in the Northern Hemisphere summer when one sees the highest lightning activity in these regions. Since these months are in the Southern Hemisphere winter the flash rate densities are very low over South America, South Africa and Australia and these regions will have a very small contribution to the WEP rates. There is a small contribution from lightning over Australia. There is still some lightning activity around 30°–40° geomagnetic longitude, the effect of which is not observed in the WEP rate distribution. This is possibly due to L-shell coupling. Since the Rothera WEP rates were used to determine the global WEP rates one would expect there to be values over the Antartic Peninsula. However due to only primary WEP rates being used the lightning activity at Rothera is not high enough to show on Figure 4.24. The WEP rates for June–August were found to be in the range of $0.25 - 1.5$ WEP/ min.

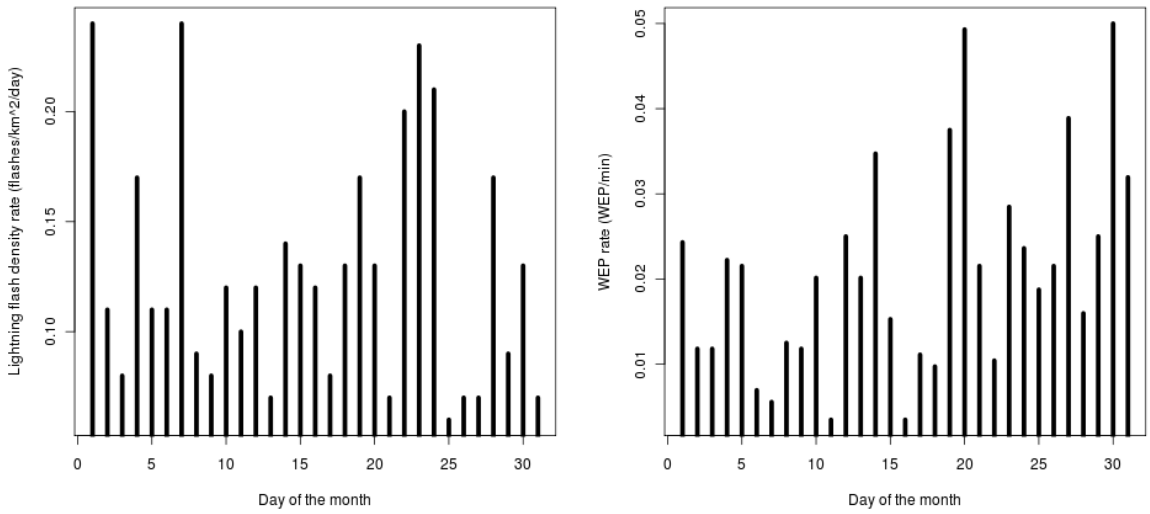

(a) (b)

Figure 4.23: (a) The lightning flash density rate over North America at $L \sim 2$ thought to contribute to (b) the WEP rate at Rothera during July 2010.

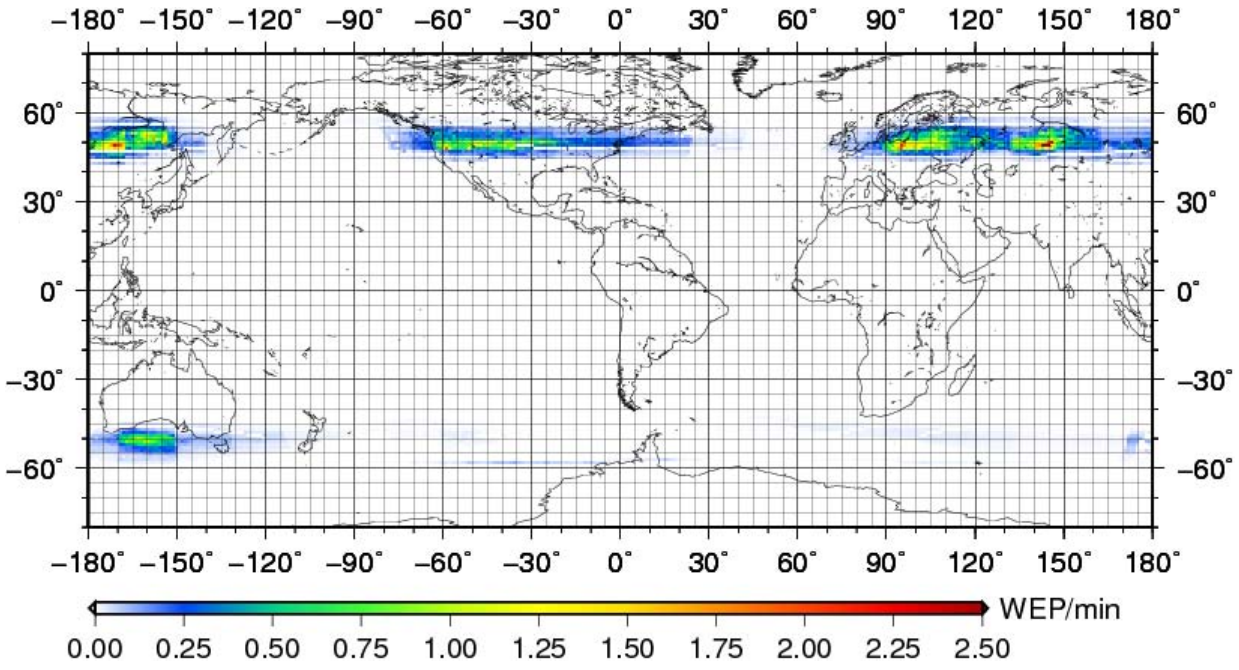

Figure 4.24: The distribution of the expected global WEP producing Trimpi rate in geomagnetic coordinates using June–August flash rate densities and Rothera Trimpi data .

Chapter 5

Discussion

Even though lightning's properties have been studied extensively, its spatial and temporal effect on the Earth's radiation belts is not yet fully understood. It is known that the precipitation of energetic electrons from the radiation belts is mainly due to the pitch angle scattering of the electrons by lightning induced whistler mode waves. This prompted a study of using lightning flash densities to examine the seasonal variation of the effect that energy radiated by lightning has on the magnetosphere and the loss of electrons from it.

First a statistical lightning model was created. WWLLN data was used since it has excellent time resolution. WWLLN has been fully operational since 2005 and started with only a few nodes. By 2009 the system had grown to more than 40 nodes distributed globally. The system uses the TOGA of VLF wavetrains. This allows for a receiver spacing of thousands of km s. However, the system needs at least 4 receivers to make an accurate detection. Over certain regions like the African continent the receiver density is very low with only about two or three spread over the whole region, which leads to a low DE.

Data from the LIS and OTD satellites were used to normalise the WWLLN data. Since LIS and OTD formed part of satellite based operations, the data has very good spatial resolution and high DE. The two datasets have been intercalibrated and merged to give a good representation of global lightning activity over 1995–2005.

The WWLLN data was transformed into a $0.5^\circ \times 0.5^\circ$ grid in units of strokes /km^2/yr. To be able to compare the two datasets, an average multiplicity of 3.5 strokes/flash was incorporated by multiplying it with the WWLLN stroke rate density data. Thereafter the mean and standard deviation of WWLLN were scaled to that of LIS/OTD and normalisation factors were applied to the WWLLN flash rate densities. This allowed for the normalisation of the WWLLN data with reference to that of the LIS/OTD data. The normalisation factors were found to vary with the node distribution with the normalisation factors over the ocean and in a region of high node density being low whilst the normalisation factors in close proximity to a node in a low node density region were higher.

The variation of the DE of WWLLN over the years Abarca et al. (2010) might also cause variations in the normalisation factors. When comparing the normalisation factors averaged over 2005-2009, Figure 5.1, to those from 2009, Figure 5.2, a few differences and similarities are clearly visible. In general the normalisation factors for 2009 appear to be very close to those from the averaged data set. The normalisation factors over North America, Europe and Asia appear to be slightly lower than the average values due to the increased DE of WWLLN in 2009 with an increase in lightning detecting nodes in these regions. This also seems to be the case across the higher latitudes ($> -15°$) of South America and Africa. However from the ratio of 2009 to 2005-2009 averaged normalisation factors, 120 out of the 288 values were > 1 from which 19 were > 2 which means that 19 of the normalisation factors for 2009 are much larger than their 2005-2009 averaged counterparts. This could be due to higher than average lightning activity rates in 2009. These variations might cause errors in the calculation of the energy flux rate values which in future should be examined in more depth.

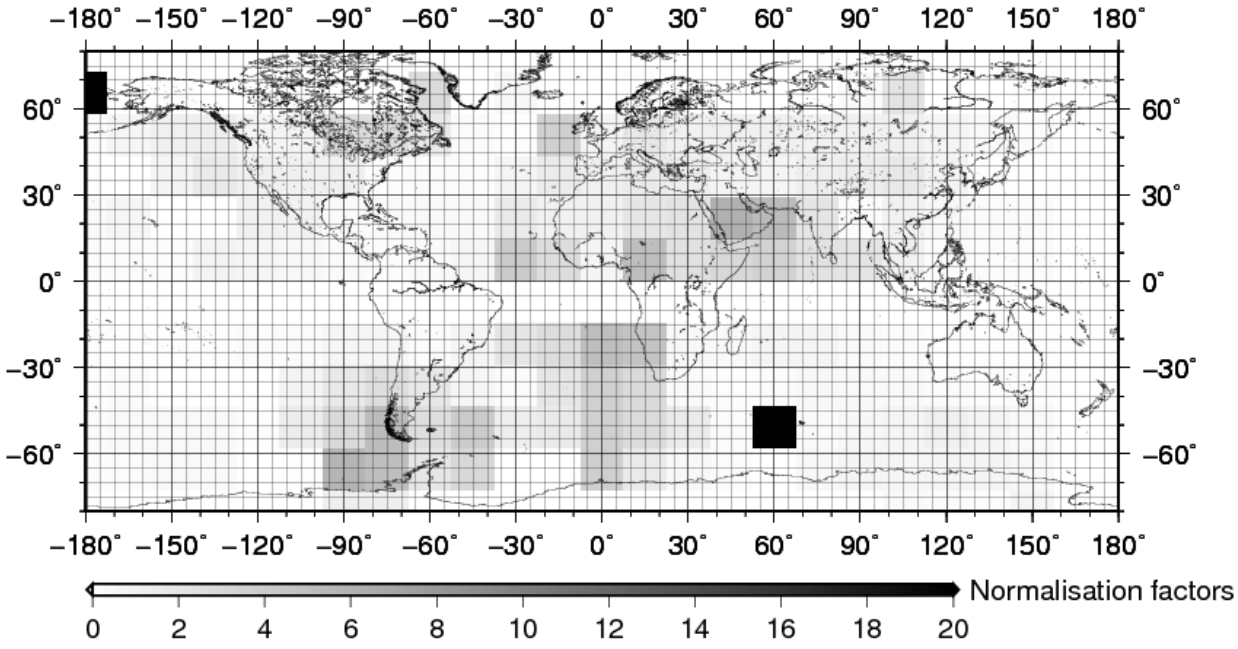

Figure 5.1: Normalisation factors, averaged over 2005-2009.

The model had to be validated in order to ensure its accuracy. Therefore it was compared to regional datasets over South Africa, the United States and the greater Europe region. The regional and WWLLN flash density rates were all converted to a $1.0° \times 1.0°$ grid to view the lightning activity on a larger scale. The χ-square test was used to do a statistical comparison of WWLLN with the regional networks. Most of the chosen days seemed to agree quite well. There was a visible improvement of WWLLN flash rate densities over all of the days and for all of the regional datasets used in the comparison after normalisation.

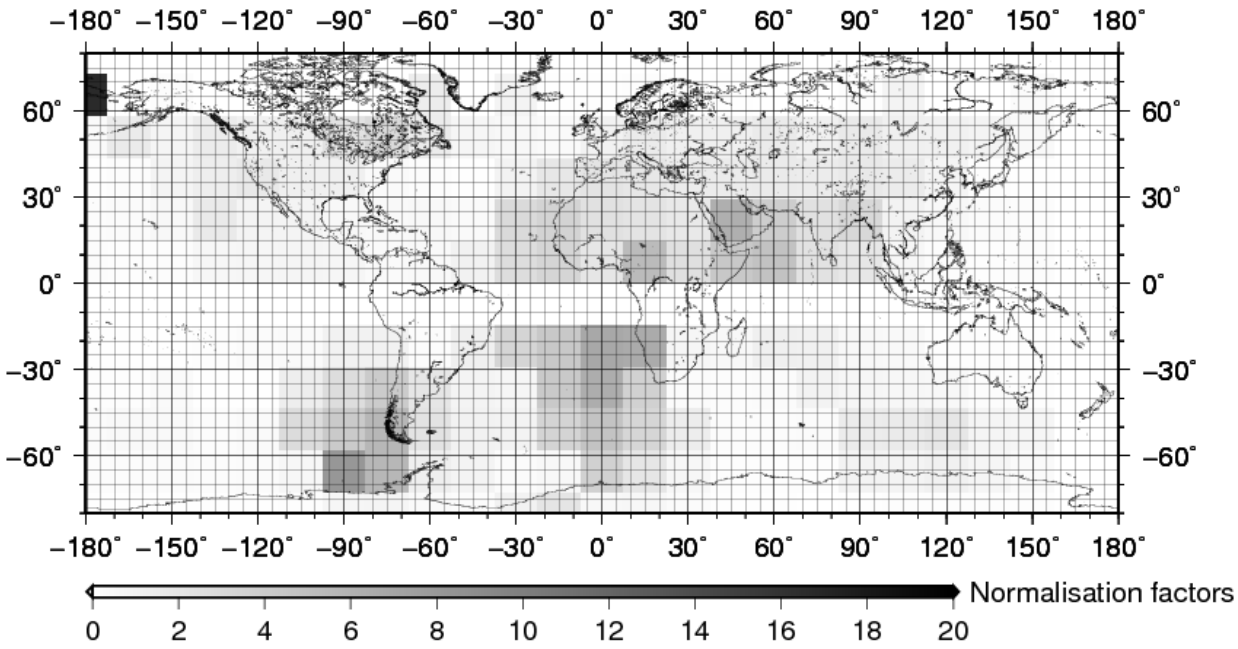

Figure 5.2: Normalisation factors for 2009.

One thing that was noted is that the scale for the flash rate densities for the NLDN comparison was noticeably higher than those of both the SAWS and LINET lightning detection networks. This is probably due to the fact that the lightning activity in the United States (22.6–35.4 flashes/km^2/ yr) is much higher than for South Africa (23.0 flashes/km^2/ yr in Bloemfontein) and Europe (8.0–9.4 flashes/km^2/ yr) (Christian et al., 2003).

The normalised WWLLN data was then used to estimate the VLF lightning power at the ionosphere. This was done using the PSD function. The PSD function was integrated over the VLF range and the spherical area surrounding the lightning stroke. A value of 2.951628×10^5 J/s was then multiplied with the average duration of a lightning stroke (0.25 s) and the average multiplicity (3.5 strokes/flash. Thereafter the flash rate densities were multiplied with the average VLF energy per flash of 2.582674×10^2 kJ giving the energy flux rate, in units of J/km^2/yr incident on the ionosphere.

The normalised seasonal WWLLN flash rate densities were then transformed to AACGM coordinates. This is an important step since the effect of a specific lightning discharge on the radiation belts will be depend on its geomagnetic latitude (Rodger et al., 2005).

The VLF wave energy will undergo attenuation while traveling through the ionosphere. Therefore attenuation curves for a day- and nighttime ionosphere over

frequencies from $3 - 30$ kHz from Helliwell (1965) were applied to account for the reduction in energy. From the subsequent data it was estimated that the highest energy flux rates will occur during the Northern Hemisphere summer months (June–August), at night. The values during June–August were found to be on a scale of $10^5 - 10^6$ J/km^2/yr and had a mean value of 1.6×10^5 J/km^2/yr. The lowest energy flux rate values were found to occur during the day when the absorption in the ionosphere is at its highest due to an increase in ionisation.

A global WEP rate map for June–July was produced, by scaling the normalised WWLLN global flash rate densities to ratio between Trimpi produced WEP rates at Rothera and flash rate densities over North America at $L \sim 2$, thought to be the expected source region of the Rothera WEP. There is however a latitude variation of WEP events. This was accounted for by using satellite measurements of the variation in L-shell coupling (Voss et al., 1998). Since June–July are the months of the Northern Hemisphere summer, one would expect a great contribution to WEP from lightning in this region. The region that was found to have the biggest contribution to the WEP rates is North America and then Europe and Asia. The initial WEP trimpi rate was found to be WEP rates were mostly found to be between 0.25 WEP/ min and 1.75 WEP/ min.

Chapter 6

Conclusion and Future studies

The normalisation of WWLLN data with reference to LIS/OTD data seems to have been successful. This is based on the comparison of the normalised WWLLN flash rate densities to that of regional lightning detection networks using χ-square tests. The calculated VLF energy per flash was found to be on the small side, however the value compared well to the results of Hill (1957). The VLF energy from a lightning flash is expected to be lower than the energy values found from other lightning studies (Borucki and Chameides, 1984; Cooray, 1997) since most of these determined lightning flash energy over all frequencies. The attenuation curves of Helliwell (1965) were used to account for the absorption of waves traveling through the ionosphere. Estimates of the seasonal energy flux rates into the magnetosphere were calculated using the normalised WWLLN flash rate densities that now have good time resolution and DE. The months of June–August in the Northern Hemisphere summer were found to be the greatest contributer to the VLF lightning energy flux rates with some of the greatest values over North America. A global WEP rate map was generated for the months of June–August with the greatest WEP rates found to be over North America.

In future it would be good if one could focus more of the effect of the EIWG on VLF propagation when estimating the energy from lightning in the VLF range. After model-observation comparisons by Starks et al. (2008) the absorption curves of Helliwell (1965) have been found not be as accurate as initially thought. The discrepancies are probably due to enhanced D-region absorption and reflection as well as the conversion to other waveguide modes that were not included in the Helliwell (1965) study (Lehtinen and Inan, 2009). For further studies it would be good to use FWM techniques that have been used to model the trans-ionospheric propagation of electromagnetic waves (Lehtinen and Inan, 2009; Tao et al., 2010). The composite model of Starks et al. (2008) that combines a simulation of fields in the EIWG, ionospheric absorption estimates and geomagnetic and plasma density models might be another method that could be used. Finally by using the seasonal geomagnetic lightning energy flux rates on the magnetosphere and ray tracing techniques the distribution of whistler wave energy in the magnetosphere could be estimated. This could be used to determine the flux and energy of the precipitating electrons on a seasonal basis.

Bibliography

Abarca, S., Corbosiero, K., and Galarneau, T. (2010). An evaluation of the worldwide lightning location network (wwlln) using the national lightning detection network (nldn) as ground truth. *Journal of Geophysical Research*, 115.

Abel, B. and Thorne, R. (1998a). Electron scattering loss in earth's inner magnetosphere 1.dominant physical processes. *Journal of Geophysical Research*, 103(A2):2385–2396.

Abel, B. and Thorne, R. (1998b). Electron scattering loss in earth's inner magnetosphere 2.sensitivity to model parameters. *Journal of Geophysical Research*, 103(A2):2397–2407.

Baker, K. and Wing, S. (1989). A new magnetic coordinate system for conjugate studies at high latitudes. *Journal of Geophysical Research*, 94(A7):9139–9143.

Barkhausen, H. (1919). Zwei mit hilfe der neuen verstärker entdeckte erscheinungen. *Physik A.*, 20:401–403.

Betz, H., Schmidt, K., Oettinger, W., and Montag, B. (2008). Cell-tracking with lightning data from linet. *Advances in Geosciences*, 17:55–61.

Biagi, C., Cummins, K. L., Kehoe, K. E., and Krider, E. P. (2007). National lightning detection network (nldn) performance in southern arizona, texas, and oklahoma in 2003–2004. *Journal of Geophysical Research*, 112.

Boccippio, D., Cummins, K., Christian, H., and Goodman, S. (2001). Combined satellite- and surface-based estimation of the intracloud-cloud-to-ground lightning ratio over the continental United States. *Monthly Weather Review*, 129(1):108–122.

Bortnik, J. (2004). *Precipitation of radiation belt electrons by lightning-generated magnetospherically reflecting whistler waves*. PhD thesis, stanford university.

Bortnik, J., Inan, U., and Bell, T. (2003a). Energy distribution and lifetime of magnetospherically reflecting whistlers in the plasmasphere. *Journal of Geophysical Research*, 108(A1):SMP19–1–SMP19–12.

Bortnik, J., Inan, U., and Bell, T. (2003b). Frequency-time spectra of magnetospherically reflecting whistlers in the plasmasphere. *Journal of Geophysical Research*, 108(A5):SMP12–1–SMP12–10.

Borucki, W. and Chameides, W. (1984). Lightning: Estimates of the rates of energy dissipation and nitrogen fixation. *Reviews of Geophysics*, 22(4):363–372.

Brooks, C. (1925). The distribution of thunderstorms over the globe. *Geophysical Memoirs*, 24:147–164.

Bruce, C. and Golde, R. (1941). The lightning discharge. *Journal of the Insitute of Electrical Engineers*, 88:487–505.

Budden, K. (1988). *The propagation of radio waves: The theory of radio waves of low power in the ionosphere and magnetosphere*. Cambridge Univ Press.

Chen, F. (1984). *Introduction to plasma physics and controlled fusion: plasma physics*, volume 1. Springer.

Christian, H., Blakeslee, R., Boccippio, D., Boeck, W., Bucchler, D., Driscoll, K., Goodman, S., Hall, J., Koshak, W., Mach, D., and Stewart, M. (2003). Global frequency and distribution of lightning as observed from space by the optical transient detector. *Journal of Geophysical Research*, 108(D1):ACL4–1–ACL4–15.

Clilverd, M., Nunn, D., Lev-Tov, S., Inan, U., Dowden, R., Rodger, C., and Smith, A. (2002). Determining the size of lightning induced electron precipitation patches. *Journal of Geophysical Research*, 107(A8):SIA10–1–SIA10–10.

Clilverd, M., Rodger, C., and Nunn, D. (2004). Radiation belt fluxes associated with lightning. *Journal of Geophysical Research*, 109(12).

Collier, A. B., Bremner, S., Lichtenberger, J., Downs, J. R., Rodger, C., Steinbach, P., and McDowell, G. (2010). Global lightning distribution and whistlers observed at dunedin, new zealand. *Annales Geophysicae*, 28:499–513.

Collier, A. B., Delport, B., Hughes, A., Lichtenberger, J., Steinbach, P., Oster, J., and Rodger, C. (2009). Correlation between global lightning and whistlers observed at tihany, hungary. *Journal of Geophysical Research*, 114.

Cooray, V. (1997). Energy dissipation in lightning flashes. *Journal of Geophysical Research*, 102(D17):21401–21410.

Cummer, S. and Inan, U. (1997). Measurement of charge transfer in sprite-producing lightning using elf radio atmospherics. *Geophysical Research Letters*, 24:1731–1734.

Cummins, K., Murphy, M., Bardo, E., Hiscox, W., Pyle, R., and Pifer, A. (1998). A combined toa/mdf technology upgrade of the u.s. national lightning detection network. *Journal of Geophysical Research*, 103:9035–9044.

De Souza, P., Pinto Jr, O., Pinto, I., Ferreira, N., and dos Santos, A. (2009). The intracloud/cloud-to-ground lightning ratio in southeastern brazil. *Atmospheric Research*, 91:491–499.

Dowden, R., Brundell, J., and Rodger, C. (2002). VLF lightning location by time of group arrival (TOGA) at multiple sites. *Journal of Atmospheric and Solar-Terrestrial Physics*, 64(7):817–830.

Fiser, J., Chum, J., Diendorfer, G., Parrot, M., and Santolik, O. (2010). Whistler intensities above thunderstorms. 28:37–46.

Friedel, R. and Hughes, A. (1992). Trimpi events on low latitude paths: An investigation of gyroresonance interactions at low values. *Journal of Atmospheric and Solar-Terrestrial Physics*, 54(10):1375–1386.

Gill, T. (2008). A lightning climatology of south africa for the first two years of operation of the south afircan weather service lightning detection network: 2006-2007. In *20th International Lightning Detection Conference and 2nd International Lightning Meteorology Conference*.

Gustafsson, G., Papitashvili, N., and Papitashvili, V. (1992). A revised corrected geomagnetic coordinate system for epochs 1985 and 1990. *Journal of atmospheric and terrestrial physics*, 54(11):1609–1631.

Helliwell, R. (1965). *Whistlers and Related Ionospheric Phenomena*. Stanford University Press, Palo Alto, California.

Helliwell, R., Katsufrakis, J., and Trimpi, M. (1973). Whistler-induced amplitude perturbation vlf propagation. *Journal of Geophysical Research*, 78:4679–4688.

Hill, E. (1957). Very low-frequency radiation from lightning strokes. *Proceedings of the IRE*, 45(6):775–777.

Hill, R. (1979). A survey of lightning energy estimates. *Reviews of Geophysics*, 17(1):155–164.

Johnson, M., Inan, U., and Lauben, D. (1999). Subionospheric vlf signatures of oblique (nonducted) whistler-induced precipitation. *Geophysical Research Letters*, 26(23):3569–3572.

Kennel, C. and Petschek, H. (1966). A limit on stably trapped particle fluxes. *Journal of Geophysical Research*, 71(1):1–28.

Kivelson, M. and Russell, C. (1995). *Introduction to space physics*. Cambridge University Press.

Lauben, D., Inan, U., and Bell, T. (1999). Poleward-displaced electron precipitation from lightning-generated oblique whistlers. *Geophysical Research Letters*, 26(16):2633–2636.

Lauben, D., Inan, U., and Bell, T. (2001). Precipitation of radiation belt electrons induced by obliquely propagating lightning-generated whistlers. *Journal of Geophysical Research*, 106(A12):29745–29770.

Lazutin, L., Kuznetsov, S., and Panasyuk, M. (2009). Solar cosmic rays as a source of the temporary inner radiation belts. *Advances in Space Research*, 44:371–375.

Lehtinen, N. and Inan, U. (2009). Full-wave modeling of transionospheric propagation of vlf waves. *Geophysical Research Letters*, 36(L03104):1–5.

Lynch, D. K., editor (1980). *Atmospheric phenomena: readings from Scientific American*. W.H. Freeman and Company, 660 Market Street, San Francisco, California 94104.

Mackerras, D., Darveniza, M., Orville, R., Williams, E., and Goodman, S. (1998). Global lightning: Total, cloud and ground flash estimates. *Journal of Geophysical Research*, 103(D16):19791–19809.

Mariott, W. (1908). Brontometer records at west norwood. *Quaterly Journal of the Royal Meteorological Society*, 34(210):210–212.

Nickolaenko, A. and Hayakawa, M. (2002). *Resonances in the Earth-ionosphere cavity*. Kluwer Academic Publications.

Ogawa, T. (1995). *Lightning Currents*, volume 1 of *Handbook of Atmospheric Electrodynamics*. CRC Press.

Orville, R. and Huffines, G. (2001). Cloud-to-ground lightning in the united states:nldn results in the first decade, 1989-98. *Monthly Weather Review*, 129:1179–1193.

Orville, R., Weisman, R., Pyle, R., Henderson, R., and Orville, R. (1987). Cloud-to-ground lightning flash characteristics from june 1984 through may 1985. *Journal of Geophysical Research*, 92(D5):5640–5644.

Pinto, O., Gin, R., Pinto, I., Mendes, O., Diniz, J., and Carvallo, A. (1996). Cloud-to-ground lightning flash characteristics in southeastern brazil for the 1992-1993 summer season. *Journal of Geophysical Research*, 101(D23):29627–29635.

Pinto Jr., O. (2008). An overview of cloud-to-ground lightning research in brazil in the last two decades. In *20th International Lightning Detection Conference and 2nd International Lightning Meteorology Conference*, Sao Jose dos Campos, SP, Brazil. Brazilian Institute of Space Research - INPE.

Poulsen, W., Inan, U., and Bell, T. (1993). A multiple-mode three-dimensional model of vlf propagation in the earth-ionosphere waveguide in the presence of localized d-region disturbances. *Journal of Geophysical Research*, 98(A2):1705–1717.

Prasad, R. and Singh, R. (1982). Various features of vlf waves generated by lightning discharge. *Il Nuovo Cimento C*, 5(4):462–476.

Prentice, S. (1977). The ratio of cloud-to-ground lightning flashes in thunderstorms. *Journal of Applied Meteorology*, 16:545–550.

Rakov, V. and Huffines, G. (2003). Return-stroke multiplicity of negative cloud-to-ground lightning flashes. *Journal of Applied Meteorology*, 42:1455–1462.

Rakov, V. and Uman, M. (2003). *Lightning: Physics and Effects*. Cambridge University Press.

Rodger, C., Brundell, J., Dowden, R., and Thomson, N. (2004a). Location accuracy of long distance VLF lightning location network. *Annales Geophysicae*, 22:747–758.

Rodger, C. and Clilverd, M. (2002). Inner radiation belt electron lifetimes due to whistler-induced electron precipitation (wep) driven losses. *Geophysical Research Letters*, 29(19):30–1–30–4.

Rodger, C., Clilverd, M., and McCormick, R. (2003). Significance of lightning-generated whistlers to inner radiation belt electron lifetimes. *Journal of Geophysical Research*, 108(A12):1462.

Rodger, C., Clilverd, M., Thomson, N., Nunn, D., and Lichtenberger, J. (2005). Lightning driven inner radiation belt energy deposition into the atmosphere: regional and global estimates. *Annales Geophysicae*, 23:3419–3430.

Rodger, C. and McCormick, R. (2004). Testing the importance of precipitation loss mechanisms in the inner radiation belt. *Geophysical Research Letters*, 31:1–5.

Rodger, C., Nunn, D., and Clilverd, M. (2004b). Investigating radiation belt losses though numerical modeling of precipitating fluxes. *Annales Geophysicae*, 22:3657–3667.

Rodger, C., Werner, S., Brundell, J., Lay, E., Thomson, R., Holzworth, R., and Dowden, R. (2006). Detection efficiency of the vlf world-wide lightning location network (wwlln): initial case study. *Annales Geophysicae*, 24:3197–3214.

Russell, C. (1971). Geophysical coordinate transformations. *Cosmic Electrodynamics*, 2(2):184–196.

Rycroft, M. (1973). Enhanced energetic electron intensities at 100 km altitude and a whistler propagating through the plasmasphere. *Planetary and Space Science*, 21(2):239–240.

Scherer, K., Fitcher, H., Heber, B., and Mall, U., editors (2005). *Space Weather*. Springer, Berlin Heidelberg.

Schultz, W. and Diendorfer, G. (2006). Flash multiplicity and interstroke intervals in austria. In *28th Conference on Lightning Protection*, pages 402–404, Austria, Kahlenberger Str. 2A, A-1190 Vienna. OVE-ALDIS.

Schulz, W., Cummins, K., Diendorfer, G., and Dorninger, M. (2005). Cloud-to-ground lightning in austria: A 10-year study using data from a lightning location system. *Journal of Geophysical Research*, 110.

Starks, M., Quinn, R., Ginet, G., Albert, J., Sales, G., Reinisch, B., and Song, P. (2008). Illumination of the plasmasphere by terrestrial very low frequency transmitters: model validation. *Journal of Geophysical Research*, 113.

Tao, X., Bortnik, J., and Friedrich, M. (2010). Variance of transionospheric vlf wave power absorption. *Journal of Geophysical Research*, 115.

Thomson, E. (1980). The dependence of lightning return stroke characteristics on latitude. *Journal of Geophysical Research*, 85(C2):1050–1056.

Thomson, E., Galib, M., Uman, M., Beasley, W., and Master, M. (1984). Some Features of Stroke Occurrence in Florida Lightning Flashes. *Journal of Geophysical Research*, 89:4910–4916.

Tsurutani, B. and Lakhina, G. (1997). Some basic concepts of wave-particle interactions in collisionless plasma. *Reviews of Geophysics*, 35(4):491–501.

Uman, M. (1984). *Lightning*. Dover Publications.

Voss, H. D., Walt, M., Imhof, W. L., Mobilia, J., and Inan, U. S. (1998). Satellite observations of lightning-induced electron precipitation. *Journal of Geophysical Research*, 103(11):11725–11744.

Walt, M. (2005). *Introduction To Geomagnetically Trapped Radiation*. Cambridge University Press.

Watkins, N., Clilverd, M., Smith, A., Rodger, C., Bharmal, N., and Yearby, K. (2001). Lightning atmospherics count rates observed at halley, antarctica. *Journal of Atmospheric and Solar-Terrestrial Physics*, 63:993–1003.

White, R. (1970). *Space physics*. Gordon & Breach Science Pub.